SELECTIVE TRANSPORT OF SULFUR DIOXIDE THROUGH POLYMER MEMBRANES

Thesis by

Donald L. Kuehne

In Partial Fulfillment of the Requirements

for the Degree of

Doctor of Philosophy

California Institute of Technology

Pasadena, California

1979

(Submitted December 6, 1978)

ACKNOWLEDGMENTS

Many people have contributed directly or indirectly to the completion of this thesis and deserve special recognition.

Dr. Sheldon K. Friedlander, my faculty advisor, suggested the research topic and provided valuable insights at crucial points in the work.

Financial support was provided by the National Science Foundation, the Environmental Protection Agency, the Pasadena Lung Association, the Air Pollution Foundation, and the National Institute of Health.

Technical discussions with the following people were very helpful: Rick Flagan, Daryl Roberts, Mike Barcelona, Tony Miguel, and Ray Stagner. Other friends who made the work environment at Caltech more pleasant include Dave Bruns, Art Stelson, Jim Ouimette, Seong Lee, Masato Koda, Susanne Hering, Pete McMurry, and Cliff Davidson.

The design and construction of the apparatus was facilitated by the expertise of Elton Daly, Joe Fontana, Richard Eastvedt, and Larry McClellan.

The following secretaries and librarians were especially friendly and helpful: Elaine Granger, Bonnie Sherburn, Helen Fabel, Adelaide Massengale, Joan Mathews, Rayma Harrison, and Gunilla Hastrup.

Beth Cooper did an excellent job of typing the thesis, despite numerous other responsibilities and illness in her family. Ruth Stratton assisted in preparing the tables and figures.

Life at Caltech was enriched by friends actively involved with Lake Ave. Congregational Church and the Caltech Christian Fellowship. Foremost among these were Ray Stagner, Dave Bruns, Nancy Mowell, Tom Greenlee, Don Page, and Daryl Roberts. Ray was a loyal friend and faithful leader of our Bible Study for over three years. Special thanks go to Dave for his friendship and for typing much of the first draft of the thesis. I thank Nancy for her understanding and interest in my work. Tom and Don were fellow Keck House residents with whom I shared many enjoyable times. Daryl, my illustrious office mate, provided technical advice, spiritual wisdom, and comic relief, not necessarily in that order.

I am especially indebted to my parents who have faithfully supported me throughout my education and encouraged me to continue my graduate studies, even when other alternatives looked more attractive. Their love and concern sustained me through the difficult times.

Finally, I thank and praise God who gave me the ability to do scientific research and who enabled me to successfully complete this work.

ABSTRACT

The purpose of this research was to identify and characterize polymeric materials which are selective to SO_2 for possible applications in the monitoring or control of SO_2 emissions from stationary sources. Preliminary studies indicated that polyacrylate and cellulose triacetate were very selective to SO_2. The SO_2 solubility of polyacrylate was 0.215 lb/lb (25 °C, 1 atm), comparable to the SO_2 solubilities of sulfolane (tetrahydrothiophene-1,1-dioxide) and polyethylene glycol, two excellent SO_2 solvents.

To achieve the high SO_2 transport rates required for a membrane separation process, two techniques were investigated for preparing ultrathin films of these polymers. Polyacrylate films were cast on mercury, and cellulose triacetate films were formed on glass plates which were withdrawn at constant velocity from dilute polymer solutions. The glass plate technique was also used to make composite films consisting of a 0.2-0.5 μm layer of polyacrylate over a 0.002-0.005 μm layer of cellulose triacetate. All the films were placed on microporous filter materials for support.

The performance of the membranes was initially determined by measuring their permeability to pure N_2, CO_2, and SO_2. The N_2 and CO_2 permeabilities were nearly independent of pressure, but the SO_2 permeability increased rapidly with increasing pressure. The SO_2 permeation data were correlated with two- and three-parameter exponential models. The three-parameter model had the same functional

form as the free volume theory and gave a better fit to the data than the two-parameter model. The SO_2 permeability was affected by previous conditioning of the membranes and time-dependent processes occurring in the polymer. There was evidence that some SO_2 molecules became immobilized in clusters within the membranes.

The composite membranes were also tested with binary mixtures of N_2 and SO_2 at 10 atm upstream pressure with a steady-state flow system. A typical membrane produced an enriched permeant stream of 2% SO_2 from 0.1% SO_2 upstream, 35% from 2%, and over 90% from 10%. N_2 permeation was enhanced by the presence of SO_2, but the presence of N_2 inhibited SO_2 permeation at high SO_2 partial pressures. Interactions between N_2 and SO_2 made it difficult to accurately predict the permeation rates of the mixtures from data for the pure gases.

The composite membranes were superior in performance to the single-layer membranes and those developed by others for SO_2 separations; however, they were unable to meet the stringent design goals for combustion and smelter gas cleaning. The unique properties of the composite membranes do make them attractive for instrumentation and other specialty applications.

TABLE OF CONTENTS

TABLE OF CONTENTS (Cont.)

TABLE OF CONTENTS (Cont.)

TABLE OF CONTENTS (Cont.)

TABLE OF CONTENTS (Cont.)

LIST OF FIGURES

LIST OF FIGURES (Cont.)

LIST OF TABLES

LIST OF SYMBOLS

Symbol	Definition
a	constant, Eq. (1.29) or (2.9)
A	membrane area
A_d	constant in free volume theory, Eq. (1.19)
b	constant, Eq. (1.29) or (2.9)
B_d	constant in free volume theory, Eq. (1.19)
c	concentration of component in membrane or solution
c_o	concentration of penetrant at upstream surface of membrane
c_ℓ	concentration of penetrant at downstream surface of membrane
D	diffusion coefficient
$\overline{D}$	mean value of diffusion coefficient
D_o	pre-exponential constant for diffusion coefficient
D_T	thermodynamic diffusion coefficient
ΔE	energy of vaporization
E_d	activation energy for diffusion
E_q	activation energy for permeation
f	average fractional free volume
g	gravitational constant
$\Delta\overline{H}_c$	molar heat of condensation
$\Delta\overline{H}_m$	molar heat of mixing
$\Delta\overline{H}_s$	molar heat of solution
J	gas flux through membrane
k	constant, Eq. (3.2)

LIST OF SYMBOLS (Cont.)

Symbol	Definition
ℓ	membrane thickness
ℓ_{liq}	thickness of liquid film on glass plate
ℓ_p	thickness of polymer film on glass plate
L	length of channel for plug flow model
m_d	mobility of diffusant
n	moles of gas in downstream chamber of manometric system
n_d	molar flow rate leaving downstream chamber of flow system
n_u	molar flow rate through upstream chamber of flow system
$n_{u,in}$	molar flow rate entering upstream chamber of flow system
$n_{u,out}$	molar flow rate leaving upstream chamber of flow system
P	pressure
ΔP	pressure difference across membrane
P(0)	pressure on upstream side of membrane
$P(\ell)$	pressure on downstream side of membrane
P_d	pressure on downstream side of flow system
P_u	pressure on upstream side of flow system
P_s	standard pressure of 1 atm
Q	permeability
$\overline{Q}$	mean value of permeability
Q_o	pre-exponential constant for permeability
R	gas constant
S	solubility
S_o	pre-exponential constant for solubility
t	time

LIST OF SYMBOLS (Cont.)

Symbol	Definition
T_c	critical temperature
T_g	glass transition temperature
T_s	standard temperature of 273 °K
v	molar volume, Eq. (1.30), or withdrawal rate of glass plate, Eqs. (2.1) and (3.1)
$\dot{v}$	volumetric flow rate leaving downstream chamber of flow system
v_d	penetrant volume fraction
V	volume of downstream chamber of manometric system
W	width of channel for plug flow model
x	coordinate normal to membrane surface
x_d	SO_2 mole fraction of gas in downstream chamber of flow system
x_u	SO_2 mole fraction of gas in upstream chamber of flow system
$x_{u,in}$	SO_2 mole fraction of gas entering upstream chamber of flow system
$x_{u,out}$	SO_2 mole fraction of gas leaving upstream chamber of flow system
z	coordinate parallel to flow through channel for plug flow model
α	constant in three-parameter exponential model, Eq. (2.24)
α_f	constant in free volume theory, Eq. (1.24)
β	constant in three-parameter exponential model, Eq. (2.24)
$\beta(T)$	parameter in free volume theory, Eq. (1.21)
β_1, β_2	molecular relaxation frequencies, Eqs. (1.27) and (1.28)
γ	plasticizing parameter, Eqs. (1.13) and (2.11)
δ	solubility parameter, Eq. (1.30)
θ	time lag

LIST OF SYMBOLS (Cont.)

Symbol	Definition
λ	constant in three-parameter exponential model, Eq. (2.19)
μ	viscosity of pure liquid or solution
ρ	density of pure liquid or solution
ρ_p	density of polymer
σ	surface tension of pure liquid or solution

Chapter 1

INTRODUCTION, PERMEATION THEORY, AND PRELIMINARY WORK

1.1 Incentive for Research

1.1.1 Introduction

Sulfur dioxide (SO_2) is a major air pollutant which has received widespread attention in recent years. Perkins (1974) estimated the nationwide emissions of common pollutants and found that over 95% of SO_2 emissions come from stationary sources such as power plants. The combustion of coal was responsible for over 60% of SO_2 emissions. The national energy policy recommends the use of the vast coal reserves in the U.S. to meet future energy needs. Thus, there is considerable interest in developing suitable control technologies for minimizing SO_2 emissions.

1.1.2 Sulfur Dioxide Control Technologies

Ponder et al. (1976) estimated the commercial availabilities and economics for promising SO_2 control technologies. The principal technologies that will be available for continuous SO_2 emission control through 1980 are naturally occurring low-sulfur coal, physical coal cleaning, and flue gas desulfurization (FGD) processes. Low-sulfur coal has a sulfur content which is low enough so that it can be burned without violating SO_2 emission standards. New Source Performance Standards (NSPS) limit emissions to 1.2 lb of SO_2 per 10^6 BTU. In 1980 it is projected that less than 50% of the utility

coal demand will be supplied from low-sulfur coal production. Physical coal cleaning is effective in removing ash and inorganic sulfur, but less than 13.5% of U.S. coal reserves can be cleaned to meet NSPS. The FGD processes include the nonregenerable lime, limestone, and double-alkali processes and numerous regenerable processes of which the magnesium oxide and Wellman-Lord are the most significant. Details on these and other proposed processes are given in the "Annual Report" (1977) of the Industrial Environmental Research Laboratory-RTP. The lime and limestone scrubbing processes have been demonstrated commercially and will be used almost exclusively in major FGD applications into the early 1980s. One of the major drawbacks of these processes is the disposal of large amounts of sludge in an environmentally acceptable manner.

Other technologies which are currently being studied for later application are chemical coal cleaning, coal gasification, coal liquefaction, and fluidized bed combustion of coal. Chemical coal cleaning utilizes reagents to remove both inorganic and organic sulfur from finely ground coal and requires much further development. Coal gasification has been demonstrated commercially for some applications, but more work is necessary in the areas of H_2S and particulate matter removal systems for utility applications. Industry is reluctant to pursue this option because coal gasification systems are highly capital intensive. With coal liquefaction there is also the need for further technological development and economic analysis is incomplete. Fluidized bed combustion is the most

promising of the advanced technologies. The coal is burned in a fluidized bed of limestone, dolomite, or coal ash which reacts with SO_2. The spent bed material may be continuously withdrawn and discarded or regenerated. The advantages of this process include increased combustion rate and boiler heat flux, the use of lower grade coals, and control of particulate, SO_2, and NO_x emissions.

The application of SO_2 control technologies to utility boilers will add to the total cost of power. Using a conventional coal-fired boiler as the base case, the percentage increase in the cost of power for each of the control technologies is given in Table 1.1. The additional costs range from 4.8% for physical coal cleaning to 25.7% for low-sulfur coal. A fluidized bed combustor operated at atmospheric pressure is the only technology that would be competitive with a conventional coal-fired boiler with no controls if present cost estimates are correct. These cost estimates from Ponder et al. (1976) indicate that controlling SO_2 emissions is very expensive. The optimum control strategy may involve using a combination of the above technologies. There is also a strong incentive to develop new or improved processes which are less costly.

1.1.3 Advances in Membrane Technology

A significant contribution to the cost of regenerable FGD processes is the regeneration of the SO_2 sorbent. It is advantageous to consider new processes which do not require this regeneration. One alternative is to use membranes which are selectively permeable

Table 1.1

Increase in the Cost of Power for SO_2 Control Technologies

Control Technology	Additional Cost (%)
Atmospheric Fluidized Bed Combustion	0
Physical Coal Cleaning	4.8
FGD Processes	8.3-12.7
Pressurized Fluidized Bed Combustion	12.7
Chemical Coal Cleaning	14.3
Coal Gasification	22.9
Coal Liquefaction	not available
Low-Sulfur Coal	25.7

Reference: Figures were calculated from data published by Ponder et al. (1976).

to SO_2. Recent advances in the field of membrane technology have made it possible to perform novel separations using membranes. Michaels (1976) reviewed the history of synthetic polymeric membranes and cited many important practical applications, including particulate separations, water purification, food by-product recovery, isolation and purification of biological substances, oxygen enrichment of air, and controlled release of drugs at specific sites in the body. However, at the time of his publication, there still did not exist any industrial scale membrane processes for gas or vapor separation. The two major reasons for this are (1) the selectivity of synthetic membranes to most commercially important chemical species is too low to make single-stage mixture resolution feasible and (2) the capital and operating costs for multistage membrane separation of gases or liquids are substantially greater than those encountered with traditional separation methods. The prospects for industrial applications have brightened with the recent development of high flux membranes consisting of ultrathin polymer films deposited on microporous substrates and immobilized liquid membranes containing chemical species which enhance the selectivity and rate of transport. These new types of membranes will be discussed in more detail later.

1.1.4 Research Objectives and Strategy

The objectives of this research were to identify and characterize membrane materials which selectively pass SO_2 and to obtain a better understanding of the permeation of condensable vapors, such as SO_2, through polymer membranes. Numerous studies in the literature

have focused on the permeation of permanent gases through polymers. For permanent gases, which do not interact appreciably with the polymer, the permeation data are usually well correlated with existing theories for ideal permeation. With condensable vapors, however, there are often strong interactions between the vapor and the polymer which result in nonideal behavior such as concentration-dependent diffusion. A study of SO_2 transport through membranes will shed light on this and other anomalous behavior.

The work on this project was divided into three phases. The first phase consisted of a literature survey and testing of selected polymers to see which might have the necessary properties for SO_2 applications. Two of the most promising polymers were designated for further study. Next, several techniques were investigated for preparing thin films from these polymers and chemicals were added to the polymers to improve their performance. A novel technique was developed for making two-layer composite films from these same two polymers which were superior in strength and performance to those consisting of a single layer and those of previous studies. The final phase of this work involved testing the composite membranes with binary mixtures of N_2 and SO_2 and comparing the results with those for the pure gases. The remainder of Chapter 1 is devoted to a discussion of permeation theory and the first phase of this research. Chapter 2 describes the fabrication, testing, and evaluation of single-layer films of the two most promising polymers. Chapter 3 deals exclusively with the fabrication, testing, and evaluation of the composite membranes.

1.2 Fundamentals of Membrane Permeation

1.2.1 Basic Permeation Theory

A good discussion of the fundamentals of membrane permeation is given by Crank and Park (1968a). The following derivation is for ideal steady-state permeation through a plane sheet or membrane of thickness ℓ, whose surfaces are maintained at the constant concentrations $c(0)$ and $c(\ell)$. The driving force for permeation is the concentration gradient across the membrane. Gas molecules are absorbed in the polymer at the high concentration interface, diffuse through the membrane, and are desorbed at the other interface. The quantity of gas which dissolves in the polymer is usually proportional to the pressure. Assuming that Fick's law holds for the diffusion process through the membrane, the gas flux is given by

$$J = -D\frac{dc}{dx} \tag{1.1}$$

where c is the concentration of gas in the membrane and the x-direction is normal to the surface. For ideal permeation the diffusion coefficient, D, is independent of concentration and (1.1) can be integrated from $x = 0$ to $x = \ell$ to give for the steady-state flux

$$J = \frac{D[c(0)-c(\ell)]}{\ell} \tag{1.2}$$

If the interfacial concentration of gas in the polymer is proportional to the pressure in the gas phase, then

$$c = SP \tag{1.3}$$

Substitution for c in (1.2) gives

$$J = \frac{DS[P(0)-P(\ell)]}{\ell} \tag{1.4}$$

The product of the diffusion coefficient, D, and the solubility, S, is the permeability, Q. The units of Q which appear most frequently in the literature are

$$\frac{cm^3(STP)\cdot cm}{cm^2\cdot sec\cdot cm\ Hg} \tag{1.5}$$

Expressed in words, the permeability is the volume of gas in cubic centimeters (measured at 0 °C and 1 atm pressure) which passes through a membrane one centimeter thick and one square centimeter in area per second per centimeter of mercury pressure difference across the membrane. The units of the diffusion coefficient are cm^2/sec and it follows that the units of solubility are $cm^3(STP)/(cm^3\cdot cm\ Hg)$.

The permeability is easily calculated from a measurement of the steady-state gas flux using (1.4). If the solubility is known, then the diffusion coefficient follows from

$$D = Q/S \tag{1.6}$$

If the diffusion coefficient varies with concentration, the value of D deduced from (1.6) is a mean value given by

$$\overline{D} = \frac{1}{c(0)-c(\ell)} \int_{c(\ell)}^{c(0)} D\,dc \tag{1.7}$$

When the diffusion coefficient is constant, it may also be determined by the time-lag method (Daynes, 1920). At t = 0 a membrane which is initially completely free of diffusant is exposed to a constant concentration on one side while maintaining zero concentration on the other side. A plot of the total amount of diffusant which has passed through the membrane versus time approaches a straight line which has an intercept θ on the t-axis given by

$$\theta = \ell^2/6D \tag{1.8}$$

Time-lag analysis for concentration-dependent diffusion coefficients is more complicated (Frisch, 1957; Meares, 1965).

1.2.2 Factors Affecting Permeability

Many factors affect membrane permeability. These may be divided into external or state properties, such as temperature and pressure, properties of the penetrant, properties of the polymer, interactions between penetrant and polymer, and membrane structure and support. Review articles which are helpful in gaining a basic understanding of these factors have been written by Michaels and Bixler (1968), Li and Long (1970), and Rogers et al. (1972). The following discussion draws heavily on the material presented by Rogers et al.

1.2.2.1 Temperature and Pressure

For homogeneous polymers the temperature dependence of the permeability, diffusion, and solubility coefficients can be represented by Arrhenius-type equations over moderate ranges of temperature:

$$Q = Q_o \exp(-E_q/RT) \tag{1.9}$$

$$D = D_o \exp(-E_d/RT) \tag{1.10}$$

$$S = S_o \exp(-\Delta\bar{H}_s/RT) \tag{1.11}$$

where $Q = DS$, $Q_o = D_o S_o$, and E_q is the activation energy for permeation equal to the sum of the activation energy for diffusion, E_d, and the heat of solution, $\Delta\bar{H}_s$. The diffusion of a gas molecule through an amorphous polymer is an activated process in which the polymer chain segments must be sufficiently mobile to permit hole formation for successive stepwise displacements of the gas molecule. As the temperature increases, segmental motion and polymer volume increase so that hole formation occurs more frequently and diffusion is more rapid. The process of absorption involves condensation of molecules on the polymer surface followed by solution. Thus, $\Delta\bar{H}_s$ is the sum of the molar heat of condensation and the molar heat of mixing:

$$\Delta\bar{H}_s = \Delta\bar{H}_c + \Delta\bar{H}_m \tag{1.12}$$

$\Delta\bar{H}_m$ depends mainly on the cohesive energy densities of condensed penetrant and polymer. As the cohesive energy densities of the components become more equal, $\Delta\bar{H}_m$ decreases and S increases. For a gas well above its critical point, the hypothetical value of $\Delta\bar{H}_c$ is negligible and $\Delta\bar{H}_s$ is essentially determined by $\Delta\bar{H}_m$, which is usually small and positive. S, therefore, increases slightly with increasing temperature for permanent gases. For more condensable

gases and vapors, $\Delta\overline{H}_s$ is dominated by the negative $\Delta\overline{H}_c$, and S decreases with increasing temperature.

The pressure dependence of the permeability coefficient is usually small for penetrants which do not interact appreciably with the polymer. At high pressures mechanical stress or compaction may lead to a slight decrease in permeability. Stress on a thin membrane may enlarge pinhole defects and greatly increase the permeability. Solubility follows Henry's law for most gases up to the critical pressure, above which there may be substantial deviations from linearity.

In the subcritical pressure region, most nonideal behavior manifests itself by altering the diffusion coefficient. Pressure- or concentration-dependent diffusion coefficients are observed in systems in which there are strong interactions between penetrant and polymer. Stern et al. (1971) studied the permeation of gases through polyethylene membranes at pressures up to 60 atm. The permeability coefficients for N_2 and He decreased slightly with increasing pressure, probably due to the membrane support. The permeability coefficients for C_2H_6, C_2H_4, CO_2, and N_2O exhibited exponential dependence on pressure at reduced temperatures of the penetrant below and near unity. This pressure-dependent behavior will be discussed in more detail in Section 1.2.2.4.

1.2.2.2 Properties of the Penetrant

The properties of the penetrant which affect permeability are molecular size and shape. Diffusion coefficients generally decrease

as the molecular weight or the volume of the penetrant increases. A change in shape which makes the penetrant molecule more bulky or increases its cross-sectional area has a greater effect on the diffusion coefficient than simply an increase in the chain length. E_d is often correlated with the cross-sectional area or diameter of the penetrant.

The dependence of the solubility on molecular size is related to the condensability of the penetrant. Larger molecules are more easily condensable because of stronger intermolecular forces and, consequently, are more soluble in a given polymer. The boiling point, critical temperature, and Lennard-Jones force constant are measures of the condensability of a gas or vapor. Linear relationships have been found between log S and each of these quantities.

1.2.2.3 Properties of the Polymer

Properties of the polymer which are important in understanding permeability include transition temperatures, polymer segmental chain mobility, crystallinity and orientation, and porosity. At the glass transition temperature, T_g, most polymers exhibit abrupt changes in the second-order thermodynamic properties. There are corresponding changes in the second-order gas transport properties. Above T_g, E_d is more positive and $\Delta\overline{H}_s$ is less negative. D_o increases significantly in going from the glassy state to the flexible state. The Arrhenius equations still apply, but the constants have different values above and below T_g.

The nature of the segmental motions in polymers determines the size distribution of holes available for the diffusion process. Any factor which reduces segmental chain mobility will decrease the overall rate of permeation. The local segmental mobility may be affected by chain interactions arising from hydrogen bonding, polar functional groups, or even van der Waal's forces. Polar functional groups increase the cohesive forces between neighboring polymer chains. As more functional groups are added per unit chain length, the permeation rate decreases and the activation energy for diffusion increases. Other factors which decrease chain segmental mobility are crosslinking, crystalline domains, high density, and solid additives or fillers on which the polymer is strongly adsorbed. Plasticizers and penetrants which solvate the polymer increase chain mobility and permeation rates.

Polymer crystallinity and chain orientation can have profound effects on membrane permeability and selectivity. Crystalline regions in a polymer are usually highly ordered and tightly packed so that it is nearly impossible for gas molecules to penetrate them. The solubility is directly proportional to the noncrystalline content and diffusion is confined to the amorphous regions which interconnect the crystallites. Crystalline regions increase the tortuosity of the diffusion path and may also restrict the mobilities of neighboring chain segments. Depending on the size and shape of the crystallites, the diffusion coefficient may be greatly reduced, particularly as

the size of the gas molecule is increased. Crystallite size and shape are governed by the thermal history of the polymer membrane. A membrane which is slowly cooled from the melt will have larger, well-formed crystallites as opposed to one which is quenched. High-temperature annealing of a quenched membrane causes the polymer to recrystallize in a more relaxed state which results in a larger permeability. Crystallinity also restricts the degree of swelling by solvating penetrants and tends to increase membrane selectivity.

Molecular orientation has similar effects on the transport properties as crystallinity. The rate of diffusion parallel to the direction of orientation is less than the rate perpendicular to the direction of orientation which is less than the rate in an isotropic sample. Orientation may be induced by mechanically deforming a crystalline polymer. If a polymer film is uniaxially stretched well below its melting point, it is much more resistant to swelling by good solvents than its undrawn counterpart. Moreover, its permeability may be reduced by a couple orders of magnitude and its selectivity greatly enhanced. If the stretched film is subsequently annealed, the permeability increases with some loss in selectivity. By combining stretching and annealing treatments, it is possible to produce a large number of structurally different membranes from the same polymer with wide variation in permeability and selectivity.

Polymer porosity is another factor which affects sorption and transport in membranes. In many investigations it is tacitly

assumed that the membrane is a homogeneous continuum through which diffusion occurs by a single activated mechanism. However, there is evidence for the presence of a microporous structure in certain amorphous polymers below or near their glass temperatures and in semicrystalline polymers above their glass temperatures. The occurrence of voids in semicrystalline polymers is very dependent on the nature of the polymer, crystallization conditions, annealing procedures, and induced orientation. The distribution of void size may range from submicron voids of unit-cell dimensions to much greater dimensions. These voids are to be distinguished from the free volume associated with liquids or amorphous solids, and their magnitude is not a thermodynamic quantity.

The effect of a microporous structure on the solubility and transport properties depends on the degree to which the pores are interconnected and on the nature of the penetrant. The presence of interconnected channels permits convection of penetrant to occur through the membrane in addition to activated diffusion. For the case of noninterconnected microvoids, the diffusion process may be slightly enhanced due to the lower overall density. However, when the cohesive forces between penetrant molecules are greater than the attractive forces between penetrant and polymer, the incoming penetrant tends to cluster within the polymer. Molecules within a cluster are less mobile than isolated free molecules because of the additional energy required to break free from the cluster. Consequently, the diffusion rate usually declines when cluster formation occurs.

1.2.2.4 Interactions between Penetrant and Polymer

Interactions between penetrant and polymer often result in nonideal behavior such as a concentration- or time-dependent diffusion coefficient. A penetrant which is strongly absorbed by a polymer acts as a plasticizer which increases chain segmental mobility and hence the rate of diffusion. The increase in the diffusion coefficient depends on the concentration of penetrant in the polymer. Many models and theories have been proposed to account for this concentration dependence. Representative of these are the exponential model, the free volume theory, and the molecular relaxation model.

The exponential model gives the concentration dependence of D as

$$D = D_o e^{\gamma c} \tag{1.13}$$

where D_o is the extrapolated value of D at zero concentration and γ is the plasticizing parameter. The advantage of this simple model is that it is easy to integrate with respect to c to obtain an analytic expression for the permeability. Starting with Fick's law, the gas flux is given by

$$J = -D_o e^{\gamma c} \frac{dc}{dx} \tag{1.14}$$

In the steady-state (1.14) may be integrated from x = 0 to x = ℓ to give

$$J\ell = \frac{D_o}{\gamma}\left[e^{\gamma c(0)} - e^{\gamma c(\ell)}\right] \tag{1.15}$$

The concentration of absorbed penetrant is usually proportional to pressure up to about 10 weight percent. Then,

$$c = SP \tag{1.16}$$

and substitution for c in (1.15) yields

$$J\ell = \frac{D_o}{\gamma}\left[e^{\gamma SP(0)} - e^{\gamma SP(\ell)}\right] \tag{1.17}$$

If $Q_o = D_o S$, then the permeability is

$$Q = \frac{J\ell}{\Delta P} = \frac{Q_o}{\gamma S[P(0)-P(\ell)]}\left[e^{\gamma SP(0)} - e^{\gamma SP(\ell)}\right] \tag{1.18}$$

The disadvantage of the exponential model is that it cannot be used to predict or correlate the separation behavior of multicomponent systems.

A number of theories which are based on free volume concepts have been proposed to explain the concentration and temperature dependence of diffusion coefficients, primarily for organic vapors in amorphous polymers above T_g. The free volume is a measure of the unoccupied volume available for the mobility of polymer segments and

diffusant molecules. The presence of plasticizer or solvent molecules within the polymer structure has the effect of increasing polymer segmental mobility and lowering T_g. The free volume is an increasing function of penetrant concentration. The simplest and most widely used free volume theory is that of Fujita et al. (1960). A number of publications have presented summaries of Fujita's approach (Fujita, 1968; Rogers et al., 1972; Machin and Rogers, 1972).

Fujita assumes that the mobility of the diffusant, m_d, is a function of the average fractional free volume of the system, f:

$$m_d = A_d \exp(-B_d/f) \tag{1.19}$$

A_d and B_d are parameters which are assumed to be independent of diffusant concentration and temperature. B_d is a measure of the minimum free volume required for diffusion. The thermodynamic diffusion coefficient, D_T, is related to m_d by the equation

$$D_T = RTm_d \tag{1.20}$$

For small values of the penetrant volume fraction, v_d, f increases linearly with v_d at constant temperature:

$$f(T,v_d) = f(T,0) + \beta(T)v_d \tag{1.21}$$

Here f(T,0) is the free volume of the polymer at zero penetrant concentration and $\beta(T)$ is a function which relates the increase in free volume to the volume fraction of penetrant. Combining the above

equations leads to the following two relations:

$$\ln(D_o/RT) = \ln A_d - B_d/f(T,0) \tag{1.22}$$

$$\frac{1}{\ln(D_T/D_o)} = \frac{f(T,0)}{B_d} + \frac{[f(T,0)]^2}{B_d\beta(T)v_d} \tag{1.23}$$

D_o denotes the value of D_T at the limit of zero diffusant concentration. The temperature dependence of $f(T,0)$ is usually represented by an equation of the form:

$$f(T,0) = f(T_s,0) + \alpha_f(T-T_s) \tag{1.24}$$

where T_s is a suitably chosen reference temperature and α_f is a parameter characteristic of the polymer. By utilizing the results of Williams et al. (1955) for the temperature dependence of the viscosity of polymers, values of $f(T_s,0)$ and α_f can be deduced.

To evaluate the parameters of the free volume theory, absorption or desorption experiments are usually performed and the data carefully analyzed. The desorption method requires a computer solution of a highly nonlinear differential equation to find the optimum values of the parameters. Absorption data can be plotted so that the slope and intercept of a line through the data are functions of the parameters. However, many experiments must be done to obtain an accurate value of the intercept which is typically far from the range of the data. One of the major disadvantages of the free volume theory is that the expressions for D cannot be integrated analytically with respect to c.

Fels and Li (1974) studied the permeation of n-heptane and cyclohexane through polyethylene. They evaluated the free volume parameters for the individual components and then predicted the permeabilities of n-heptane and cyclohexane for various mixtures of the two components. The agreement between the actual and predicted permeabilities for the mixtures was only fair. The main reason given for this discrepancy was inaccuracy in the values of the free volume parameters and diffusion coefficients. Another possibility was that conditioning of the membrane by the organic liquids caused the polymer chains to undergo irreversible rearrangement. The conditioning effects were likely to be different for the steady-state permeation of the mixtures and the unsteady-state absorption/desorption experiments from which the free volume parameters were calculated. Fels and Li concluded that the model was somewhat impractical for predicting separation behavior.

The molecular relaxation model is one of three models for anomalous diffusion discussed by Petropoulos and Roussis (1974). This model takes into account the molecular rearrangement in the polymer necessary to accommodate a change in penetrant content. It has been applied to systems in which the penetrant is a good swelling agent of the polymer. It is customary to start with Fick's diffusion equation:

$$\frac{\partial c}{\partial t} = \frac{\partial}{\partial x}\left(D\frac{\partial c}{\partial x}\right) \qquad (1.25)$$

The following boundary equations apply for c(x,t):

$$c(0,t) = c_0, \quad c(\ell,t) = c_\ell, \quad c(x,0) = c_1 \tag{1.26}$$

The above formation is modified by following the treatments of Crank (1953) or of Long and Richman (1960). Crank made D a function of t. The initial value, D(c,0), is assumed to approach the final equilibrium value, D(c,∞), by first-order kinetics. Accordingly, (1.25) and (1.26) have to be solved simultaneously with

$$\frac{\partial D(c,t)}{\partial t} = \frac{\partial D(c,0)}{\partial c}\frac{\partial c}{\partial t} + \beta_1[D(c,\infty)-D(c,t)] \tag{1.27}$$

Similarly, Long and Richman made c_0 a function of t with initial and equilibrium values of $c_0(0)$ and $c_0(\infty)$, respectively. The auxiliary equation in this case is

$$c_0(t) = c_0(\infty) - [c_0(\infty)-c_0(0)]\exp(-\beta_2 t) \tag{1.28}$$

The rate constants or relaxation frequencies, β_1 and β_2, may also depend on c. Absorption, desorption, or time-lag experiments are necessary to evaluate the functions and parameters.

One criticism of the above treatment is that the concentration gradient is not the proper driving force if c is affected directly by the relaxation process. It is more appropriate to use the chemical potential gradient as the driving force. This refinement does not change the form of the equations, and the results are very similar to those obtained with the original models, too. The molecular

relaxation models can explain in a physically meaningful way a wide diversity of nonideal behavior.

1.2.2.5 Membrane Structure and Support

The factors most often overlooked in permeation studies deal with membrane structure and support. For homogeneous membranes the permeability is ideally independent of thickness. However, a thickness dependence is observed when there are boundary resistances at the surfaces of the membrane, when the membrane is composed of different layers or has a gradient of inhomogeneity, and when the membrane is supported on a microporous medium which has a limited surface porosity.

Hwang and Kammermeyer (1974) give methods for analyzing the effect of thickness. For membranes consisting of a single homogeneous phase, the reciprocal of the permeability is plotted versus the reciprocal of membrane thickness. The intrinsic or invariant permeability, which is a property of the polymer, and the boundary resistances are calculated from the intercept and slope of the line through the data. When a membrane consists of two or more layers of different permeability, the analysis is modified by plotting the concentration driving force divided by flux versus membrane thickness.

Rogers et al. (1957) investigated the permeability of composite membranes consisting of more than one layer. If the permeability coefficient of each layer is independent of pressure, the overall rate of permeation is independent of the order in which the individual

layers are assembled. If the permeability coefficients are pressure dependent, however, the permeation rate will depend on the order. For a membrane composed of two layers, the permeation rate will be greater if the layer having the more pressure dependent permeability coefficient is exposed to penetrant on the high pressure side of the permeation cell. Rogers et al. verified these conclusions with experimental results for the transmission of water vapor through membranes composed of nylon and Ethocell layers. Rogers (1965) observed similar behavior with polyethylene membranes having a gradient of structural composition. The rate at which certain vapors passed through these membranes depended on the direction of flow relative to the gradient of polymer composition.

Composite membranes consisting of a thin homogeneous film supported on a microporous medium exhibit thickness-dependent permeation rates due to the limited surface porosity of the substrate. This effect was observed and characterized by Lonsdale et al. (1971) with reverse osmosis composite membranes. For ideal permeation the flux is inversely proportional to film thickness. The effect of surface porosity is to make the flux lower than the value predicted from data on thick films and this inverse relationship. The factors which govern the flux reduction are film thickness, pore size, and pore density. As the film thickness is decreased, the flux asymptotically approaches the "porosity limit," which is just the surface porosity times the ideal flux. The surface porosity cannot be deduced from a gravimetric determination of the bulk porosity but must be estimated

from electron micrographs of the surface. Pore size and density determine the open area available for transport and the minimum film thickness which can be adequately supported. Mechanical failure will occur at high pressure if the pore diameter is much larger than the film thickness. To achieve good membrane performance, the microporous substrate should have a high density of small pores and a smooth surface.

1.3 Survey of Sulfur Dioxide Permeation Through Membranes

1.3.1 Literature Survey

A survey of the recent chemical literature was conducted to find SO_2 permeation data and to identify polymers having the necessary properties for SO_2 gas separations. Chemical Abstracts was reviewed through December, 1977, under the headings "membranes" and "permeability." A computer search was also done to insure that no important references were missed.

Felder et al. (1975) compiled all the available data on SO_2 transport through polymers and discussed the effects of temperature, pressure, humidity, and plasticizers on SO_2 permeability. A large proportion of the data was for teflon and silicone rubbers. Teflon typically has a very low permeability for SO_2. Silicone rubber is one of the most permeable membrane materials but is not very selective. Other synthetic rubbers and some cellulosic polymers looked more attractive for SO_2 applications. These materials have large SO_2 solubilities and the rubbers, of course, also have large

diffusion coefficients. A polyethylene glycol liquid membrane developed by Ward (1971) had the highest SO_2 permeability of all the materials tabulated by Felder et al.

One of the earliest permeation studies of rubbers was done by Van Amerongen (1946). He measured the permeability of nine rubbers to H_2, He, O_2, N_2, CO_2, and CH_4 and independently determined solubilities and diffusivities which he related to the nature of the gases and the rubbers. He found that gases with high critical temperatures or boiling points dissolve more readily in rubbers. The solubility is related to the critical temperature by the equation

$$\log S = a + bT_c \tag{1.29}$$

where a and b are constants. Polymers with strong polar functional groups absorb the polar gases SO_2 and NH_3 much more readily than the nonpolar gases N_2 and O_2. The SO_2 solubilities of several rubbers were 2 to 3 orders of magnitude greater than the N_2 solubilities, indicating that rubbers may be good candidates for SO_2 gas separations.

The problem most often encountered in applying polymer membranes to gas separation is that high selectivity and high flux rates cannot be achieved with the same membrane. Ward and Neulander (1970) chose to look at immobilized liquid membranes as a viable alternative. Liquids have much larger diffusion coefficients than solid polymers and they may also have enormous solubilities for reactive gases such as SO_2. The permeation of SO_2 is enhanced by the mechanism of "facilitated transport" in which ionic sulfur species contribute to

the total flux of sulfur by reversible chemical reactions. Ward and Neulander measured the SO_2 solubilities of 20 liquids having essentially zero vapor pressure at 100 °C and found that polyethylene glycol had the highest solubility. Next, they immobilized the liquid by forming a rigid gel about 1 mil thick. The resulting membrane had excellent selectivity but the flux rate was an order of magnitude too low for practical applications. A procedure was developed for preparing much thinner membranes to obtain the desired flux. However, these membranes were unable to withstand a pressure difference across them, which is essential to produce a concentrated stream of SO_2.

In an extension of this work, Juliano and Ward (1972) found that polyethylene glycols could also be immobilized by forming a block copolymer of bisphenol-A polycarbonate and polyethylene glycol. This copolymer could be dissolved in chloroform, and membranes were readily cast from the solution and supported on microporous backings or 1-mil silicone rubber membranes. The block copolymer membranes had the same selectivity as pure polyethylene glycol, but the SO_2 fluxes were too low for large-scale separations.

Matson et al. (1977) described an approach for fabricating immobilized liquid membranes for the removal of H_2S from gasified coal. A 30 weight percent K_2CO_3 solution was immobilized by impregnating it in a microporous hydrophilic polymer membrane 1-3 mils thick with 60-70% porosity. Surface tension forces held the liquid in the pores of the support even when a pressure difference of 300 psi was applied across the membrane. The facilitated transport of H_2S

through these membranes was inhibited by side reactions with oxygen and other species. One solution to this chemical deactivation problem was to arrange for a gradual replacement of the membrane liquid. Other potential problem areas with these liquid membranes were evaporation and fouling from dust and tar fog in the coal gas.

The performance of a polymer membrane may be improved by adding chemicals which alter its properties. Seibel and McCandless (1974) plasticized vinylidene fluoride (Kynar) with sulfolane (tetrahydrothiophene-1,1-dioxide) and found that the resulting membranes were effective in separating SO_2 from a binary mixture with N_2. The optimum membrane composition was about 8.2 weight percent sulfolane. The membrane selectivity was highly dependent on gas composition and pressure. Gas fluxes were very low because of the relative impermeability of Kynar and the 1-mil thickness of the films. Zavaleta and McCandless (1976) extended this work by testing several sulfones as modifiers and discovered that a membrane with 18 weight percent sulfolene (dihydrothiophene-1,1-dioxide) was the best. The highest SO_2 permeabilities and selectivities were obtained at low temperatures and high partial pressures of SO_2.

In addition to homogeneous polymer membranes and immobilized liquid membranes, a third type of membrane that has been considered for gas separations is the asymmetric cellulosic membrane which was originally prepared by Loeb and Sourirajan (1964). The membrane structure consists of a dense surface layer about 0.2 μm thick supported by a finely porous substrate. The membranes were used in reverse osmosis

processes to desalinate brackish water but were not sufficiently selective for single-stage seawater desalination. To apply these membranes for gas separations, they were dried by an elaborate procedure involving heat treatment, quick-freezing, and vacuum sublimation. The entire procedure is highly empirical and not easily adapted to other polymers.

Agrawal and Sourirajan (1970) studied the permeation of pure gases and several binary gas mixtures, including N_2/SO_2, through porous freeze-dried cellulose acetate membranes. Due to the porosity of the membranes, separation factors were rather low but flux rates were reasonable. Schell (1975) prepared asymmetric cellulose acetate films which had selectivities characteristic of nonporous cellulose acetate films but much higher permeation rates. He used these membranes to separate H_2 from CH_4 and CO and suggested applications in coal utilization processes.

1.3.2 Criteria for Screening Polymers

The preceding literature survey shows that little work has been done in the specific area of SO_2 permeation through polymers. A more comprehensive survey is needed in which many different types of polymers are examined. Elastomers and cellulosic polymers have already been identified as good candidates for further study. That leaves, perhaps, several hundred other polymers for which no SO_2 permeation data are available. To facilitate the screening of these polymers, it is necessary to develop criteria which do not require physical testing, since this would be impractical for a large number of samples.

The solubility parameter is an obvious choice for screening purposes. High solubility is expected when the solubility parameters of penetrant and polymer are nearly the same. Of course, other factors such as crystallinity and crosslinking will affect solubility, too. The solubility parameter, δ, is defined as

$$\delta = (\Delta E/v)^{1/2} \tag{1.30}$$

where ΔE is the energy of vaporization and v is the molar volume. For SO_2 at 21 °C, δ = 10.1 $(cal/cc)^{1/2}$. A list of solubility parameters for selected rubbers and resins is given in Table 1.2. Amino resins, epoxy, and ethyl cellulose have solubility parameters closest to the value for SO_2. This criterion is a practical guide for nonpolar systems but may not hold for polar systems in which there are specific interactions such as hydrogen bonding.

The solubility parameter has limited applicability and has not been determined for all polymers so other criteria are necessary for identifying SO_2 selective polymers. The permeability of a few polymers has been measured for many gases. If the gases are listed in order of increasing permeability, the order is usually the same for polymers selective to SO_2. N_2 is the least permeable gas, followed by O_2, CO_2, SO_2, and H_2O. Permeation data are available for most polymers for at least N_2, CO_2, and H_2O. Since the SO_2 permeability usually falls between the CO_2 and H_2O permeabilities, these data can be used to estimate the value for the SO_2 permeability. One of the best sources for gas permeation data is a review article by Hwang et al. (1974) which lists data for seventy-four different

Table 1.2

Solubility Parameter, Crystallinity, and Modulus of Rubbers and Resins

Rubber/Resin	Solubility Parameter	Crystallinity	Modulus at Room Temperature (after cure, for thermosets)
Polytetrafluoroethylene	6.2	High	Medium
Silicone, polydimethyl	7.3	Low-medium	Medium
Butyl rubber	7.7	Low	Low
Polyethylene	7.9	High	Medium
Natural rubber	7.9-8.3	Low	Low
Butadiene-styrene	8.1-8.5	Low	Low
Polyisobutylene	8.0	Low	Low
Polystyrene	8.6-9.7	Low	High
Polysulfide rubber (Thiokol)	9.0-9.4	Low	Low
Epichlorohydrin-ethylene oxide	9.1	Low	Low
Neoprene	9.2	Varies	Low
Butadiene-acrylonitrile	9.2-9.6	Low	Low
Polyvinyl acetate	9.4	Low	Low-medium
Epichlorohydrin	9.4	Low	Low
Polymethyl methacrylate	9.0-9.5	Low	High
Polyvinyl chloride	9.5-9.7	Medium	Medium-high
Amino resins	9.6-10.1	Low	High
Epoxy	9.7-10.9	Low	Medium-high
Ethyl cellulose	10.3	Low	Medium-high
Polyvinyl chloride acetate	10.4	Low-medium	Medium
Polyglycol terephthalate	10.7	High	High
Cellulose acetate	10.9	Medium	Medium-high
Cellulose nitrate	10.6-11.5	Low-medium	Medium
Phenolic	11.5	Low	High
Polyvinylidene chloride (saran)	12.2	High	Medium-high
Nylon	12.7-13.6	High	Medium-high
Polyacrylonitrile	15.4	High	Medium-high

Table 1.2 (continued)

Reference: "Hycar Nitrile Rubber in Adhesives," Manual HM-12, B. F. Goodrich Chemical Company.

kinds of polymers for A, H_2, He, N_2, O_2, CO_2, CH_4, and H_2O. Two other sources of data are Major and Kammermeyer (1962) and Baer (1964). Baer's tables include data for the activation energy of permeation.

When no permeation data are available for a particular polymer, it is necessary to examine the polymer structure. Polymers with polar functional groups, such as carbonyl or amine groups, absorb SO_2 more readily than nonpolar gases. For example, Lesky and Fuest (1972) found that selected basic-nitrogen containing polymers had high solubility for acidic materials and when blended with thermoplastic resins such as polyolefins, polyesters, or polyamides could be spun into fibers for use in gas absorbers.

The above criteria were helpful in identifying polymers that might be selective to SO_2. For polymers for which data were lacking or incomplete, commercial samples were obtained and tested by measuring their permeability to N_2, CO_2, and SO_2. These gases are the principal constituents in gas mixtures containing SO_2 and have permeabilities which usually differ by several orders of magnitude. Briefly, the permeability was determined by the Manometric Method in which a sample is mounted in a permeation cell and is exposed to gas at 1 atm pressure on the upstream side. The downstream side is initially completely evacuated, but the pressure gradually increases with time as a result of gas permeation through the sample. From this pressure versus time data and system parameters, the permeability can be calculated. The apparatus and procedure are described in detail in Chapter 2.

1.3.3 Membrane Design Goals

The objective of the literature survey and testing of selected polymers was to find the most promising materials for SO_2 separations. In their work on immobilized liquid membranes, Ward and Neulander (1970) proposed the following design goals for a membrane for recovering SO_2 from combustion or smelter gases:

(1) The SO_2 flux should be on the order of

$$4 \times 10^{-3} \frac{cm^3(STP)}{cm^2 \cdot sec \cdot cm\ Hg} \tag{1.31}$$

This is equivalent to a permeability of

$$1 \times 10^{-5} \frac{cm^3(STP) \cdot cm}{cm^2 \cdot sec \cdot cm\ Hg} \tag{1.32}$$

for a membrane 1 mil thick, which is a typical minimum commercial thickness. This goal was deduced from economic considerations. The SO_2 flux determines the membrane area necessary for a particular application. By assuming a total cost per unit area, it is possible to calculate the SO_2 flux which will make the membrane separation process competitive with existing processes. Lacking the details of these calculations, the SO_2 flux goal will be considered only an order of magnitude estimate.

(2) The membrane should be highly selective for SO_2. The SO_2/CO_2 permeability ratio should be on the order of several hundred for application in the removal of SO_2 from combustion gases, which typically contain on the order of 0.2% SO_2. O_2 and N_2 permeabilities would not be a problem since they are usually at least 10 times smaller than the CO_2 permeability. For the membrane to have application for more concentrated stack gases, such as 2-10% SO_2 which might be produced in a smelter, the permeability ratio should be at least 10.

(3) The membrane should operate at elevated temperatures of at least 100 °C.

(4) The membrane should be chemically inert and nonvolatile at the operating temperature.

(5) The membrane should have an effective life of at least one year and preferably more.

1.3.4 Summary of Attractive Membranes

The most attractive membranes revealed by the literature survey and testing of commercial samples are listed in Table 1.3 with their N_2, CO_2, and SO_2 permeabilities and permeability ratios to indicate their selectivity for SO_2. Tables of data for all the polymers that were examined are given in Appendix A. The data of this study were taken by the method described at the end of Section 1.3.2. The methods

Table 1.3

Permeability of Attractive Membranes

Membrane	$Q(N_2)$	$Q(CO_2)$	$Q(SO_2)$	$Q(SO_2)/Q(N_2)$	$Q(SO_2)/Q(CO_2)$	Reference
1. Dimethyl Silicone	229	2470	11500	50	4.6	General Electric (1970)
2. Buna N on Nylon	1.8	39.7	800	444	20	Present Study
3. Polyacrylate on Dacron	2.04	46.7	1920	941	41	Present Study
4. Cellulose Triacetate	0.20	5.6	270	1350	48	Present Study
5. Cellulose Acetate-Butyrate	1.5	39.2	720	480	18	Present Study
6. Ethyl Cellulose	4.7	104	970	206	9.3	Present Study
7. Parylene N	0.046	1.3	11.3	246	8.7	Union Carbide (1974)
8. Polyvinylidene Fluoride (w/18 wt % sulfolene)	0.093	2.0	430	4620	215	Zavaleta and McCandless (1976)
9. Polyethylene Glycol	1.65	92.7	4100	2480	44	Ward (1972)

Units of Permeability, Q: $\frac{cm^3(STP)\cdot cm}{cm^2\cdot sec\cdot cm\ Hg} \times 10^{10}$

for the literature data were not specified in some cases. For this reason, the data from different references should only be compared qualitatively.

The first three entries in Table 1.3 are elastomers and the next three are cellulosic polymers. The last three entries were included for their unique properties. Dimethyl silicone rubber is clearly the most permeable material but has the lowest selectivity for SO_2. The Buna N and polyacrylate elastomers were obtained from Du Pont as coatings on fabric supports. Polyacrylate has the highest selectivity of the elastomers. With the cellulosic polymers, a tradeoff between permeability and selectivity is again apparent. Cellulose triacetate has the highest selectivity for SO_2 but is the least permeable.

Parylene N has only moderate selectivity and its permeability is very low but was included in Table 1.3 for its thin film capabilities By a special vapor deposition process developed by Union Carbide (1974), films as thin as 250 Å are routinely made. Unfortunately, even at this thickness, gas fluxes would not be adequate for SO_2 applications. The modified polyvinylidene fluoride membrane has the highest SO_2 selectivity but rather low permeability. The immobilized polyethylene glycol membrane appears to be the most attractive of the membranes in Table 1.3. The problem with immobilized liquid membranes is the difficulty in preparing thin films which will withstand a pressure difference across them.

1.3.5 Ways of Meeting Sulfur Dioxide Flux Goal

The importance of the magnitude of the SO_2 permeability is better understood in light of the membrane design goals mentioned earlier. For a dimethyl silicone membrane to meet the SO_2 flux goal, its thickness would have to be about 3 μm. For the other materials which were more selective to SO_2, membrane thicknesses would need to be much less. This means that the development of practical gas separation membranes depends on the availability of technology to produce thin, durable films.

Other ways of increasing the gas flux include changing the temperature or pressure or plasticizing the polymer. The permeability may increase or decrease with increasing temperature, depending on the temperature dependence of the diffusion coefficient and solubility. Zavaleta and McCandless (1976) found that the permeation of SO_2 through sulfolene-modified membranes was "solubility controlled" because it decreased sharply with increasing temperature. The nitrogen permeability was an increasing function of temperature. Consequently, higher temperatures led to lower SO_2 fluxes and selectivity.

Similar results were obtained for the temperature dependence of the air and SO_2 permeabilities of the Buna N and polyacrylate elastomers (Table 1.4). The air permeability of both elastomers increased by a factor of 10 as the temperature was increased from 25 to 75 °C; whereas, the SO_2 permeability exhibited only a slight temperature dependence over the same range. The reason for the

Table 1.4

Temperature Dependence of the Air and SO_2 Permeabilities of Buna N on Nylon and Polyacrylate on Dacron

Elastomer	T (°C)	Q(air)	$Q(SO_2)$	$Q(SO_2)/Q(air)$	$D(SO_2)$	$S(SO_2)$
Buna N	25	1.51	968	640	2.48	0.391
Buna N	50	5.07	1080	213	6.45	0.167
Buna N	75	13.8	1160	84	12.9	0.090
Polyacrylate	25	1.42	2530	1780	2.39	0.987
Polyacrylate	50	5.01	1610	320	5.27	0.304
Polyacrylate	75	14.7	1670	114	19.9	0.084

Units: Q, $\frac{cm^3(STP)\cdot cm}{cm^2\cdot sec\cdot cm\ Hg} \times 10^{10}$; D, $\frac{cm^2}{sec} \times 10^7$; S, $\frac{cm^3(STP)}{cm^3\cdot cm\ Hg}$

nearly constant SO_2 permeability is apparent from the values for the diffusion coefficient and solubility given in Table 1.4. The SO_2 solubility decreased rapidly with increasing temperature but this effect was compensated by the increase in the diffusion coefficient.

Higher operating pressures can lead to higher fluxes two ways. For a gas whose permeability is independent of pressure, the gas flux will be proportional to the pressure difference across the membrane. For a gas or condensable vapor which interacts strongly with the membrane, the permeability is pressure dependent and the gas flux will increase much more rapidly. Therefore, it is possible to achieve higher fluxes and selectivity at elevated pressures for this kind of penetrant. A disadvantage of operating at high pressures is the cost of compressing the gases.

Adding plasticizer to a polymer can alter its properties greatly and improve its permeability. This was demonstrated by Zavaleta and McCandless (1976) with the sulfolene-polyvinylidene fluoride system. Sulfolene, a good SO_2 solvent, enabled the polyvinylidene fluoride membrane to absorb more SO_2. Acting as a plasticizer, the sulfolene also increased segmental chain mobility and thereby increased the diffusion coefficient. These effects combine to give a higher SO_2 permeability and make the membrane more attractive for SO_2 separations.

1.3.6 Summary

The purpose of Chapter 1 was to provide background material for the work which will be presented in Chapters 2 and 3 on the development of practical membranes. The motivation for studying SO_2 transport through polymers comes from a desire to devise better systems for monitoring and controlling SO_2 emissions from stationary sources. A large section on the fundamentals of membrane permeation was included in Chapter 1 to provide a basic understanding of the factors affecting permeability and to show the limited applicability of current theories. From the literature survey of SO_2 permeation and testing of selected materials, several polymers were identified as having desirable properties for SO_2 gas separations. However, the SO_2 transport rates through typical commercial thicknesses of these polymers were inadequate for practical applications. Several ways of achieving higher transport rates were presented at the end of Chapter 1 and will be explored in more detail in the following chapters.

Chapter 2

POLYACRYLATE AND CELLULOSE TRIACETATE SINGLE-LAYER MEMBRANES

2.1 Introduction

A summary of the most attractive membranes for SO_2 separations was given in Table 1.3. For SO_2 applications a membrane must satisfy SO_2 flux and selectivity design goals in addition to having physical durability. The polymeric membranes with the highest selectivity for SO_2 were polyacrylate and cellulose triacetate. Zavaleta and McCandless (1976) were able to achieve higher selectivity by modifying a polyvinylidene fluoride film with sulfolene (dihydrothiophene-1,1-dioxide), but their method of measurement was different. All of the membranes that were very selective to SO_2 suffered one major limitation - the SO_2 fluxes through the test samples were too low for most practical applications. In this chapter several ways will be investigated for obtaining higher SO_2 fluxes with the polyacrylate and cellulose triacetate polymers.

Higher transport rates through a membrane may be achieved by increasing the pressure difference across the membrane, by changing the temperature, by reducing the thickness,or by including additives which alter its properties. Operating a membrane separation process at high pressure requires heavy duty equipment and is not practical if large volumes of gas must be compressed. It is preferred to keep the pressure near 1 atm. Raising the temperature will increase the

permeation rate for permanent gases but may have the opposite effect for condensable gases such as SO_2. If SO_2 is present in a mixture with permanent gases, higher temperatures will produce higher overall fluxes but there will be a significant decline in selectivity for SO_2. Lower temperatures are preferred for maximum SO_2 selectivity. Reducing the film thickness will yield higher fluxes without changing the selectivity. This is an attractive alternative if technologies are available for making thin films and adequately supporting them. Additives may be included in a membrane to increase its solubility for a particular gas or vapor or to loosen the polymer chains and increase the rate of diffusion.

The first two alternatives for increasing the flux deal with the external factors of temperature and pressure. The properties of the membrane are not considered adjustable parameters. To achieve the best performance with a membrane system, however, it is desirable to first optimize the membrane by changing its thickness and other physical properties which affect the permeation rate. In this chapter techniques are described for preparing thin films of the polyacrylate and cellulose triacetate polymers in which SO_2 solvents may be included as additives. The performance of the resulting membranes was evaluated by measuring their permeability to N_2, CO_2, and SO_2 at room temperature and atmospheric pressure.

2.2 Membrane Preparation

2.2.1 Previous Studies

Many techniques are available for making thin films and development in this area is occurring at a rapid pace. One method which works well for many polymers is to prepare a dilute solution of the polymer and pour it on an immiscible liquid. The polymer solution must possess surface activity so that it will spread spontaneously over the lower liquid. The solvent evaporates and leaves a thin film floating on the liquid surface. Wellons and Stannett (1966) made ethyl cellulose films by casting an acetone solution on mercury and drying under vacuum. Ward et al. (1976) formed silicone/polycarbonate membranes as thin as 0.015 μm by dissolving the copolymer in 1,2,3-trichloropropane and spreading the solution on a water surface.

Another method for making thin films involves vapor or plasma deposition of a monomer onto the surface of a substrate. The monomer polymerizes in place on the surface. Union Carbide (1974) produces films of parylene ranging from 250 Å to several mils in thickness by vaporizing and pyrolizing the dimer (di-para-xylylene for parylene N) and then depositing the monomer on objects in a vacuum chamber at room temperature. Parylene N has excellent barrier properties which have led to its use as a protective coating for electronics equipment.

The most active area of membrane research has been in the development of membranes for water purification. Many of the

advances in thin-film technology have also occurred in this area. Loeb and Sourirajan (1964) prepared the first asymmetric cellulosic membranes by a complicated process using mixed solvents with evaporation, heat treatment, and quenching steps. The entire procedure is highly empirical and not easily adapted to other polymers. The asymmetric membrane structure consists of a dense surface layer about 0.2 μm thick supported by a finely porous substrate. Most of the resistance to mass transfer occurs across the thin surface layer so that large water fluxes are obtained.

After the structure and properties of the asymmetric membranes were well understood, Riley et al. (1967) proposed an alternative method for making reverse osmosis membranes based on the procedure described by Carnell and Cassidy (1961) and subsequently modified by Carnell (1965). Briefly, the procedure involves dipping a clean glass plate into a dilute polymer solution and withdrawing the plate at constant velocity. After the solvent evaporates, the thin film is floated off the glass onto a water surface and placed on a microporous support. This procedure works well for a limited number of polymers which do not stick to the glass and is convenient for making small membranes for research purposes; however, it is not adaptable for large-scale membrane production.

Riley et al. (1973) improved their thin-film capabilities by developing a continuous process for making cellulose acetate composite membranes. The support for the thin film consists of a finely porous cellulose nitrate-cellulose acetate membrane which has been

coated with polyacrylic acid so that the polymer solution cannot intrude into the pores. A thin film is formed on the surface of the masked support by continuously passing the support across a wick saturated with a dilute solution of cellulose acetate in chloroform. To maximize membrane area per unit volume, the membrane may be coiled into a spiral-wound element (Riley et al., 1974). When the membrane module is placed in operation, water dissolves the polyacrylic acid masking layer and washes it through the support so that it does not lower the water flux.

Another way of forming thin films is by in situ interfacial polymerization (Cadotte and Rozelle, 1972). Riley et al. (1976) applied this technique to make poly(ether/amide) composite membranes. The procedure involves depositing a thin layer of an aqueous solution of an epichlorohydrin-ethylene diamine condensate on the finely porous surface of a polysulfone support membrane and then contacting the poly(ether/amine) layer with a water immiscible solution of isophthalyldichloride. A thin semipermeable film, a crosslinked poly(ether/amide) copolymer, is formed at the interface. Subsequently, the membrane is dried at an elevated temperature. Riley et al. also designed a continuous process for making fabric-reinforced poly(ether/amide) membrane in a 38-in. width which may be packaged in spiral-wound modules.

2.2.2 Methods of This Study

In this study polyacrylate films were made by dissolving the polymer in toluene and casting the solution on mercury. Samples of

uncured polyacrylate were obtained from B. F. Goodrich Chemical Company. The two types most suitable for solution applications were Hycar 4021-45 and Hycar 4041CG. The Hycar acrylic polymers are made from two types of monomeric acid esters:

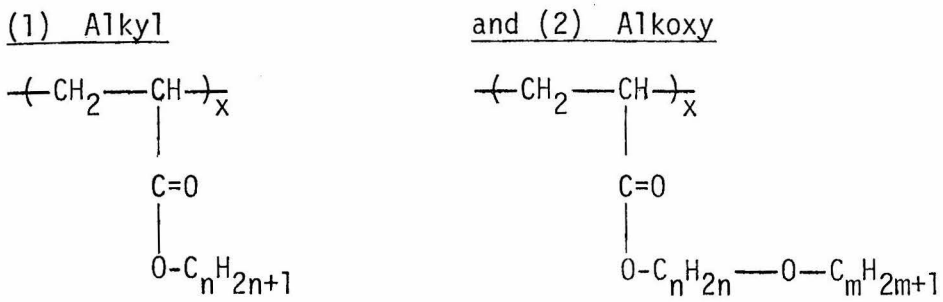

n and m are small integers.

The procedure for making the polyacrylate membranes is described briefly below and in more detail in Appendix B. First, the desired film thickness is selected and an appropriate amount of the crude polymer is dissolved in toluene in a beaker. After the solution process is complete and all residue in the polymer has settled to the bottom of the beaker, the polymer solution is transferred with a pipet to a small petri dish containing a clean pool of mercury. The petri dish is covered with a bell jar to slow down the evaporation and to prevent dust particles from settling on the solution. After all the solvent has evaporated, a small disk of Celgard 2500, a porous polypropylene film manufactured by Celanese, is laid on top of the thin polymer film. Next, a disk of paper having a slightly smaller diameter than the petri dish is laid on top of the Celgard film. The polymer film is cut away from the edge of the petri dish with a razor blade and is removed from the mercury by lifting the

paper disk to which it adheres with a pair of forceps. The paper backing is cut to the size of the Celgard disk and then separated from it. The end result is a composite membrane consisting of a thin polyacrylate film supported on Celgard. The thickness of the polyacrylate layer is estimated by weighing the Celgard disk before and after picking up the thin film and by assuming that the density of the thin film is the same as that of the bulk polymer.

Pinhole-free films from 25 to less than 1 μm in thickness were successfully made following this procedure. For the thinner films extreme care was taken to prevent defects from particles in the air or impurities in the polymer solution. Many of the membranes were prepared in a glove box.

The above procedure is somewhat tedious, and there are a number of drawbacks. For example, it is difficult to keep the mercury clean and to avoid scattering tiny droplets of mercury outside the petri dish when removing the polymer film. Films cannot be made quickly because it may take many hours for the solvent to evaporate. Film thickness is not uniform because the surface of the mercury is not perfectly flat, particularly near the glass-mercury interface.

The procedure for making cellulose triacetate films is similar to that discussed by Carnell and Cassidy (1961). Cellulose triacetate (type 436-80S, Eastman Chemical Products, Inc.) is dissolved in chloroform and filtered through a fritted glass filter. A thin film is formed on the surface of a clean glass plate by lowering it into the cellulose triacetate solution and withdrawing it at constant

velocity. The thin film is removed from the glass plate by slowly dipping the plate in a water bath at a slight angle to the horizontal. A microporous support taped to a flat, rigid surface is raised from the bottom of the water bath until the thin film adheres to its surface. The membrane is then removed from the water bath and allowed to dry. Quite often, it is possible to remove the film on the other side of the glass plate and estimate the thickness from its mass, dimensions, and the bulk density of cellulose triacetate. Details on this procedure are also given in Appendix B.

The apparatus was enclosed in a glove box with unsealed port holes which permitted easy access to materials inside. A stream of filtered air was continuously fed to the box to minimize the influx of room air and to sweep out solvent vapors. Polymer solutions, glass plates, a water bath, and accessories were kept inside the box. A variable speed motor was mounted on top to raise and lower the glass plates via a fine wire connected to a Y-shaped holder inside.

The glass plates were manufactured by the tin-float process and were relatively free of surface features which might produce defects in the films. The thin films of cellulose triacetate were supported on MF-Millipore filters with a 0.050 μm pore size and Celgard 3501, a porous hydrophilic polypropylene film. These microporous media are representative of materials that are suitable for this application but are not necessarily the preferred choice since they were not optimized with respect to pore size and distribution.

Cellulose triacetate films approximately 0.05 and 0.12 μm in thickness were prepared using 0.25 and 0.50 weight percent solutions of cellulose triacetate in chloroform and a withdrawal rate of 4 cm/sec. The thickness of the thin films may be predicted from an equation derived by Levich (1962). He found that the limiting thickness of the liquid layer entrained by a plate withdrawn vertically from a quiescent liquid is given by

$$\ell_{liq} = \frac{0.93(\mu v)^{2/3}}{\sigma^{1/6}(\rho g)^{1/2}} \tag{2.1}$$

where μ, σ, and ρ are the viscosity, surface tension, and density, respectively, of the liquid; v is the withdrawal rate; and g is the gravitational constant. To apply (2.1) to a dilute polymer solution, it is multiplied by the solution concentration, c (gm/gm), and the ratio of the densities of the liquid and polymer, ρ/ρ_p. The thickness of the polymer film remaining after the liquid evaporates is then given by

$$\ell_p = \frac{0.93(\mu v)^{2/3}}{\sigma^{1/6}(\rho g)^{1/2}} \frac{\rho}{\rho_p} \cdot c \tag{2.2}$$

For dilute solutions the density and surface tension of the pure liquid may be used in (2.2) without introducing much error. For chloroform σ = 26 dynes/cm and ρ = 1.47 gm/cm^3. The density of cellulose triacetate is 1.31 gm/cm^3. With these substitutions (2.2) becomes

$$\ell_p = 0.016(\mu v)^{2/3} c \qquad (2.3)$$

The viscosity of the dilute solutions was estimated from data published by Riley et al. (1973) for cellulose acetates of varying acetyl content and intrinsic viscosities. Cellulose triacetate type 436-80S is 43.6% acetyl.

The film thicknesses predicted from (2.3) were within 10-20% of the values obtained by weighing known areas. This discrepancy may be attributed to the uncertainty in the viscosity, particularly for the 0.50 weight percent solution. Films prepared by this technique have a wavy appearance, indicating some nonuniformity in thickness. The films are much thicker at the bottom edge of the plate where excess solution accumulates. To obtain more accurate values for the thickness, all four edges of the films were scored with a razor blade before removing them from the glass plates. In this way edge effects were eliminated, and only the center portion of the films was weighed to determine the thickness.

Some of the polyacrylate and cellulose triacetate films were prepared from solutions to which polyethylene glycol or sulfolane (tetrahydrothiophene-1,1-dioxide) was added. These substances have high SO_2 solubilities and, therefore, could improve membrane performance. Ward and Neulander (1970) made immobilized polyethylene glycol membranes for SO_2 separations and Seibel and McCandless (1974) found that sulfolane plasticized vinylidene fluoride films were effective in separating SO_2 from a binary mixture with N_2. The

optimum vinylidene fluoride membrane contained about 8.2 weight percent sulfolane.

2.3 Experimental Apparatus and Procedure

2.3.1 Standard Test Methods

Methods for measuring the gas permeability of polymer films have been reviewed by Crank and Park (1968b) and Hwang and Kammermeyer (1975). The two methods most often used have been described in detail in ASTM D 1434-75. These are referred to as Method M-Manometric and Method V-Volumetric. A sample film is mounted in a gas transmission cell forming a sealed barrier between two chambers. One chamber contains the test gas at a specific high pressure and the other chamber, at a lower pressure, receives the permeant gas. In Method M the low pressure chamber is initially evacuated and the transmission of gas through the test specimen is indicated by a change in pressure. In Method V the low pressure chamber is maintained near atmospheric pressure and the transmission of gas through the test specimen is indicated by a change in volume. The gas permeability is calculated from the change in pressure or volume and the physical dimensions of the apparatus.

A dynamic method described by Pasternak et al. (1970) allows permeation and diffusion rates to be measured without applying a pressure difference across the membrane. Both chambers of the permeation cell are open to the atmosphere. Initially, carrier gas flows through both chambers and a thermal conductivity detector

which is downstream of one of the chambers is zeroed. The carrier gas in the other chamber is then replaced by a test gas. The permeation rate of the test gas is proportional to the detector signal.

2.3.2 Method of This Study

The membranes were tested by measuring their permeability to N_2, CO_2, and SO_2 by the Manometric Method. The simple, inexpensive apparatus shown schematically in Figure 2.1 was assembled to take these measurements. The permeation cell holds the membrane and is connected to a differential manometer on the upstream side and an absolute manometer on the downstream side. The vacuum pump, gas source, and vent are the other essential features of the system. Additional downstream volume was provided for testing membranes with very large SO_2 permeation rates.

The permeation cell was made from two stainless steel disks 4 in. in diameter. The membrane was supported by a porous metal disk 1 $\frac{3}{4}$ in. in diameter which was fitted into the lower half of the cell. A piece of filter paper was placed over the porous metal disk followed by the membrane, a stainless steel gasket, and a rubber gasket. This cell configuration was effective in protecting the fragile membranes from excessive stress and sealing the cell vacuum tight. A thin film of high vacuum silicone grease was spread on the sealing surfaces of the cell before mounting the membrane to minimize the leakage of air into the cell when a vacuum was applied. For some membranes it was necessary to seal with nail polish the

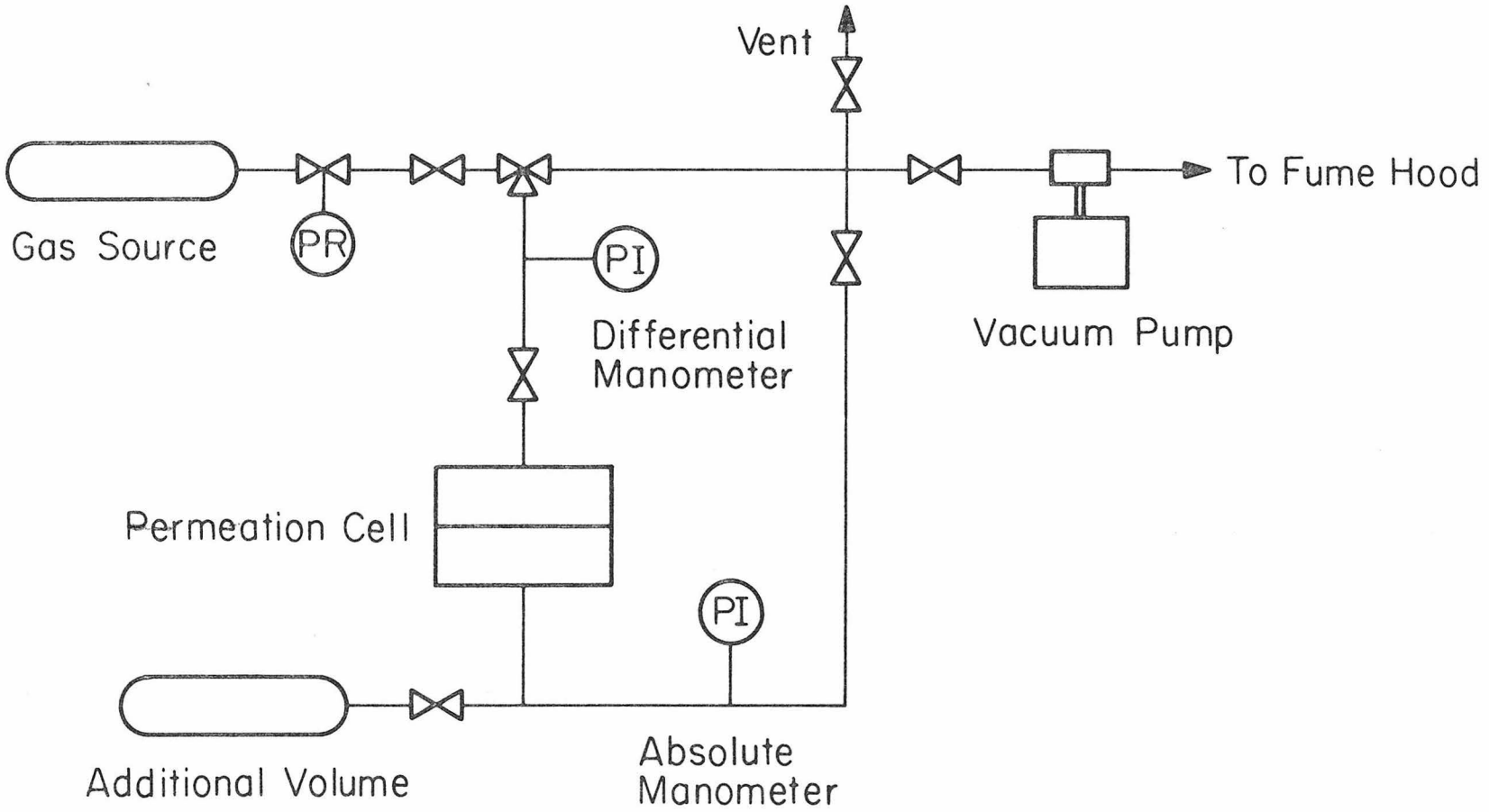

Figure 2.1 Schematic diagram of the manometric system for measuring gas permeability.

inner edge of the steel gasket where it contacted the membrane because of a tendency for the thin film to tear under pressure.

To determine the permeability, a membrane was mounted in the permeation cell and both sides of the cell were evacuated below 1 mm Hg. Sufficient time was allowed for the membrane to degas and to ascertain whether or not there were any leaks in the system. If there was a negligible pressure rise, gas at approximate 1 atm pressure was admitted to the upstream side and the pressure on the downstream side was observed as a function of time. From this pressure versus time data and the system parameters, the permeability was calculated. N_2, CO_2, and SO_2 were usually tested in the order of increasing permeability. Most of the membranes were much too thin to observe a time lag for permeation; however, a special 10-mil polyacrylate film was prepared to obtain time lags for SO_2 permeation. For a few membranes the upstream SO_2 pressure was set at several values less than 1 atm in a series of runs to determine the pressure dependence of the SO_2 permeability.

By making a slight modification of the permeation apparatus, SO_2 solubility data for sulfolane, polyethylene glycol, and polyacrylate were obtained. A small stainless steel pan was placed in the permeation cell to hold the sample and the lower half of the cell was plugged. A known volume of SO_2 gas was admitted to the cell and the absorption process was observed with the upstream manometer. After equilibrium was reached, additional gas was admitted to the cell. This procedure was repeated several times to obtain data from 0 to 1 atm pressure.

2.4 Results and Discussion

2.4.1 Permeability Calculations

To determine the permeability of a membrane to a particular gas, downstream pressure readings were taken at appropriate time intervals. It is customary to plot the pressure data versus time and then measure dP/dt to calculate the permeability. Resorting to such graphical techniques makes the data analysis very tedious. By examining the equations which apply to gas permeation, it is possible to derive expressions from which the permeability may be calculated directly from the experimental data. If ideal, steady-state permeation occurs, then the gas flux is given by (1.4):

$$J = \frac{DS[P(0)-P(\ell)]}{\ell} \tag{2.4}$$

This gas flux results in a pressure rise on the downstream side which obeys the ideal gas law. Differentiation of the pressure with respect to time, assuming the volume is constant, yields

$$\frac{dP(\ell)}{dt} = \frac{RT}{V}\frac{dn}{dt} \tag{2.5}$$

By paying due regard to units, dn/dt may be related to J. The units of J most frequently encountered in the literature are $cm^3(STP)/(cm^2 \cdot sec)$. If dn/dt is in mole/sec, then

$$\frac{dn}{dt} = \frac{76(\text{cm Hg})\ AJ}{273(°K)R} \tag{2.6}$$

where A is the membrane area. Substitution of (2.4) and (2.6) into (2.5) gives

$$\frac{dP(\ell)}{dt} = \frac{ATDS[P(0)-P(\ell)]}{3.592V\ell} \tag{2.7}$$

If the upstream pressure, P(0), is constant, (2.7) may be integrated with respect to $P(\ell)$ and t and subsequent rearrangement yields for the permeability

$$Q_{i,i+1} = DS = \frac{3.592V\ell}{AT(t_{i+1}-t_i)} \ln\left(\frac{P(0)-P(\ell)_i}{P(0)-P(\ell)_{i+1}}\right) \tag{2.8}$$

The subscripts, i and i+1, refer to consecutive datum points on the pressure versus time permeation curve.

In deriving (2.8) it was assumed that the downstream volume, V, is constant. In this study the downstream pressure was measured with a manometer which means that V varies linearly with pressure:

$$V = a+bP(\ell) \tag{2.9}$$

where a and b are constants for a particular system. Substituting this expression for V in the ideal gas law and following the above procedure gives

$$Q_{i,i+1} = \frac{3.592\ell}{AT(t_{i+1}-t_i)}\left[-2b[P(\ell)_{i+1}-P(\ell)_i] + [a+2bP(0)]\cdot \ln\left(\frac{P(0)-P(\ell)_i}{P(0)-P(\ell)_{i+1}}\right)\right] \tag{2.10}$$

All the permeation data were analyzed using (2.10). This expression for Q is strictly valid only when Q is independent of pressure and experiments are run at steady-state. However, even when Q depends on pressure, the error is small if the datum points are sufficiently close together. Other methods for evaluating Q are given in Appendix D.

The permeation of N_2 and CO_2 through the polyacrylate membranes was not dependent on pressure. Consequently, (2.10) could be used to determine the permeability. A typical permeation run contained 5-10 datum points from which a mean value for the permeability was computed. This simple procedure was not adequate to analyze SO_2 permeation data. SO_2 permeability results obtained from (2.10) for four polyacrylate membranes are plotted versus the downstream pressure in Figure 2.2. The SO_2 permeability has approximately an exponential dependence on downstream pressure. For membranes less than 10 μm thick, there is also a strong dependence on thickness, which will be discussed later.

With the pressure dependence of the SO_2 permeability, questions arise concerning the best way to correlate the data and present the results. Two important objectives in correlating the data are (1) to fit the data to a model so that it is not necessary to plot all the results and (2) to be able to predict the SO_2 permeability for any upstream and downstream pressures, particularly as both of these approach zero. The observed exponential dependence on pressure suggests that an exponential model for the diffusion coefficient

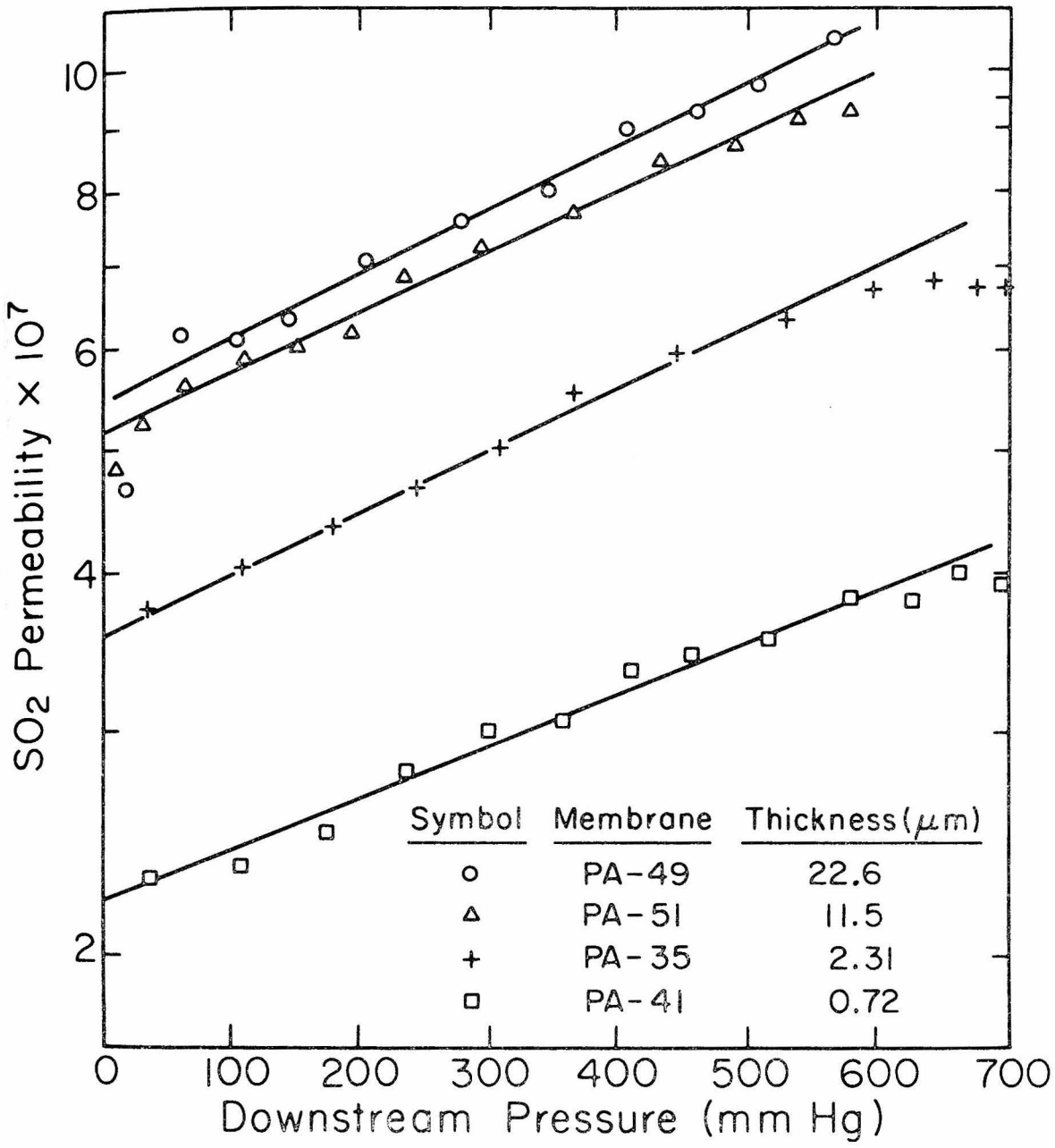

Figure 2.2 Pressure dependence of the SO_2 permeability of polyacrylate membranes for an upstream pressure of 1 atm.

may give satisfactory results. If the concentration dependence of D is assumed to be of the form

$$D = D_o e^{\gamma c} \tag{2.11}$$

then (1.17) gives for the steady-state flux

$$J = \frac{D_o}{\ell\gamma}\left[e^{\gamma SP(0)} - e^{\gamma SP(\ell)}\right] \tag{2.12}$$

Substitution of (2.6) and (2.12) into (2.5) leads to

$$\frac{dP(\ell)}{dt} = \frac{ATD_o}{3.592V\ell\gamma}\left[e^{\gamma SP(0)} - e^{\gamma SP(\ell)}\right] \tag{2.13}$$

Integrating with respect to $P(\ell)$ and t yields

$$Q_{o(i,i+1)} = D_o S = \frac{3.592V\ell\gamma S}{AT(t_{i+1}-t_i)\exp[\gamma SP(0)]}\left[\left[P(\ell)_{i+1} - P(\ell)_i\right] + \frac{1}{\gamma S}\ln\left(\frac{e^{\gamma SP(0)} - e^{\gamma SP(\ell)_i}}{e^{\gamma SP(0)} - e^{\gamma SP(\ell)_{i+1}}}\right)\right] \tag{2.14}$$

Equation (2.14) applies for a constant V. If V varies linearly with $P(\ell)$, then the integral with respect to $P(\ell)$ must be evaluated numerically:

$$I = \int_{P(\ell)_i}^{P(\ell)_{i+1}} \frac{[a+2bP(\ell)]dP(\ell)}{\left[e^{\gamma SP(0)} - e^{\gamma SP(\ell)}\right]} \tag{2.15}$$

$$Q_o(i,i+1) = \frac{3.592\ell\gamma SI}{AT(t_{i+1}-t_i)} \qquad (2.16)$$

Both (2.14) and (2.16) contain Q_o and γS as adjustable parameters. Q_o is the value of the permeability in the limit of zero upstream and downstream pressures. γS is a measure of the pressure dependence of the diffusion coefficient. If a value of γS is assumed, permeation data may be used to calculate a set of values for Q_o. By an optimization procedure successive values of γS are selected until the scatter in the set of values for Q_o is minimized.

An expression for Q is obtained by multiplying (2.12) by ℓ and dividing by $[P(0) - P(\ell)]$:

$$Q = \frac{D_o}{\gamma[P(0)-P(\ell)]}\left[e^{\gamma SP(0)} - e^{\gamma SP(\ell)}\right] \qquad (2.17)$$

Noting that $Q_o = D_o S$, (2.17) becomes

$$Q = \frac{Q_o}{\gamma S[P(0)-P(\ell)]}\left[e^{\gamma SP(0)} - e^{\gamma SP(\ell)}\right] \qquad (2.18)$$

Given Q_o and γS, Q may be estimated from (2.18) for arbitrary values of $P(0)$ and $P(\ell)$, provided they are in the range of validity of the parameters.

2.4.2 Permeability Results for Polyacrylate Membranes

The performance of the polyacrylate membranes was characterized by measuring their permeability to N_2, CO_2, and SO_2 at 1 atm upstream

pressure and room temperature (24-26 °C). Mean values for the N_2 and CO_2 permeabilities were obtained by averaging the results from (2.10). Optimum values of Q_o and γS for the SO_2 permeability were found by an iterative technique using (2.15) and (2.16). Computer programs for performing the data analysis are given in Appendix D.

Table 2.1 shows the effect of thickness on the permeability of selected polyacrylate membranes,which are tabulated in order of decreasing thickness. The column headed "Rel Error" gives the relative error in the value of $Q_o(SO_2)$, which is an indication of how well the two-parameter exponential model correlated the data. The last two columns in Table 2.1 give the ratio of $Q_o(SO_2)$ to $\bar{Q}(N_2)$ and $\bar{Q}(CO_2)$. These ratios tell how selective the membrane is likely to be for SO_2 at low concentrations. For membranes greater than 10 μm in thickness, there is some scatter in the permeability results but no significant trends. Below 10 μm the permeabilities of all three gases decrease with thickness by approximately the same amount so that there is little difference in selectivity. The permeability results for the thinnest membrane are only 50-60% of the values for the thick membranes.

One reason for the decline in permeability with decreasing membrane thickness is illustrated in Figure 2.3 in which the SO_2 fluxes through the microporous supports, Celgard 2400 and 2500, are compared with the SO_2 flux through PA-41. As the gas flux through a composite membrane approaches the limiting flux through the porous support, the mass transfer resistance of the support becomes

Table 2.1

Effect of Thickness on the Permeability of Polyacrylate Membranes

Membrane	$\ell(\mu m)$	$\bar{Q}(N_2)$	$\bar{Q}(CO_2)$	$Q_o(SO_2)$	Rel. Error (%)	γS	$Q_o(SO_2)/\bar{Q}(N_2)$	$Q_o(SO_2)/\bar{Q}(CO_2)$
PA-62	267	3.41	105	1990	2.5	0.00217	584	19.0
PA-30	27.1	3.30	101	1700	2.6	0.00267	515	16.8
PA-21	26.7	2.79	89.7	1450	0.6	0.00297	520	16.2
PA-49	22.6	3.55	95.5	1830	2.5	0.00261	515	19.2
PA-51	11.5	3.05	93.1	1820	2.2	0.00249	597	19.5
PA-38	2.64	3.14	70.0	1200	1.0	0.00258	382	17.1
PA-35	2.31	2.95	69.1	1410	2.4	0.00231	478	20.4
PA-41	0.72	2.07	45.7	941	3.2	0.00209	455	20.6

Units: Q, $\frac{cm^3(STP)\cdot cm}{cm^2\cdot sec\cdot cm\ Hg} \times 10^{10}$; γS, $(mm\ Hg)^{-1}$

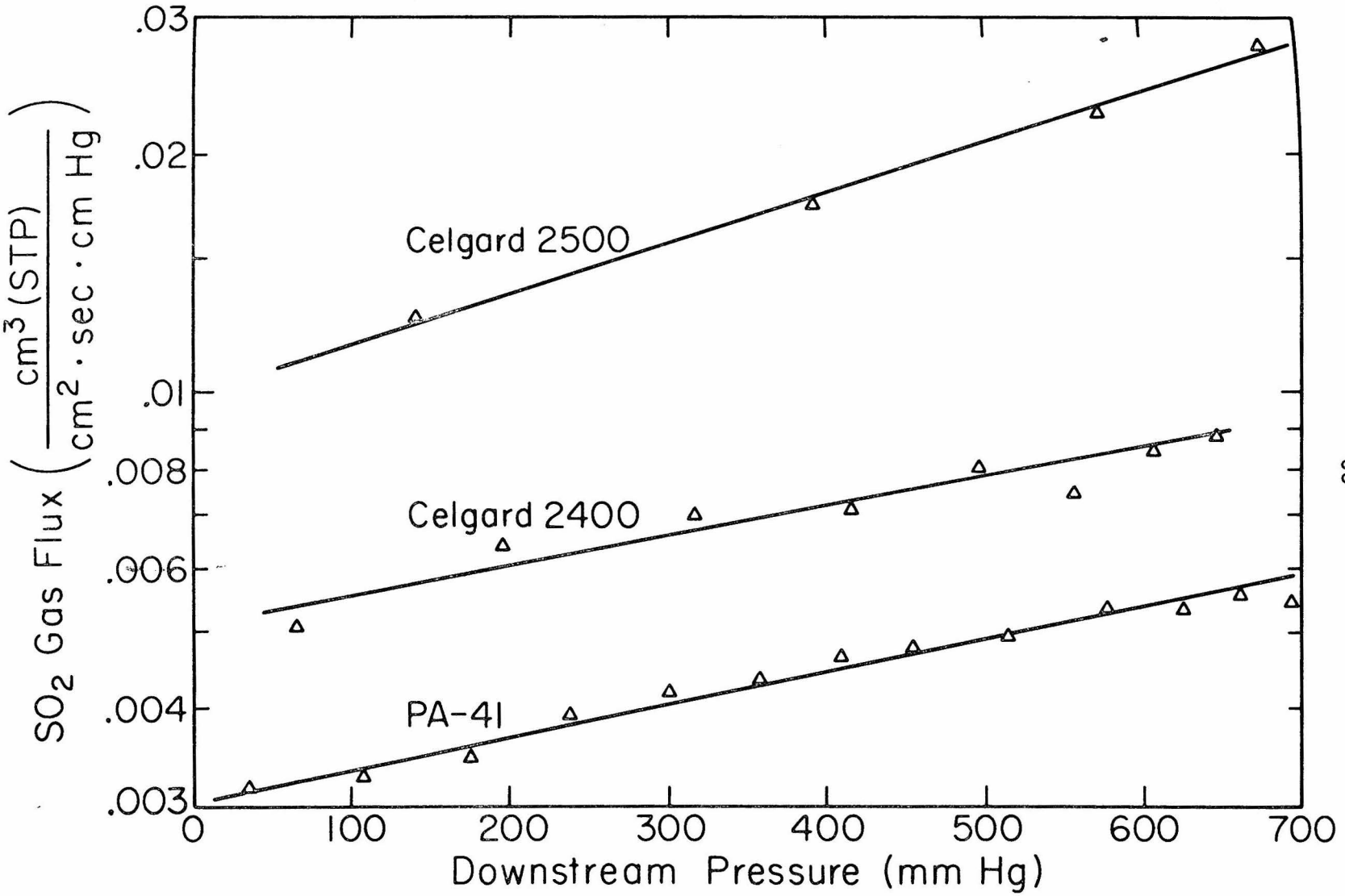

Figure 2.3 SO_2 gas flux through Celgard 2400, Celgard 2500, and PA-41 for an upstream pressure of 1 atm.

significant and causes the observed permeability of the thin film to be less than that for thicker films. The SO_2 flux through PA-41 is approximately 25% of the maximum achievable through Celgard 2500. This accounts for part of the decline in permeability.

Lonsdale et al. (1971) found that the limited open area of the porous support is an important factor which affects the permeability. For thin films that intimately contact the surface of the porous support the actual permeability will approach the "porosity limit," which is the porosity times the ideal permeability. This effect is significant when the distance between the pores in the surface of the support is large compared to the thickness of the thin film. Physical properties of the Celgard films reported by Celanese are given in Table 2.2. Using the method of Lonsdale et al. and the data in Table 2.2, the predicted reduction in permeability is about 5% for PA-41.

Several other factors may also have contributed to the permeability decline. Uncured polyacrylate tends to flow under an applied pressure and may have intruded into the pores of the Celgard and reduced the effective area for permeation. Residual solvent in a polymer film acts as a plasticizer which enhances the permeability. Loss of residual solvent would lower the permeability and is likely to occur more rapidly for the thinner films. The transport process consists of sorption of the gas at the high-pressure interface, diffusion through the film, and desorption at the low-pressure interface. For a thin film diffusion is fast enough so that the

Physical Properties of Celgard Films

Property	Celgard 2400	Celgard 2500	Units
Thickness	1.0	1.0	mil
Density	0.56	0.49	gm/cc
Porosity	38	45	%
Pore Density	10×10^9	7×10^9	pores/cm^2
Pore Dimensions (max)	.02 × .20	.04 × .40	μm

Reference: Celanese data sheets

transport rate may be limited by the sorption and desorption steps. The importance of these factors cannot be determined from the available data.

Table 2.3 shows the effect of including polyethylene glycol and sulfolane in polyacrylate membranes. The weight percentage additive was based on the relative amounts of additive and polymer in the solutions before casting the membranes. The actual amounts of additive in the membranes may have been somewhat less, particularly at the higher concentrations where the capacity of the polymer may have been exceeded. The effect of polyethylene glycol was to increase the SO_2 permeability by more than a factor of 2 for PA-57 which contained 50% polyethylene glycol. The N_2 and CO_2 permeabilities increased by smaller amounts so that selectivity was enhanced. Below 25% the polyethylene glycol had almost negligible effect on the SO_2 permeability. A similar increase in the SO_2 permeability was obtained with sulfolane; however, sulfolane also increased the permeability of N_2 and CO_2 such that there was no increase in selectivity for SO_2. The presence of both additives decreased the pressure dependence of the SO_2 permeability. At least one of the membranes, PA-59, had defects which made the N_2 permeability higher than expected.

PA-56, containing 25% polyethylene glycol, had the best overall performance. To achieve higher flux rates, thinner films containing 25% polyethylene glycol were prepared but were unable to withstand

Table 2.3

Effect of Additives on the Permeability of Polyacrylate Membranes

Membrane	Additive	ℓ (μm)	$\bar{Q}(N_2)$	$\bar{Q}(CO_2)$	$Q_o(SO_2)$	Rel. Error (%)	γS	$\frac{Q_o(SO_2)}{\bar{Q}(N_2)}$	$\frac{Q_o(SO_2)}{\bar{Q}(CO_2)}$
PA-51	none	11.5	3.05	93.1	1820	2.2	0.00249	597	19.5
PA-53	1% PEG	9.54	3.32	99.3	1680	2.5	0.00268	506	16.9
PA-54	5% PEG	8.60	3.52	114	1930	2.9	0.00260	548	16.9
PA-55	10% PEG	9.89	3.07	102	1980	3.3	0.00281	645	19.4
PA-56	25% PEG	11.8	3.22	113	3210	2.1	0.00238	997	28.4
PA-57	50% PEG	12.3	4.68	128	5160	2.6	0.00159	1100	40.3
PA-58	5% Sulfolane	11.9	3.08	85.5	1860	1.6	0.00227	604	21.8
PA-59	10% Sulfolane	11.0	7.82	84.1	1520	2.1	0.00251	194	18.1
PA-60	25% Sulfolane	12.5	3.65	107	2150	1.6	0.00219	589	20.1
PA-61	50% Sulfolane	14.8	7.46	192	4470	1.5	0.00172	599	23.3

Units: Q, $\frac{cm^3(STP)\cdot cm}{cm^2\cdot sec\cdot cm\ Hg} \times 10^{10}$; γS, $(mm\ Hg)^{-1}$

1 atm pressure difference across them. The polyethylene glycol weakened the physical structure of the polymer.

The time dependence of the permeability is conveniently divided into short term and long term effects. In the short duration of an SO_2 permeation experiment, the SO_2 permeability is expected to increase with time due to its pressure dependence. In some experiments, however, the SO_2 permeability began to decrease sharply as the downstream pressure approached the upstream pressure. This may be caused by a molecular relaxation process occurring in the polymer which makes it less permeable. Another possible explanation is that as the pressure difference across the membrane decreases, there is an increasing tendency for SO_2 molecules to become immobilized in clusters within the polymer. Cluster formation and the attendant decline in the diffusion coefficient were observed by Wellons and Stannett (1966) for the water-ethyl cellulose system.

Table 2.4 shows the effect of time on the permeability of three membranes which were retested after extended time periods. Between tests the membranes were stored in a laboratory drawer exposed to room air. For PA-51, a relatively thick membrane, there was little change in its permeability over a 10-month period. For the thinner membranes, PA-41 and PA-43, the N_2 permeability initially decreased with time and then increased sharply, indicating physical deterioration. The SO_2 permeability decreased over the entire period of observation for both membranes.

Table 2.4

Time Dependence of the Permeability of Polyacrylate Membranes

Membrane	ℓ (μm)	Elapsed Time	$\bar{Q}(N_2)$	$\bar{Q}(CO_2)$	$Q_o(SO_2)$	Rel. Error (%)	γS	$\frac{Q_o(SO_2)}{\bar{Q}(N_2)}$	$\frac{Q_o(SO_2)}{\bar{Q}(CO_2)}$
PA-51	11.5	1-3 days	3.05	93.1	1820	2.2	0.00249	597	19.5
		3 mos.	3.01	88.8	1710	1.8	0.00257	568	19.3
		10 mos.	3.38	95.2	1940	1.5	0.00215	574	20.4
PA-41	0.72	1 day	2.07	45.7	941	3.2	0.00216	455	20.6
		4-6 days	1.70	35.8	680	3.0	0.00222	400	19.0
		18-20 days	1.43	32.0	586	2.3	0.00204	410	18.3
		19 weeks	5.55	-	526	2.5	0.00222	95	-
PA-43	0.73	5 weeks	1.62	27.1	439	2.3	0.00241	271	16.2
		19 weeks	1.30	23.8	403	2.4	0.00251	310	16.9
		50 weeks	11.6	33.8	378	1.9	0.00227	32.6	11.2

Units: Q, $\frac{cm^3(STP)\cdot cm}{cm^2\cdot sec\cdot cm\ Hg} \times 10^{10}$; γS, $(mm\ Hg)^{-1}$

Some questions may be raised as to the validity of using the two-parameter exponential model to correlate SO_2 permeation data and to predict the permeability of SO_2 at low pressures. To check the applicability of the model, additional SO_2 permeation experiments were run on PA-51 and PA-62 at upstream pressures less than 1 atm. The results are plotted in Figures 2.4 and 2.5. All the data for the different upstream pressures were used in (2.15) and (2.16) to find the optimum values of Q_0 and γS. The solid curves drawn on these figures represent the permeability calculated from these optimum values. The two-parameter exponential model is able to correlate the data rather well, except for the data at 400 mm Hg upstream pressure for PA-51 and the data at 500 mm Hg upstream pressure for PA-62. In both cases the curves fall somewhat below the experimental data.

It is interesting to compare the optimum values of Q_0 and γS obtained using just the data for 1 atm upstream pressure (Table 2.1) and using four sets of data for different upstream pressures (Figures 2.4 and 2.5). The values of Q_0 in Table 2.1 are a factor of 2 larger than those in Figures 2.4 and 2.5, and the values of γS in Table 2.1 are smaller than those in the figures. This means that the parameters cannot be precisely determined from just the data for 1 atm upstream pressure. The values of $Q_0(SO_2)$ and γS presented in Tables 2.1, 2.3, and 2.4 must be regarded as rough estimates only.

One of the limitations of the two-parameter exponential model is that it does not allow for a change in γS with pressure. The

Figure 2.4 Pressure dependence of the SO_2 permeability of PA-51. The permeation data were correlated with the two- and three-parameter exponential models. The solid curves represent the two-parameter model (Eq. (2.18) with $Q_o = 1.03 \times 10^{-7}$, $\gamma S = 3.25 \times 10^{-3}$, and relative error = 8.2%). The dashed curves represent the three-parameter model (Eq. (2.24) with $Q_o = 8.46 \times 10^{-8}$, $\alpha = 5.43 \times 10^{-3}$, $\beta = 8.63 \times 10^{-4}$, and relative error = 3.4%).

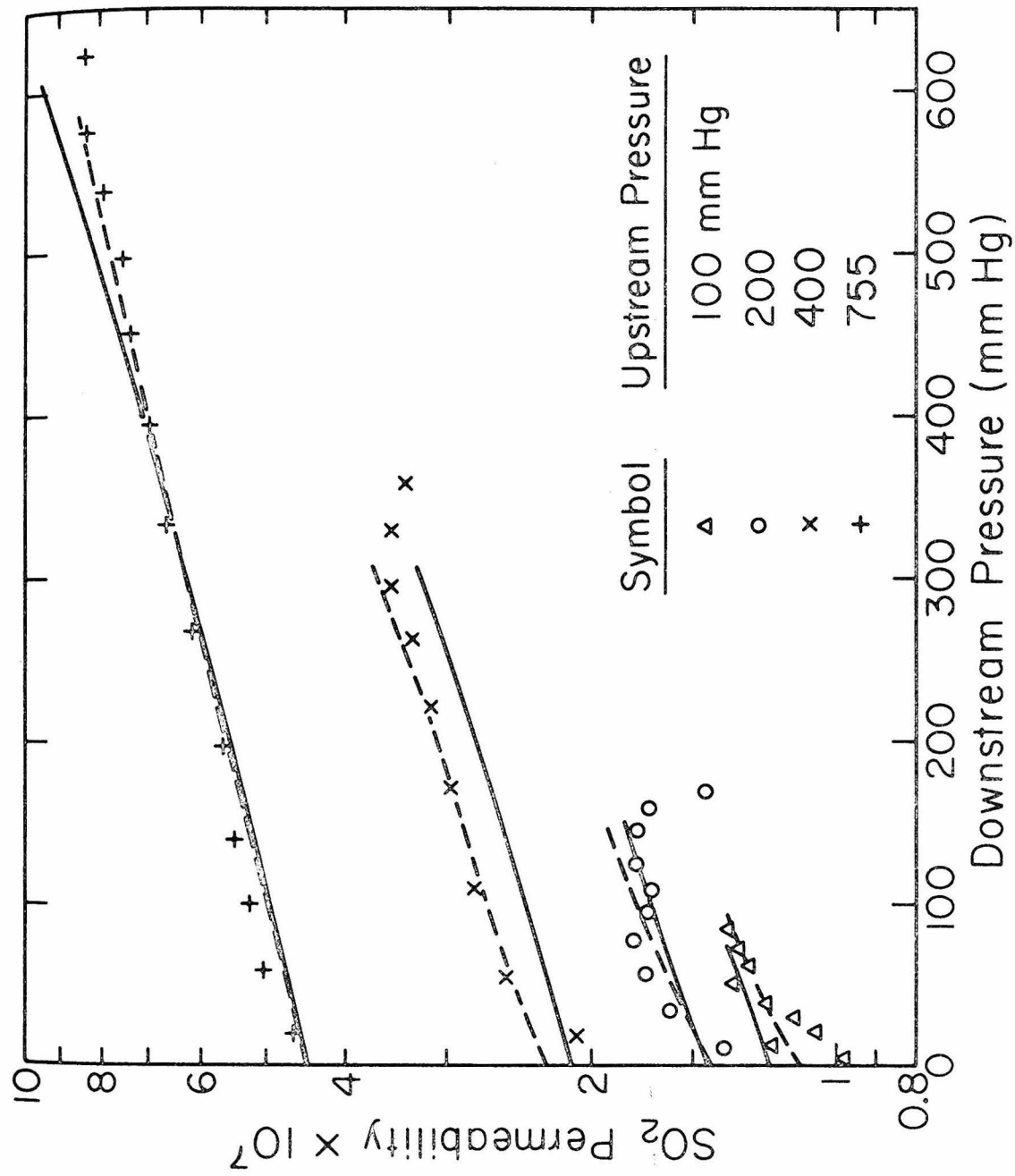
SO_2 Permeability x 10^7
Downstream Pressure (mm Hg)
Symbol
Upstream Pressure
100 mm Hg
200
400
755

Figure 2.4

Figure 2.5 Pressure dependence of the SO_2 permeability of PA-62. The permeation data were correlated with the two- and three-parameter exponential models. The solid curves represent the two-parameter model (Eq. (2.18) with $Q_o = 9.16 \times 10^{-8}$, $\gamma S = 3.68 \times 10^{-3}$, and relative error = 9.0%). The dashed curves represent the three-parameter model (Eq. (2.24) with $Q_o = 7.09 \times 10^{-8}$, $\alpha = 6.32 \times 10^{-3}$, $\beta = 9.93 \times 10^{-4}$, and relative error = 4.6%).

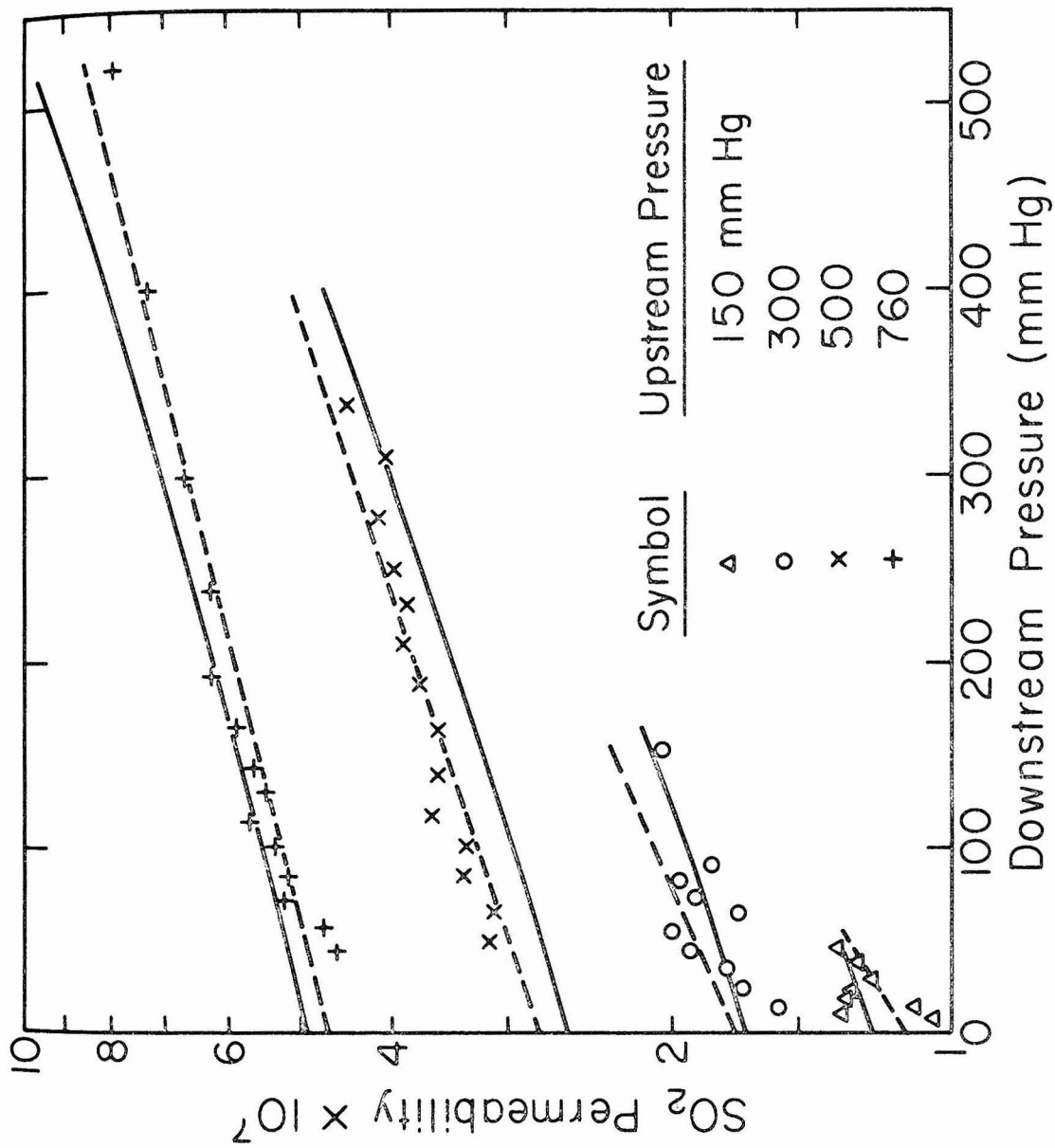
SO_2 Permeability x 10^7
10
8
6
4
2
0
100
200
300
400
500
Downstream Pressure (mm Hg)
Symbol
Upstream Pressure
150 mm Hg
300
500
760

Figure 2.5

optimum value of γS was lower for the data at 1 atm upstream pressure than it was when all four sets of data were combined. This suggests that γS may be a decreasing function of pressure. From a physical point of view, it is plausible that a small amount of absorbed vapor has a large plasticizing effect on a membrane, but as more vapor is absorbed, the incremental effect grows smaller. To account for this behavior, the exponential model was modified by adding a third parameter:

$$D = D_o \exp\left(\frac{\gamma c}{1+\lambda c}\right) \tag{2.19}$$

Assuming Fick's law holds, the gas flux is given by

$$J = -D_o \exp\left(\frac{\gamma c}{1+\lambda c}\right) \frac{dc}{dx} \tag{2.20}$$

In the steady state J is constant and (2.20) may be integrated to give

$$J\ell = -D_o \int_{c(0)}^{c(\ell)} \exp\left(\frac{\gamma c}{1+\lambda c}\right) dc \tag{2.21}$$

If Henry's law holds, $c = SP$ and

$$J\ell = D_o S \int_{P(\ell)}^{P(0)} \exp\left(\frac{\gamma SP}{1+\lambda SP}\right) dP \tag{2.22}$$

Dividing by $\Delta P = P(0)-P(\ell)$ yields an expression for Q:

$$Q = \frac{D_o S}{P(0)-P(\ell)} \int_{P(\ell)}^{P(0)} \exp\left(\frac{\gamma SP}{1+\lambda SP}\right) dP \qquad (2.23)$$

To simplify this expression, let $Q_o = D_o S$, $\alpha = \gamma S$, and $\beta = \lambda S$. Then,

$$Q = \frac{Q_o}{P(0)-P(\ell)} \int_{P(\ell)}^{P(0)} \exp\left(\frac{\alpha P}{1+\beta P}\right) dP \qquad (2.24)$$

Equation (2.24) will be referred to as the three-parameter exponential model for the permeability. Although this model was proposed on the basis of empirical considerations, it has the same functional form as the free volume theory, which was discussed in Section 1.2.2.4. The final expression for the diffusion coefficient in the free volume theory is given by Equation (1.23), which can be rearranged into the form

$$D_T = D_o \exp\left[\frac{[B_d \beta(T)/[f(T,0)]^2]v_d}{1+\frac{\beta(T)}{f(T,0)}v_d}\right] \qquad (2.25)$$

Equation (2.25) is analogous to (2.19).

The three-parameter exponential model for Q has a rather simple form but must be integrated numerically. This makes it less convenient to use than the two-parameter model and adds to the difficulty in

evaluating the optimum values of the parameters. A computer program for performing the data analysis is given in Appendix D. The results for PA-51 and PA-62 are represented by the dashed curves in Figures 2.4 and 2.5. A comparison of the solid and dashed curves with the experimental data verifies that the three-parameter model correlates the data better than the two-parameter model.

2.4.3 Diffusivity and Solubility Results for Polyacrylate

In permeation studies a better understanding of the transport process is gained by measuring the diffusion coefficient and solubility separately since their product is equal to the permeability. Diffusion coefficients may be determined by the time-lag method if a membrane is thick enough so that the time lag for diffusion is on the order of minutes rather than seconds. PA-62 was specially cast for this purpose. Permeation data were obtained for upstream pressures of 150, 300, 500, and 760 mm Hg and plotted in Figure 2.6. Time lags were determined by extrapolating the linear portion of the permeation curves to zero pressure. This was done graphically and with a least-squares fit to the data.

Some difficulty was encountered in interpreting the time-lag data because the diffusion equation has been solved explicitly only for the case of a constant diffusion coefficient (Daynes, 1920). The solution for this case is

$$\theta = \ell^2/6D \qquad (2.26)$$

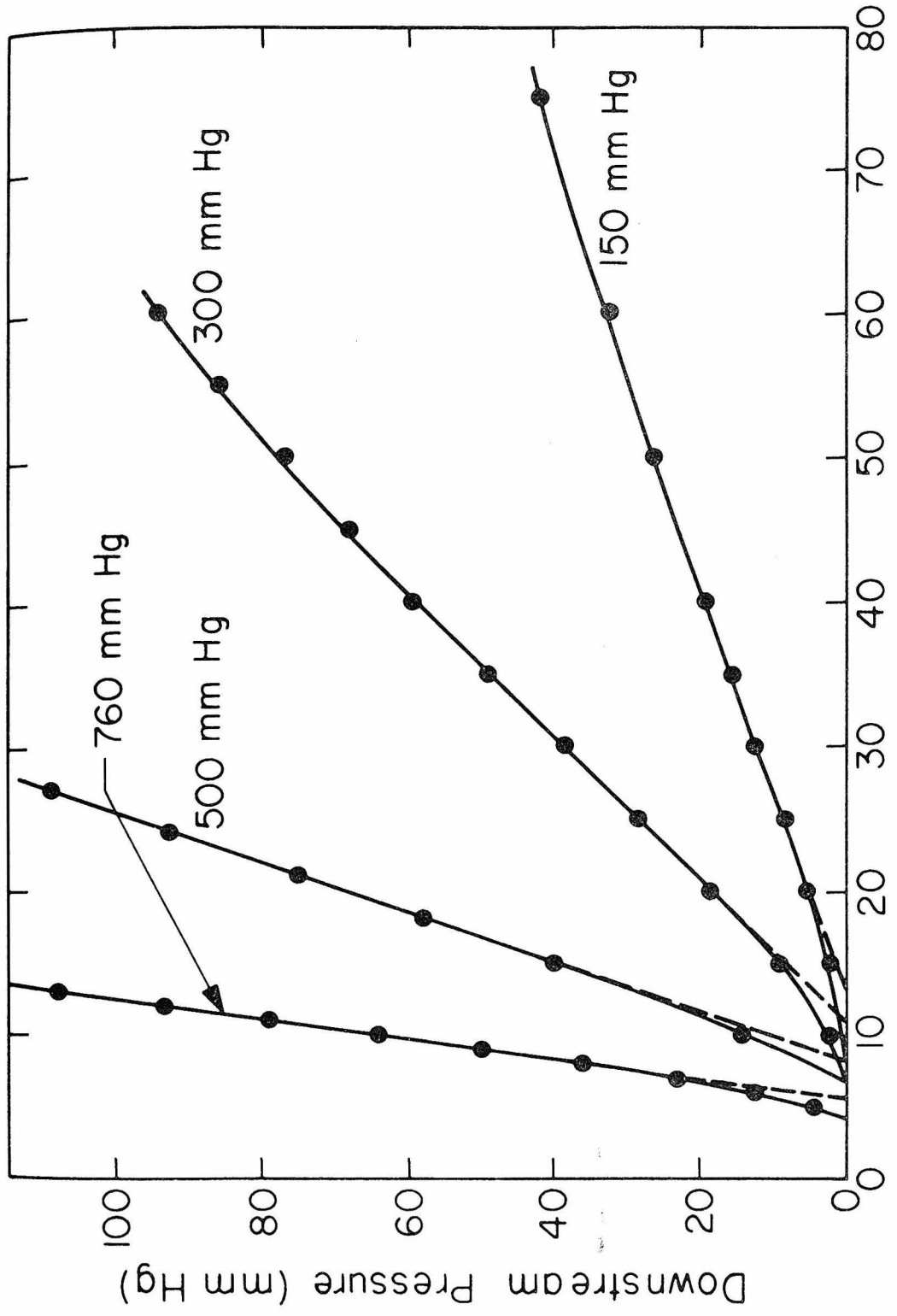

Figure 2.6 SO_2 permeation through PA-62 for upstream pressures of 150, 300, 500, and 760 mm Hg.

Frisch (1957) described a method for obtaining expressions for the time lag without explicitly solving the diffusion equation and applied it to cases in which the diffusion coefficient is constant and varies linearly with concentration. Frisch's method was applied to the case of an exponential concentration dependence by Barrer and Fergusson (1958) and Meares (1958). Their expression for the time lag in the present nomenclature is

$$\theta = \frac{\ell^2}{4D_o}\left[\frac{4e^{\gamma SP(0)}+[2\gamma SP(0)-3]e^{2\gamma SP(0)}-1}{[e^{\gamma SP(0)}-1]^3}\right] \tag{2.27}$$

Since the permeability data for the polyacrylate membranes were reasonably well correlated by the two-parameter exponential model, it is justifiable to apply (2.27) to the time-lag data. Optimum values of D_o and γS which were found by evaluating (2.27) with the time-lag data are included at the bottom of Table 2.5.

If the pressure dependence is known for the permeability and the diffusion coefficient, the solubility can be estimated. The permeability is given by Equation (2.18) or (2.24). A mean value for the diffusion coefficient is obtained by integrating (2.11) with respect to pressure over the thickness of the membrane:

$$\begin{aligned}\overline{D} &= \frac{1}{P(0)-P(\ell)}\int_{P(\ell)}^{P(0)} D_o e^{\gamma SP}\,dP \\ &= \frac{D_o}{\gamma S[P(0)-P(\ell)]}\left[e^{\gamma SP(0)}-e^{\gamma SP(\ell)}\right]\end{aligned} \tag{2.28}$$

Table 2.5

SO_2 Solubility of Polyacrylate from Time-Lag Analysis

P(0) (mm Hg)	θ (min)	Q	$\bar{D}$	S
0	-	0.709	1.36	0.521
151	12.9	1.13	1.75	0.646
302	10.8	1.72	2.31	0.745
500	8.01	2.77	3.40	0.815
762	5.57	4.67	5.95	0.785

Parameters for Q (Eq. (2.24)): $Q_0 = 7.09 \times 10^{-8}$, $\alpha = 6.32 \times 10^{-3}$, $\beta = 9.93 \times 10^{-4}$, relative error = 4.6%

Parameters for $\bar{D}$ (Eq. (2.28)): $D_0 = 1.36 \times 10^{-7}$, $\gamma S = 3.24 \times 10^{-3}$, relative error = 2.2%

Units: Q, $\frac{cm^3(STP) \cdot cm}{cm^2 \cdot sec \cdot cm\ Hg} \times 10^7$; $\bar{D}$, $\frac{cm^2}{sec} \times 10^7$; S, $\frac{cm^3(STP)}{cm^3 \cdot cm\ Hg}$; $\alpha, \beta, \gamma S$, $(mm\ Hg)^{-1}$

The solubility is simply equal to (2.18) or (2.24) divided by (2.28):

$$S = Q/\overline{D} \tag{2.29}$$

SO_2 solubilities calculated according to this analysis are given in Table 2.5. Q and $\overline{D}$ were evaluated at the tabulated upstream pressures and zero downstream pressure. The three-parameter exponential model (Equation (2.24)) was used to calculate Q. There was some variation in the solubility results with the lower values occurring at the lower upstream pressures. This suggests that the solubility has a weak pressure dependence.

Equilibrium SO_2 solubility data at room temperature were obtained for polyethylene glycol, sulfolane, and polyacrylate by making a slight modification to the permeation apparatus. The data, which are plotted in Figure 2.7, indicate that polyacrylate has a high solubility for SO_2, comparable to the SO_2 solubilities of the two SO_2 solvents. The amounts of SO_2 absorbed by sulfolane and polyacrylate increase linearly with pressure; whereas, the amount absorbed by polyethylene glycol departs slightly from linearity near 1 atm pressure. There are no literature data for polyethylene glycol or sulfolane at room temperature; however, the extrapolation of data for sulfolane reported by Lange and Evdokimova (1970) to room temperature gave values which agreed well with the data of this study.

In the units of Table 2.5, the equilibrium SO_2 solubility of polyacrylate is 1.08, somewhat higher than the values obtained from the time-lag experiments. Apparently, equilibrium was not established

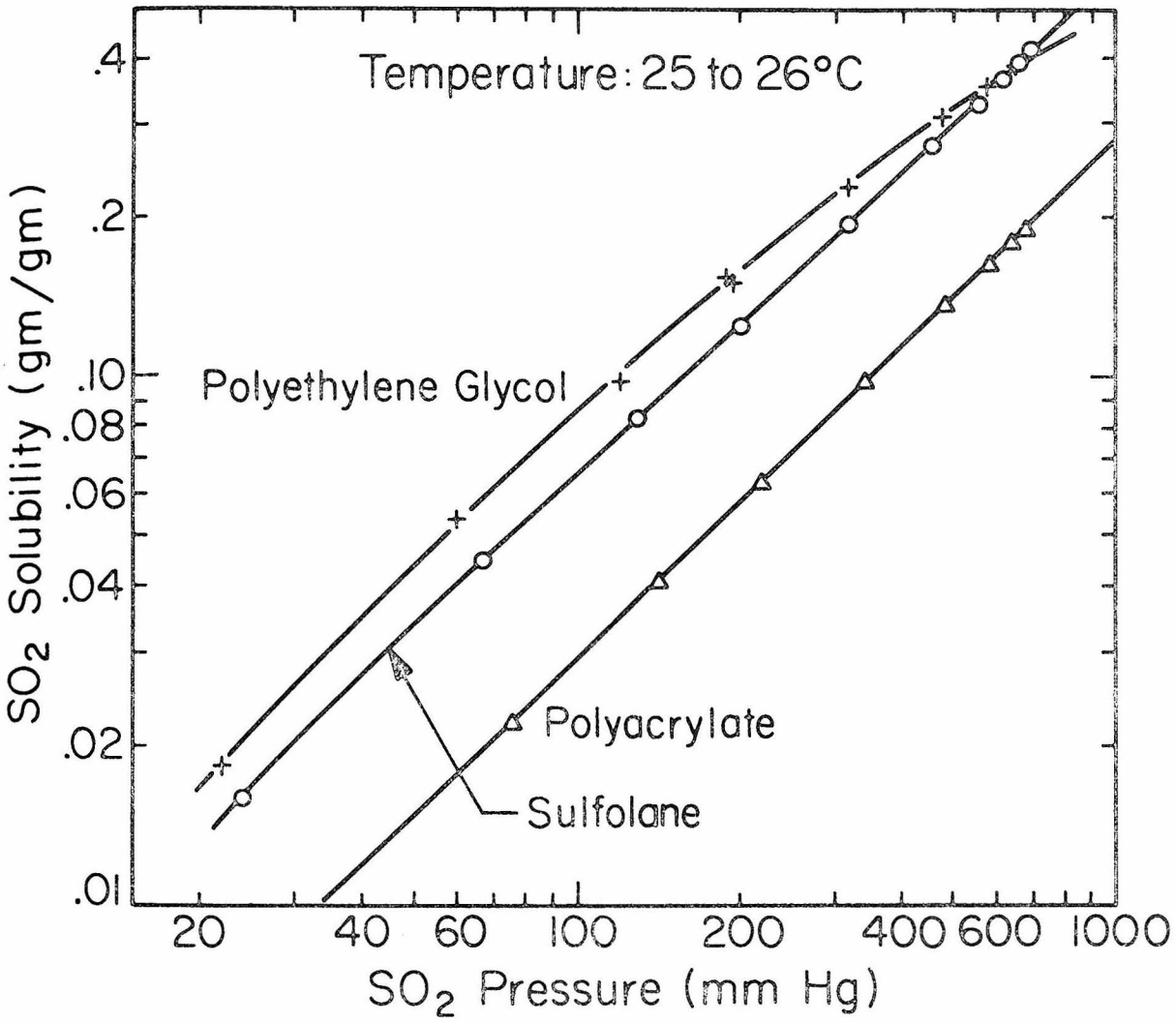

Figure 2.7 SO_2 solubility of polyethylene glycol, sulfolane, and polyacrylate.

in the short duration of the time-lag experiments, or some of the SO_2 molecules became immobilized in clusters within the polymer and did not participate in the transport process.

2.4.4 Evaluation of Polyacrylate Membrane Performance

Ward and Neulander (1970) proposed five design goals for a membrane for recovering SO_2 from combustion or smelter gases. These pertained to the SO_2 flux, selectivity, operating temperature, chemical stability, and life. The SO_2 flux should be on the order of 4×10^{-3} $cm^3(STP)/cm^2 \cdot sec \cdot cm\ Hg)$. For the thinnest membrane in Table 2.1, the SO_2 flux in the limit of zero pressure falls short of this goal by about a factor of 3. At higher pressures, though, the flux would come closer to meeting this goal because of the pressure dependence of the SO_2 permeability. The second design goal was an SO_2/CO_2 permeability ratio of several hundred for applications involving combustion gases and at least 10 for smelter gas applications. The SO_2/CO_2 permeability ratios given in the last column of Table 2.1 indicate that these membranes would only be suitable for smelter gas and other applications in which the SO_2 concentrations are on the order of 1-10%.

The third goal was a minimum operating temperature of 100 °C. The polyacrylate elastomers have a service temperature range of -40 to 200 °C; however, the transport properties would change drastically at the higher temperatures. Typically, the permeability of the noncondensable species would increase much faster than that of the condensable species, resulting in a decline in selectivity. Lower

operating temperatures are preferred for maximum selectivity. The chemical stability and life of the membranes have not been well characterized. Some deterioration was observed for the thinnest membranes over a period of several months. In conclusion, the polyacrylate membranes do not have adequate performance for large-scale industrial applications; however, they may find applications in the monitoring of SO_2 emissions and in laboratory chemical analysis or separation equipment where the requirements are less stringent.

The high solubility of SO_2 in polyacrylate (.215 lb/lb @ 25 °C and 1 atm) makes this polymer a good candidate for the solid absorbent in an SO_2 scrubber. The absorptive capacities of sulfolane and polyethylene glycol are only 2 to 2.5 times larger. A solid absorbent has the advantage of low volatility so that vapor losses would be negligible. The SO_2 scrubber could consist of a packed bed of polyacrylate in the form of small particles or fine fibers. Absorption of SO_2 would occur at low temperature. The bed could be regenerated by heating with a steam coil. For continuous operation two or more scrubbers would be required. Considering the difficulties encountered with the membranes, this is an attractive alternative for utilizing polyacrylate to remove SO_2 from a mixture of gases.

2.4.5 Permeability Results for Cellulose Triacetate Membranes

Permeability results for the cellulose triacetate membranes are given in Table 2.6. The second column of the table lists the microporous support, the elapsed time since the membrane was made, and

Table 2.6

Permeability of Cellulose Triacetate Membranes

Membrane	Support/Additive/ Elapsed Time	ℓ (μm)	$\bar{Q}(N_2)$	$\bar{Q}(CO_2)$	$Q_o(SO_2)$	Rel. Error (%)	γS	$\frac{Q_o(SO_2)}{\bar{Q}(N_2)}$	$\frac{Q_o(SO_2)}{\bar{Q}(CO_2)}$
CTA-2	Millipore/5 days	0.125	2.47	47.1	364	3.4	0.00471	147	7.73
CTA-2	12 days	0.125	1.81	-	-	-	-	-	-
CTA-6	Millipore/3 days	0.114	2.88	63.3	441	2.8	0.00403	153	6.97
CTA-6	4 days	0.114	2.67	61.4	642	3.0	0.00348	240	10.5
CTA-11	Millipore/3 days	0.051	5.32	65.7	615	2.1	0.00342	116	9.36
CTA-17	Celgard 3501/ 1-2 days	0.053	1.71	26.5	562	2.3	0.00270	329	21.2
CTA-19	Millipore/5% PEG	0.108	2.53	83.1	786	2.3	0.00268	311	9.46
CTA-24	Millipore/10% PEG	0.110	2.16	52.3	677	1.1	0.00327	313	12.9
CTA-30	Millipore/25% PEG	0.110	2.72	52.5	376	2.6	0.00413	138	7.16

Units: Q, $\frac{cm^3(STP)\cdot cm}{cm^2\cdot sec\cdot cm\ Hg} \times 10^{11}$; γS, $(mm\ Hg)^{-1}$

whether or not polyethylene glycol was included in the polymer solution. The thickness of the cellulose triacetate films ranged from 0.05 to 0.125 μm. These films are much thinner and stronger than the polyacrylate films. The N_2, CO_2, and SO_2 permeabilities are tabulated in the same manner as they were for the polyacrylate membranes. The SO_2 data were taken at 1 atm upstream pressure and were correlated with the two-parameter exponential model. Theoretically, $Q_0(SO_2)$ is the limiting value of $Q(SO_2)$ as the upstream and downstream pressures approach zero. However, as was seen with the polyacrylate membranes, extrapolation of the data at 1 atm upstream pressure to zero may give an inaccurate value for the intercept. This problem with the two-parameter model will be examined in more detail later.

The results for CTA-2 and CTA-6 indicate a slight time dependence for the permeability. The decrease in permeability with time may be due to loss of residual solvent in the membrane or to molecular rearrangements which lead to an increase in the density. The thickness dependence of the permeability cannot be deduced from the results in Table 2.6, alone, because there is very little variation in thickness. Table 1.3 has permeability results for a cellulose triacetate film 76 μm thick which are very close to the results for the 0.1-μm films in Table 2.6. The lack of an appreciable dependence on thickness is surprising because the permeability of the 0.1-μm films should be affected by the limited open area of the porous support. The films may be rigid enough so that they do not intimately contact the surface of the porous support.

The importance of the porous support in determining membrane performance is further illustrated by the results for CTA-11 and CTA-17. CTA-11, supported on a Millipore filter, has an N_2 permeability larger than expected because of defects in the film. These defects were produced either when the film was cast or when it was transferred to the Millipore filter. The glossy side of a Millipore filter has a smooth surface when it is dry; however, when the filter is soaked in water, it swells and the surface becomes covered with a high density of sharp, needle-like projections. This was observed when the Millipore filter and its attached film were removed from the water bath and allowed to dry. The phenomenon is analogous to the raising of the grain in a piece of wood when it is wet. The sharp projections on the surface of the Millipore filter could puncture tiny holes in the thin film. The surface of Celgard 3501, a hydrophilic version of Celgard 2500, was much smoother when it was wet. This is verified by the lower N_2 permeability for CTA-17.

The last three membranes in Table 2.6 show the effect of adding polyethylene glycol (PEG) to the polymer solution. Each polymer solution contained the same amount of polymer; only the amount of PEG was different. The membranes with more PEG should be thicker, but all three membranes had approximately the same thickness. This means that PEG is insoluble in cellulose triacetate and is ineffective as an additive. The permeability results support this conclusion.

CTA-17 had the best performance of the membranes in Table 2.6. The pressure dependence of the SO_2 permeability, however, was only characterized from data at 1 atm upstream pressure. To more adequately determine the pressure dependence, four permeation experiments were run at upstream pressures of 100, 200, 400, and 740 mm Hg. The permeability results are plotted as a function of the mean pressure across the membrane in Figure 2.8. The mean pressure is simply the average of the upstream and downstream pressures and is an appropriate variable for clearly illustrating the pressure dependence. Mathematically, the mean pressure leads to some ambiguity because the permeability is not a single-valued function of the mean pressure. Upstream and downstream pressures may be selected which give the same mean pressure but different permeabilities. For this reason, one continuous curve cannot be drawn through the four sets of data in Figure 2.8.

The pressure dependence of the SO_2 permeability of CTA-17 is much larger than expected. The SO_2 permeability increases two orders of magnitude as the mean pressure goes from 0 to 700 mm Hg. The pressure dependence decreases with increasing mean pressure so that the two-parameter exponential model cannot correlate the results. The curves in Figure 2.8 represent the three-parameter exponential model, which fits the data very well. The optimum values of the parameters were obtained by substituting the four sets of data into the model. A few points at the beginning and end of each run were not included because of their departure from ideality. At the end of a run, there was a tendency for the permeability to drop sharply

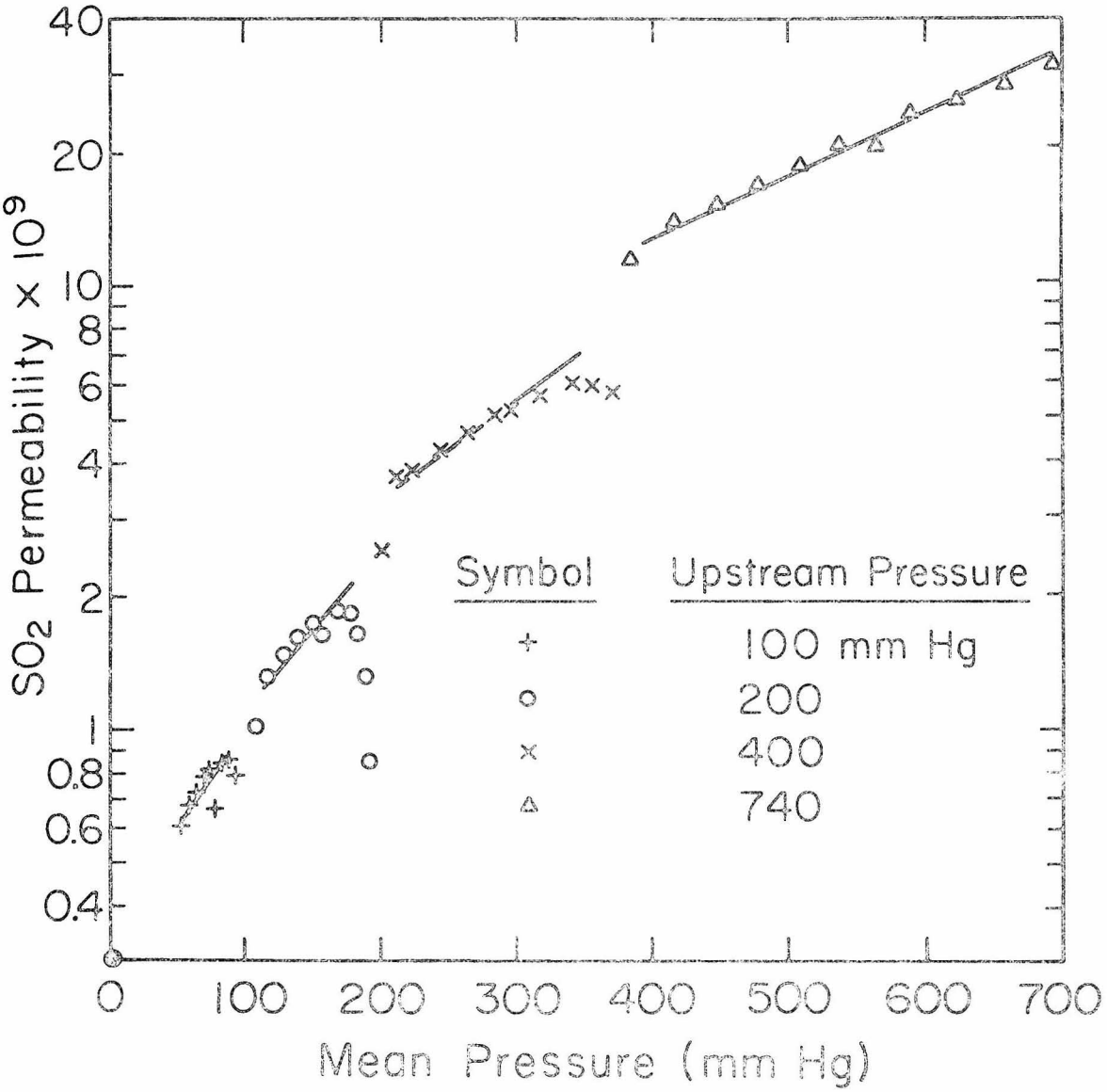

Figure 2.8 Pressure dependence of the SO_2 permeability of CTA-17. The permeation data were correlated with the three-parameter exponential model (Eq. (2.24) with $Q_o = 3.06 \times 10^{-10}$, $\alpha = 1.37 \times 10^{-2}$, $\beta = 1.51 \times 10^{-3}$, and relative error = 5.0%), represented by the line segments.

as the downstream pressure approached the upstream pressure. This may be attributed to the immobilization of gas molecules in clusters within the polymer or to some molecular relaxation process which makes the polymer less permeable.

From the three-parameter exponential model, $Q_0(SO_2)$ is more than an order of magnitude smaller than the value predicted from the two-parameter model using only the data at 1 atm upstream pressure. This low value makes the membrane unattractive for applications in which a large SO_2 flux and high selectivity are required. These results also demonstrate that the two-parameter model is inadequate for extrapolating the data taken at 1 atm upstream pressure to lower pressures. Therefore, the SO_2 permeability results in Table 2.6 apply only for 1 atm upstream pressure.

2.5 Summary

Ultrathin films of the polyacrylate and cellulose triacetate polymers were prepared to achieve the high SO_2 fluxes which are required for practical applications. Polyacrylate films were cast on mercury and cellulose triacetate films were formed on glass plates which were withdrawn at constant velocity from dilute polymer solutions.

The performance of the membranes was characterized by measuring their permeability to N_2, CO_2, and SO_2. N_2 and CO_2 did not interact appreciably with the membranes and their permeabilities were independent of pressure. The permeation of SO_2 was highly nonideal,

increasing rapidly with pressure. The SO_2 permeation data were correlated with two- and three-parameter exponential models. The three-parameter model had the same functional form as the free volume theory and gave a better fit to the data than the two-parameter model. The third parameter was needed to account for a decrease in the pressure dependence with increasing pressure. Physically, this means that the plasticizing effect of the SO_2 diminished as more SO_2 was absorbed by the membrane.

With the polyacrylate membranes the effects of membrane thickness, additives, and time were studied extensively. The permeability decreased for membranes less than 10 μm in thickness. The inclusion of polyethylene glycol and sulfolane in some membranes increased the SO_2 permeability but reduced the physical strength of the membranes. The overall effect was little improvement in performance. During some permeation experiments the permeability dropped sharply at the end of the run as the downstream pressure approached the upstream pressure. This was caused by cluster formation or a change in orientation of the polymer chains. Over long periods of intermittent testing, the permeability of the thin membranes first decreased and later increased as they deteriorated.

Time-lag experiments were performed on one polyacrylate membrane to estimate the functional dependence of the diffusion coefficient for SO_2. The data were well correlated with a two-parameter exponential model. From the permeability and diffusivity results, values of the SO_2 solubility were obtained which were less than the

equilibrium solubility determined independently. The SO_2 solubility of polyacrylate was only a factor of 2 to 2.5 lower than the SO_2 solubilities of polyethylene glycol and sulfolane, two excellent SO_2 solvents. With such a high solubility polyacrylate may find application as a solid absorbent in SO_2 scrubbers.

The cellulose triacetate membranes exhibited much of the same behavior as the polyacrylate membranes. The SO_2 permeability had a large pressure dependence, even greater than for polyacrylate. The few results for membranes of different thicknesses indicated that there was little or no dependence on thickness. Membranes which were retested after some time had elapsed exhibited a decrease in permeability. An attempt was made to prepare membranes containing polyethylene glycol, but it was insoluble in cellulose triacetate. The cellulose triacetate membranes were much stronger than the polyacrylate membranes and were not as subject to pinhole defects and deterioration with time.

Preliminary permeation studies on thick samples of the polyacrylate and cellulose triacetate polymers indicated that they were very selective to SO_2. To achieve high SO_2 transport rates, techniques were developed for preparing thin films of both polymers. The results of this chapter revealed the large pressure dependence of the SO_2 permeability, which makes both the SO_2 flux and the selectivity pressure dependent. In the limit of zero pressure both of these were much smaller than anticipated, even for the thinnest membranes.

Consequently, the polyacrylate and cellulose triacetate membranes do not meet the design goals for large-scale industrial applications; however, they may be useful for SO_2 monitoring and laboratory gas separations.

Chapter 3

CELLULOSE TRIACETATE/POLYACRYLATE COMPOSITE MEMBRANES

3.1 Introduction

In Chapter 2 we described the preparation of thin membranes of the polyacrylate and cellulose triacetate polymers by two conventional methods and the measurement of their permeability to N_2, CO_2, and SO_2. Because of the pressure dependence of the SO_2 permeability, the SO_2 flux and selectivity were low, compared with the design goals,for gases containing low concentrations of SO_2. Of these two polymers, polyacrylate was better for SO_2 separations because it was over ten times as permeable as cellulose triacetate and the pressure dependence of the SO_2 permeability was smaller. The main problem with polyacrylate was the difficulty in casting thin, pinhole-free films. Forming films on the surface of mercury was tedious and for good results was limited to film thicknesses greater than 1 μm.

Polyacrylate would be more attractive as a membrane material if it could be cast into much thinner films. The desired thickness could be achieved with the glass-plate technique; however, polyacrylate is very adhesive and would not float off the glass. In this chapter it is shown how the glass-plate technique can be applied to polyacrylate and many other soluble polymers by making composite membranes consisting of more than one layer.

The performance of the composite membranes was first determined by measuring their permeability to pure N_2, CO_2, and SO_2 with the

gas permeation apparatus described in Section 2.3.2. For practical applications it is also important to know how the membranes will behave with gas mixtures. A steady-state flow system was built to measure the permeability of binary mixtures of 0.1-10% SO_2 in N_2. The permeation results for the mixtures are compared to those for the pure gases. Chapter 3 concludes with discussions of the design of membrane gas separators, possible applications for the membranes, and recommendations for future work.

3.2 Membrane Preparation

Cellulose triacetate/polyacrylate (CTA/PA) composite membranes were made by modifying the glass-plate technique described in Section 2.2.2 and Appendix B. The principal feature of the modified technique is the formation of layers of different polymers on the same glass plate. Each layer serves a particular function which determines its thickness. For the CTA/PA composite membranes the CTA layer served as a nonadhesive agent so that the PA layer could be removed from the plate. The PA layer was selected for its large SO_2 permeability and good selectivity. The permeability results of Chapter 2 indicate that the SO_2 permeability of PA is at least a hundred times greater than it is for CTA in the limit of zero pressure. This means that the thickness of the CTA layer should be small compared to the thickness of the PA layer to minimize its effect on the mass transfer.

Film thickness was estimated from the theory of Levich (1962):

$$\ell_p = \frac{0.93(\mu v)^{2/3}}{\sigma^{1/6}(\rho g)^{1/2}} \frac{\rho}{\rho_p} \cdot c \qquad (3.1)$$

where μ, σ, ρ, and c are the viscosity, surface tension, density, and concentration, respectively, of the polymer solution; v is the withdrawal rate; g is the gravitational constant; and ρ_p is the polymer density. For dilute solutions the density and surface tension of the pure solvent may be used in (3.1) without introducing much error. The solvents for CTA and PA were chloroform and toluene, respectively. When the properties of the solvent and the polymer are substituted in (3.1), the film thickness is given by

$$\ell_p = k(\mu v)^{2/3} c \qquad (3.2)$$

where k = 0.016 and 0.015 for the CTA and PA solutions, respectively.

The desired thickness range for the PA layer was 0.2-0.5 μm. Because of uncertainty in the viscosity of the PA solutions, the solution concentrations required to make films in this thickness range could not be determined exactly. Solutions of 1 and 2 weight percent PA in toluene were prepared to bracket the range. The crude polymer was dissolved in 1200 ml of reagent grade solvent. Impurities and residue in the polymer settled to the bottom of the beaker.

The desired thickness range for the CTA layer was 0.002-0.005 μm Solutions of 1.25×10^{-2} and 3.76×10^{-2} weight percent CTA in chloroform were prepared by dissolving the polymer in 1200 ml of

reagent grade solvent and filtering the solution through a fritted glass filter. Since these solutions were so dilute, the viscosity of pure chloroform (0.542 cp @ 25 °C) could be used in (3.2) to estimate film thickness. For the above solutions and a withdrawal rate of 4 cm/sec, the calculated film thicknesses are 0.0016 and 0.0047 μm. If the amount of residue in the chloroform (0.001%) is taken into account, the calculated film thicknesses are 0.0017 and 0.0048 μm. This is probably the most accurate way to determine the film thickness, because films this thin are very difficult to see and handle.

The smoothness of the glass plates is important in preparing the composite films. The first films were formed on glass plates manufactured by the tin-float process and did not come off when they were dipped in a water bath. Polished glass plates ($4 \times 5 \times \frac{1}{8}$ in.) were obtained from Pacific Universal Products which had a smoothness of approximately four fringes per inch, almost optical quality. The films formed on these plates came off very slowly, provided the plates were sufficiently clean. The plates were cleaned by vigorous scouring with a nonabrasive liquid soap using plastic gloves. The plates were then rinsed with distilled water. If the plates did not hold a continuous film of water, further cleaning was needed. After rinsing with the distilled water, the plates were blown dry with a stream of compressed N_2 and quickly placed in the glove box which contained the apparatus. Inside the box they were inspected for defects and dust particles.

The microporous supports for the thin polymer films included MF-Millipore filters with 0.050 μm pore size, Celgard 2500, a porous hydrophobic polypropylene film, and Celgard 3501, a hydrophilic version of Celgard 2500. Both Celgard products were developed and distributed by Celanese, and their properties are summarized in Table 2.2. These microporous media are representative of materials that are suitable for this application, but they do have some drawbacks. Dry Millipore filters have a glossy side which is very smooth and a dull side which has a much coarser structure. When a Millipore filter is soaked in water, it swells and needle-like projections appear on the surface of the glossy side which could damage the thin polymer film. The Celgard films have a surface smoothness intermediate between that of dry and wet Millipore filters. Surface smoothness, pore size, and pore density determine the minimum film thickness supportable by a particular substrate and affect the performance of the resulting membrane.

The general procedure for making the composite membranes is the same as that described in Section 2.2.2 and Appendix B for the CTA membranes. A brief summary and modifications to this procedure are given below. A clean, polished glass plate is first lowered into one of the CTA solutions, withdrawn at constant velocity, and allowed to dry. This is repeated for one of the PA solutions. CTA is insoluble in toluene so that it does not come off the plate when the PA layer is applied. When the plate is dry, the edges are carefully scraped with a sharp razor blade. Next, the plate

is slowly dipped into a water bath at a slight angle from the horizontal. The composite film slowly detaches from the plate and floats on the surface of the water. Two methods are employed for removing the composite film from the water bath:

(1) A microporous support taped to a flat, rigid plate is raised from the bottom of the water bath until the composite film adheres to its surface. The plate is removed from the water bath and the membrane is allowed to dry.

(2) A microporous support is laid directly on the composite film while it is floating on the water. The film sticks to the support and both are removed together.

Details on the preparation of five composite membranes are given in Table 3.1. The withdrawal rate of the glass plates was held constant at 4 cm/sec. Film thickness was estimated by weighing the thin film on the other side of the glass plate if it came off; otherwise, a thin film prepared under identical conditions was weighed. The first three membranes in Table 3.1 were removed from the water bath by method 1 and the last two by method 2. CTA/PA-43 had the thickest CTA layer and was stronger and more stable than the other four membranes. The thickness of the CTA layer was more critical in determining the strength of the composite film than the thickness of the PA layer. There is a tradeoff between mechanical

Table 3.1

Details of Composite Membrane Preparation

Membrane	CTA Solution (%)	PA Solution (%)	Thickness (μm)	Porous Support
CTA/PA-43	0.0376	1	0.190	Millipore filter--glossy side wet
CTA/PA-52	0.0125	1	0.179	Celgard 3501--wet
CTA/PA-53	0.0125	2	0.461	Celgard 3501--wet
CTA/PA-58	0.0125	2	0.485	Millipore filter--glossy side dry
CTA/PA-59	0.0125	2	0.460	Celgard 2500--dry

strength and permeability because the thicker the CTA layer is, the greater its resistance to permeation. The microporous support and the thickness of each of the layers can be selected to optimize membrane performance.

3.3 Experimental Apparatus and Procedure

The permeability of the composite membranes to pure N_2, CO_2, and SO_2 was determined by the Manometric Method (Section 2.3). N_2 and CO_2 were tested at 1 atm upstream pressure. SO_2 was tested at upstream pressures of 100, 200, 400, and 760 mm Hg to more accurately characterize its permeability which exhibited a strong pressure dependence. A steady-state flow system was designed and built to measure the permeability of mixtures of N_2 and SO_2.

3.3.1 Design Equations for Flow System

A schematic diagram of the flow system permeation cell is shown in Figure 3.1. A binary mixture of SO_2 mole fraction $x_{u,in}$ enters the upstream chamber of the permeation cell at a rate of $n_{u,in}$ moles/sec and a pressure P_u and leaves at a rate of $n_{u,out}$ with a mole fraction $x_{u,out}$. The downstream chamber of the cell is maintained at a lower pressure P_d. N_2 and SO_2 permeate across the membrane as a result of their respective partial pressure driving forces. If the upstream chamber is well mixed, then the composition is x_u throughout and is equal to $x_{u,out}$. From the definitions of gas flux and permeability, the N_2 and SO_2 fluxes are

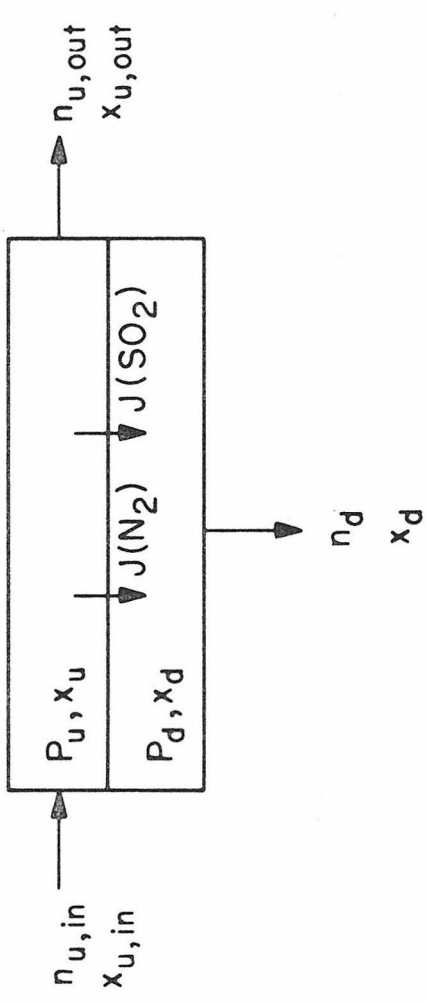

Figure 3.1 Schematic diagram of the flow system permeation cell.

$$J(N_2) = \frac{Q(N_2)}{\ell}[(1-x_u)P_u-(1-x_d)P_d] \tag{3.3}$$

$$J(SO_2) = \frac{Q(SO_2)}{\ell}[x_uP_u-X_dP_d] \tag{3.4}$$

where ℓ is the membrane thickness. By the conservation of mass,

$$x_d = \frac{J(SO_2)}{J(N_2)+J(SO_2)} \tag{3.5}$$

Substitution of (3.3) and (3.4) in (3.5) and manipulation of the resulting equation leads to a quadratic equation in x_d:

$$ax_d^2 + bx_d + c = 0 \tag{3.6}$$

where

$$a = \frac{Q(SO_2)}{Q(N_2)} - 1 \tag{3.7}$$

$$b = \frac{P_u}{P_d}\left(x_u - x_u\frac{Q(SO_2)}{Q(N_2)} - 1\right) - \frac{Q(SO_2)}{Q(N_2)} + 1 \tag{3.8}$$

$$c = x_u\frac{P_u}{P_d}\frac{Q(SO_2)}{Q(N_2)} \tag{3.9}$$

Equation (3.6) is written in dimensionless form. The three dimensionless groups which determine the downstream mole fraction, x_d, are the upstream mole fraction, x_u, the pressure ratio, P_u/P_d, and the permeability ratio, $Q(SO_2)/Q(N_2)$. This is a useful result because

it reduces the number of parameters which must be varied to characterize a permeation system.

Once x_d is found from the solution of (3.6), the permeation rate, n_d, is easily derived from the above expressions:

$$n_d = \frac{AP_s}{RT_s} [J(N_2)+J(SO_2)] \tag{3.10}$$

where A is the membrane area, R is the gas constant, and T_s and P_s are evaluated at STP (0 °C and 1 atm). The N_2 and SO_2 fluxes may be estimated from permeability data for the pure gases; however, interactions between the two gases and the membrane may make the results for the mixtures quite different from those predicted from pure-component data.

Another important quantity is the flow rate into the upstream chamber, $n_{u,in}$. The flow rate should be large enough so that there is not an appreciable change in concentration from the inlet to the outlet of the upstream chamber. Otherwise, the assumption of uniform upstream composition may be violated. A simple mass balance leads to an expression for $n_{u,in}$ in terms of n_d and the mole fractions of all the streams:

$$n_{u,in} = \frac{(x_d - x_{u,out})n_d}{(x_{u,in} - x_{u,out})} \tag{3.11}$$

For a well-mixed upstream chamber x_u is everywhere equal to $x_{u,out}$ and (3.11) becomes

$$n_{u,in} = \frac{(x_d - x_u)n_d}{(x_{u,in} - x_u)} \tag{3.12}$$

The above equations were sufficient to do the basic design of the flow system.

3.3.2 Flow System Equipment

Scale drawings of the permeation cell are shown in Figure 3.2. The entire cell is made of type 316 stainless steel. The gas mixture enters the cell through a manifold in the top which distributes the gas to four inlet ports and exits through a larger port above the center of the membrane. The bottom of the cell has a cavity which receives the permeant gas and three posts for supporting the rigid disk on which the membrane rests. The rigid disk should have a smooth surface, a large open area or porosity, and a low resistance to gas flow. Suitable materials include porous metal or glass, metal screen or laminate, and perforated plate. A porous stainless steel disk with 10 micron porosity (Mott Metallurgical Corp.) was used for most of the experiments. A piece of filter paper was placed over the porous disk followed by the membrane, a stainless steel gasket (1.750 I.D. x 2.234 O.D. x .004 in.), and a rubber gasket. This was the preferred cell configuration for protecting the fragile membranes and sealing the cell gas tight.

A schematic diagram of the entire flow system is shown in Figure 3.3. The gas flow through the system began in the upper right corner and proceeded in a counterclockwise direction. Gas mixtures were prepared by diluting pure SO_2 and 1 and 10% mixtures

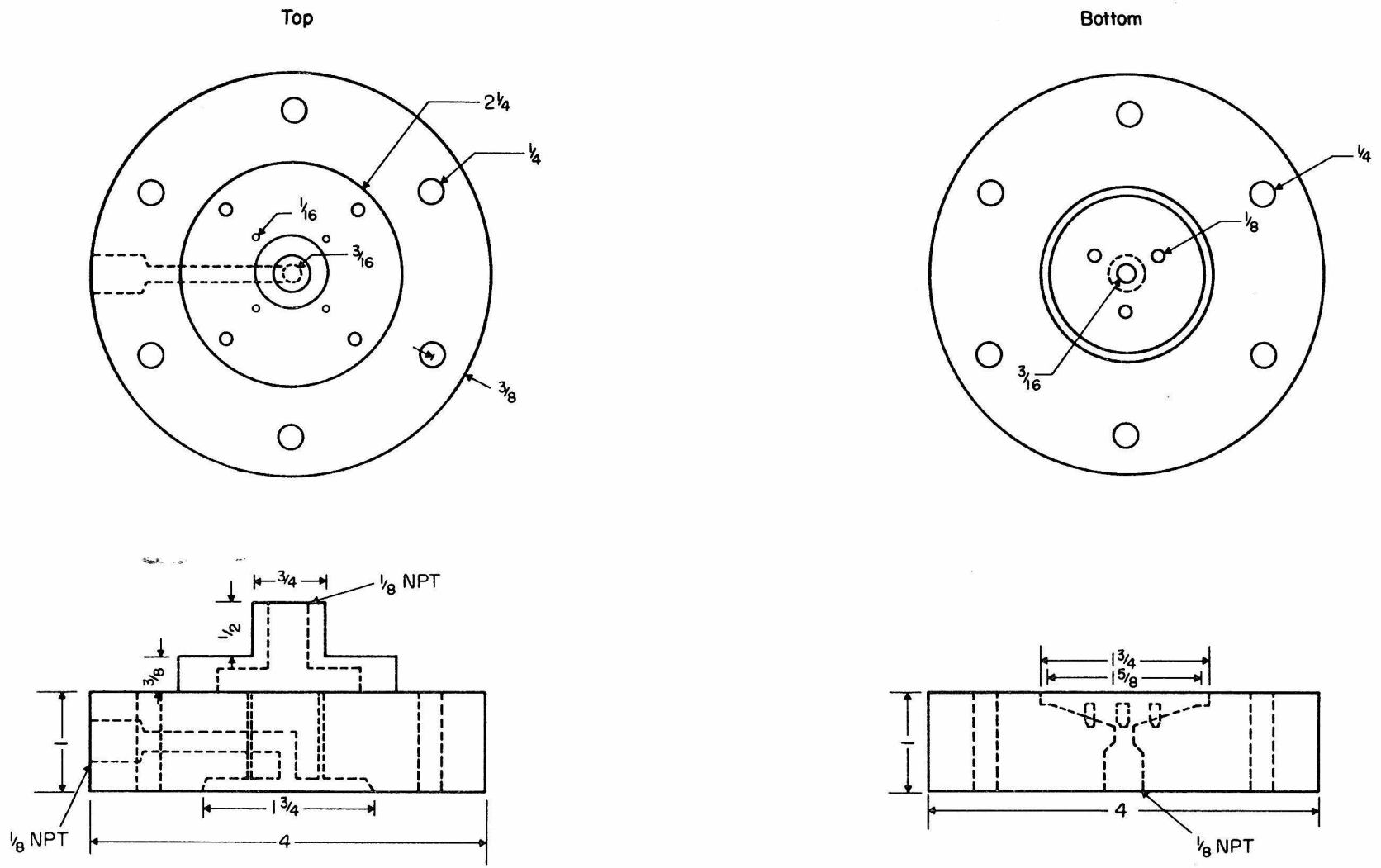

Figure 3.2 Permeation cell.

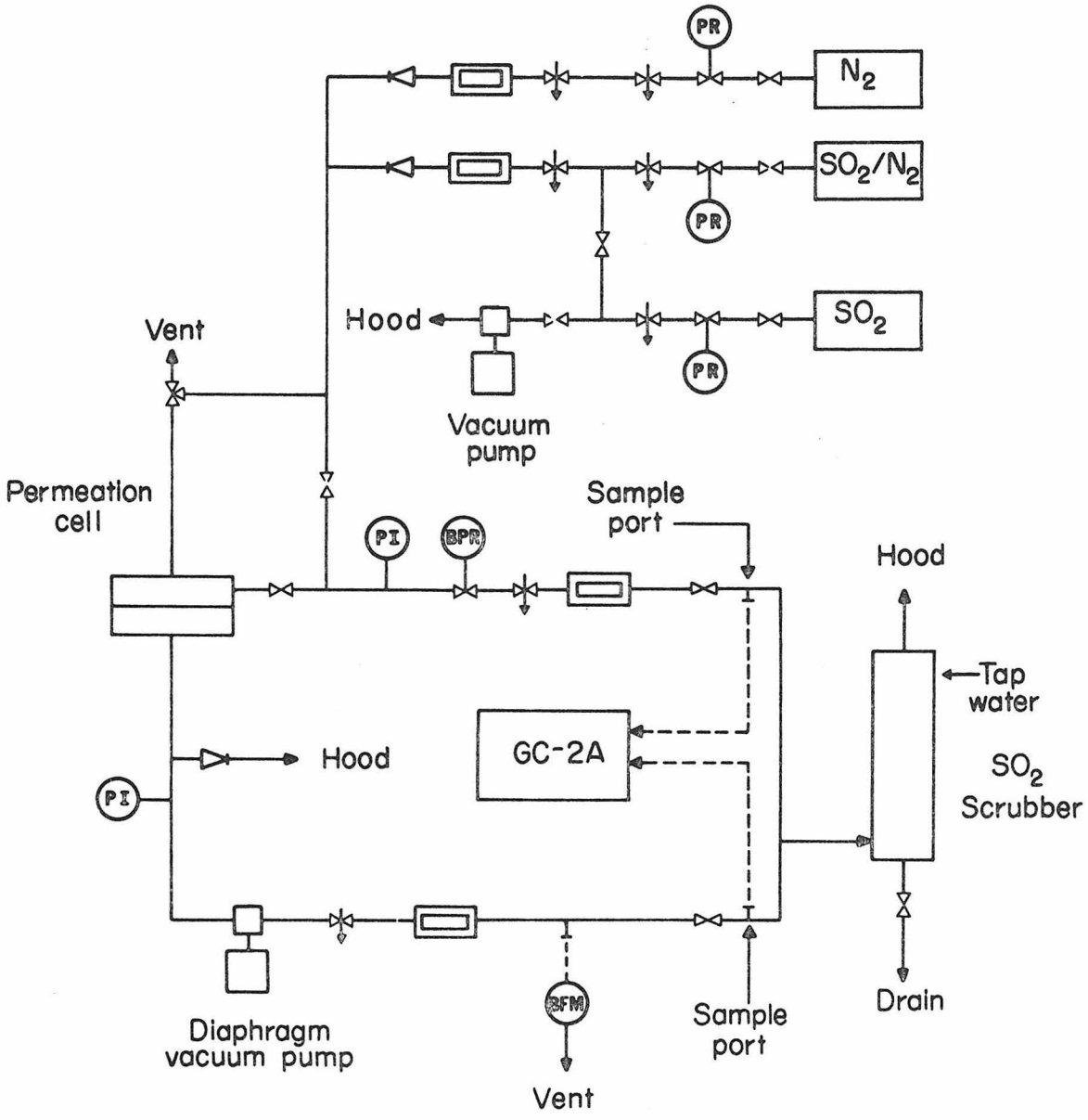

Figure 3.3 Schematic diagram of the flow system.

of SO_2 in N_2 with pure N_2. The gas mixture flowed through the upstream chamber of the permeation cell at an elevated pressure controlled by a back pressure regulator. After passing through a rotameter, the mixture was sent to an SO_2 scrubber and then exhausted to a fume hood. The downstream chamber of the permeation cell was maintained at 0.2 atm by a diaphragm vacuum pump. Flow rates on the downstream side were measured with a rotameter and a bubble flow meter. Gas analysis was done by taking 1.0-ml samples from the upstream and downstream lines with a gas-tight syringe and injecting them into a thermal conductivity gas chromatograph (Beckman GC-2A). The column for the gas chromatograph was packed with Chromosil 310 (Supelco, Inc.) and operated at a helium flow rate of 50 ml/min.

3.3.3 Instrument Calibration and Operating Conditions

The rotameters were calibrated over a wide range of flow rates and several different pressures using a wet test meter and a bubble flow meter. Pure SO_2 and mixtures of SO_2 and N_2 could not be calibrated with the wet test meter because of the high solubility of SO_2 in water. This problem was solved by applying dimensional analysis to the rotameters (McCabe and Smith, 1956). If a particular dimensionless group is the same for two gases, they will have identical calibration curves. This observation enabled all of the calibration work to be done with pure N_2. The gas chromatograph was calibrated by mixing known gases with the rotameters and

injecting samples into the instrument. Details of these and other routine instrument calibrations are given in Appendix C.

Flow system experiments were run on membranes CTA/PA-43 and CTA/PA-58 with pure N_2 and SO_2 and mixtures containing 0.1-50% SO_2. Typical operating conditions were room temperature (25-27 °C), 10 atm upstream pressure, 0.2 atm downstream pressure, and 2 l/min (25 °C, 1 atm) upstream flow rate. The upstream pressure was selected to give larger permeation rates and greater selectivity for SO_2 at the higher concentrations. The downstream pressure was set at the minimum operating pressure of the diaphragm vacuum pump. Flow rates were chosen to give good mixing and to extend the life of the gas cylinders over several experiments. A few runs were performed at different flow rates and upstream pressures to determine their effect on the permeation.

3.4 Permeability Results

3.4.1 Permeability Calculations

The permeability of the composite membranes to pure gases was determined by analyzing the permeation data with Equation (2.10). The permeation of N_2 and CO_2 through the composite membranes was independent of pressure under the test conditions of the Manometric Method. Equation (2.10) yielded a set of permeability results for each permeation run from which a mean value was computed. The permeation of SO_2 exhibited a strong pressure dependence which could not be characterized by a single value for the permeability.

In Chapter 2 a three-parameter exponential model having the same functional form as the free volume theory was proposed for correlating SO_2 permeability results obtained from (2.10). The final expression for the pressure dependence of the permeability was given by Equation (2.24), which applies to each layer of the composite membrane. Two separate equations with different values of the parameters are not needed because the resistance of the CTA layer is usually small enough to neglect. Furthermore, it is easier to analyze the data by assuming there is just a single layer. Optimum values of Q_o, α, and β in Equation (2.24) were found with the aid of a computer program (Appendix D).

The permeability of the composite membranes to mixtures of N_2 and SO_2 was studied with the flow system. Consequently, a different approach was required for the data analysis. Gas compositions were determined with a calibrated thermal conductivity gas chromatograph. Permeation rates were measured with a rotameter and a bubble flow meter. If the permeation rate is $\dot{v}$ (cm^3/sec at STP), then the N_2 and SO_2 permeabilities are

$$Q(N_2) = \frac{(1-x_d)\dot{v}\ell}{A[(1-x_u)P_u-(1-x_d)P_d]} \tag{3.13}$$

$$Q(SO_2) = \frac{x_d\dot{v}\ell}{A(x_uP_u-x_dP_d)} \tag{3.14}$$

In the above equations the driving force for permeation is the partial pressure difference across the membrane.

3.4.2 Results for Pure Gases

The permeability results for pure N_2, CO_2, and SO_2 are given in Table 3.2 and are better understood by referring to Table 3.1, also. The five composite membranes are relatively free of pinhole defects except for CTA/PA-52, which has an abnormally large N_2 permeability. The column headed "Rel Error" tells how well the three-parameter exponential model correlated the SO_2 permeability results. The last two columns in Table 3.2 give the ratio of $Q_o(SO_2)$ to $\overline{Q}(N_2)$ and $\overline{Q}(CO_2)$. These ratios indicate how selective the membrane would be for SO_2 at low concentrations.

The effect of the thickness of the CTA layer on permeability is seen from the SO_2 results. CTA/PA-43 has the thickest CTA layer and, correspondingly, the lowest value of $Q_o(SO_2)$ and the highest value of α. The CTA layer offers a significant resistance to SO_2 permeation even though it is only 2.5% of the composite film thickness. The other four membranes have CTA layers which are one-third as thick as the one for CTA/PA-43, and their SO_2 permeabilities are more characteristic of polyacrylate alone. Reducing the thickness of the CTA layer, however, made these membranes weaker and more subject to pinhole defects. The results in the last two columns of Table 3.2 show that the selectivity for SO_2 is larger for the membranes with thinner CTA layers.

Table 3.2

Permeability of CTA/PA Composite Membranes

Membrane	ℓ (μm)	$\bar{Q}(N_2)$	$\bar{Q}(CO_2)$	$Q_o(SO_2)$	α	β	Rel. Error (%)	$\frac{Q_o(SO_2)}{\bar{Q}(N_2)}$	$\frac{Q_o(SO_2)}{\bar{Q}(CO_2)}$
CTA/PA-43	0.190	2.05	23.6	50.6	0.0121	0.00219	4.8	24.7	2.14
CTA/PA-52	0.179	11.6	35.2	165	0.00810	0.00199	4.5	14.2	4.69
CTA/PA-53	0.461	2.96	42.2	311	0.00633	0.00132	3.9	105	7.37
CTA/PA-58	0.485	1.13	22.6	125	0.00767	0.00150	4.1	111	5.53
CTA/PA-59	0.460	1.98	31.0	178	0.00783	0.00150	4.9	89.9	5.74

Units: Q, $\frac{cm^3(STP)\cdot cm}{cm^2\cdot sec\cdot cm\ Hg} \times 10^{10}$; α,β, $(mm\ Hg)^{-1}$

$\bar{Q}(N_2)$ and $\bar{Q}(CO_2)$ are mean values obtained from Equation (2.10).

$Q_o(SO_2)$, α, and β are optimum values of the parameters in Equation (2.24).

The pressure dependence of the SO_2 permeability is plotted in Figures 3.4 and 3.5 for membranes supported on Millipore filters and Celgard, respectively. The abscissa is the mean pressure, the average of the upstream and downstream pressures. The use of the mean pressure reduces the number of independent variables so that the pressure dependence is easier to illustrate graphically. Experimental data were taken at 100, 200, 400, and 760 mm Hg upstream pressure, and the permeability results were correlated with the three-parameter exponential model which is represented by the line segments in these figures. The values of the parameters are given in Table 3.2. In both figures the thinner membrane has the lower SO_2 permeability because the CTA layer is a larger percentage of the total thickness. If these figures are superimposed, it is observed that the membranes supported on Celgard are more permeable than those supported on Millipore filters. This results from differences in the surface properties of the two supports. Near the end of some of the permeation runs, there is a noticeable decline in the SO_2 permeability which may be caused by the immobilization of SO_2 molecules in clusters within the membrane.

All the permeation data thus far were taken by the Manometric Method, in which the pressure difference (ΔP) across the membrane changes with time. Such experiments may yield different results from those in which ΔP is held constant, which is how the flow system experiments were run. To compare the permeability

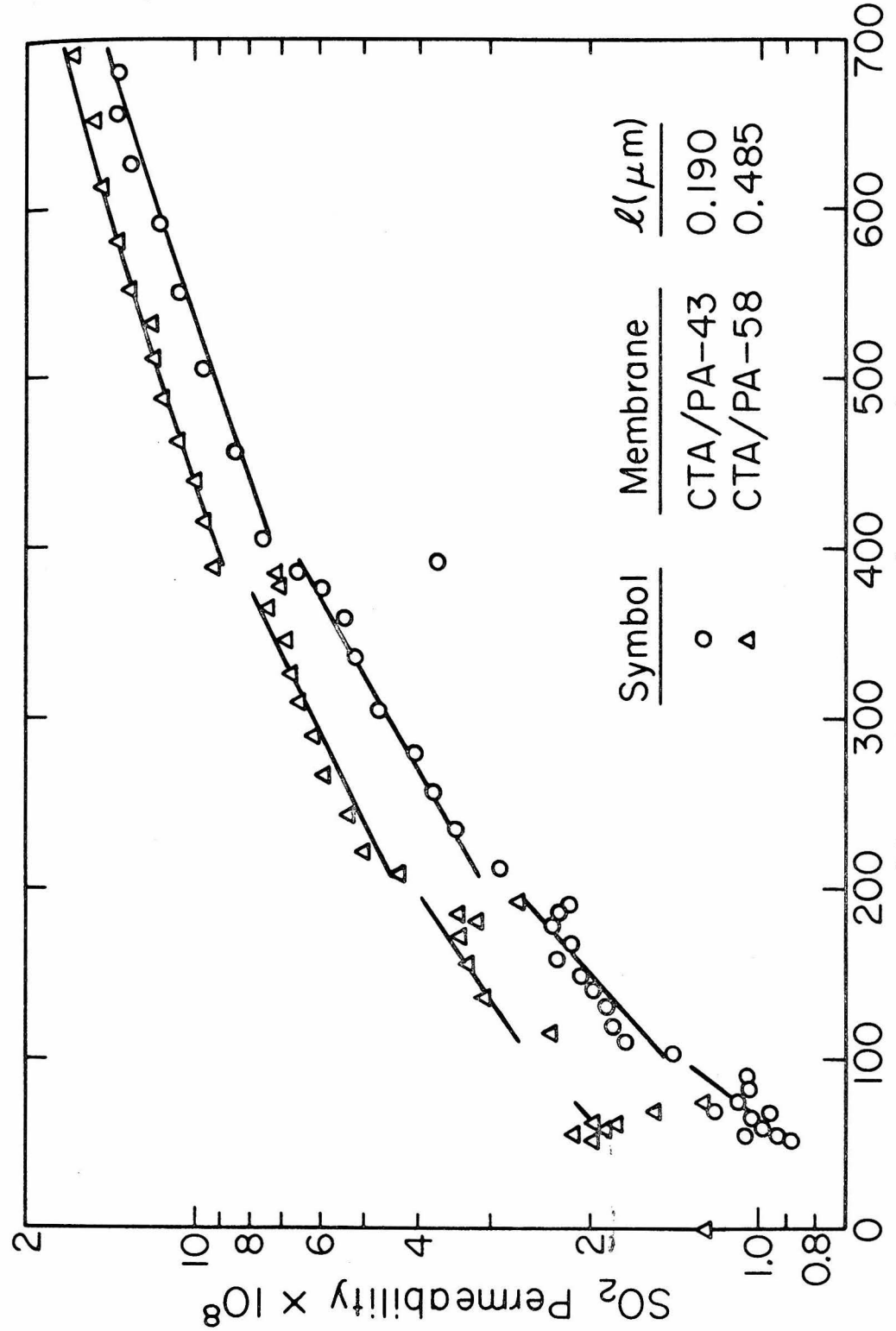

Figure 3.4 Pressure dependence of the SO_2 permeability of composite membranes supported on Millipore filters. The line segments represent the three-parameter exponential model (Eq. (2.24)). The parameters are given in Table 3.2.

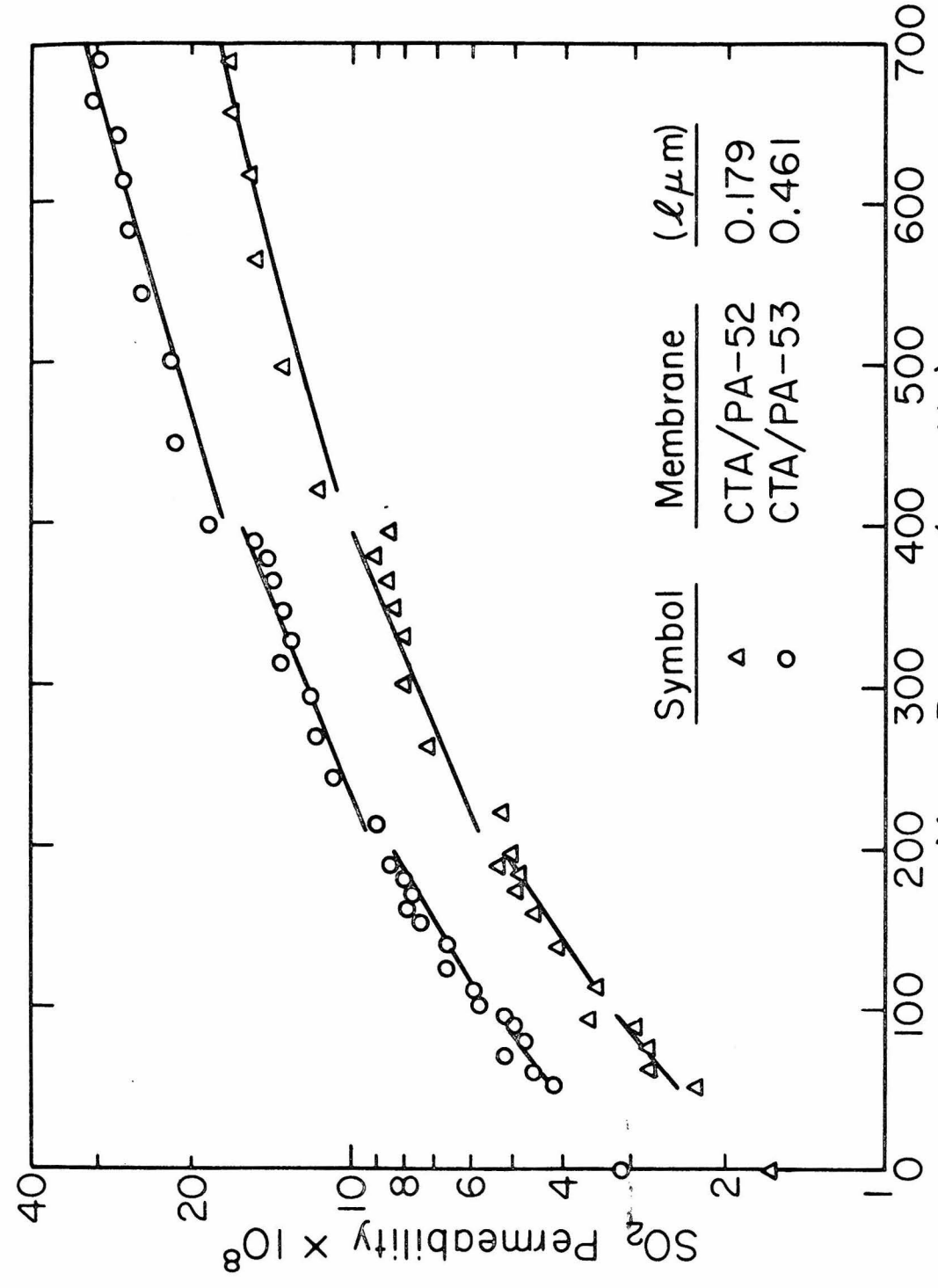

Figure 3.5 Pressure dependence of the SO_2 permeability of composite membranes supported on Celgard. The line segments represent the three-parameter exponential model (Eq. (2.24)). The parameters are given in Table 3.2.

results for the pure gases with those for the mixtures, the methods of measurement must either be the same or give comparable results.

Variable-ΔP and constant-ΔP SO_2 experiments were run on CTA/PA-59 to see whether or not the method of measurement makes a significant difference. The variable-ΔP SO_2 runs were done immediately after testing the membrane with N_2 and CO_2. At the conclusion of these experiments, the membrane was left in the permeation cell for a period of three weeks under vacuum. Then, constant-ΔP SO_2 permeation runs were made by holding the upstream pressure constant and maintaining the downstream pressure close to zero with the vacuum pump. The permeation rate was measured by closing the valve to the vacuum pump and noting the initial pressure rise on the downstream side of the membrane. After recording data for one run, the downstream side was re-evacuated and the above procedure was repeated until the initial pressure rise was the same for consecutive runs, indicating steady-state permeation.

The results for the variable-ΔP experiments were correlated with the three-parameter exponential model and are represented by the curve in Figure 3.6. For comparison, the results for the constant-ΔP experiments are plotted in the same figure. The letters next to the points indicate the order of the permeation runs. Where two letters are next to the same point, the results for consecutive runs were identical. At 100 and 200 mm Hg upstream pressure the SO_2 permeability varied over a wide range. The results at 200 mm Hg were obtained over several hours and suggest

Figure 3.6 Pressure dependence of the SO_2 permeability of CTA/PA-59 from constant- and variable-ΔP experiments. The variable-ΔP data were correlated with the three-parameter exponential model (Eq. (2.24)), which is represented by the curve. The values of the parameters are given in Table 3.2. The letters next to the plotted points indicate the order in which the constant-ΔP permeation runs were performed. The order shows that the SO_2 permeability depended on time and previous conditioning of the membrane.

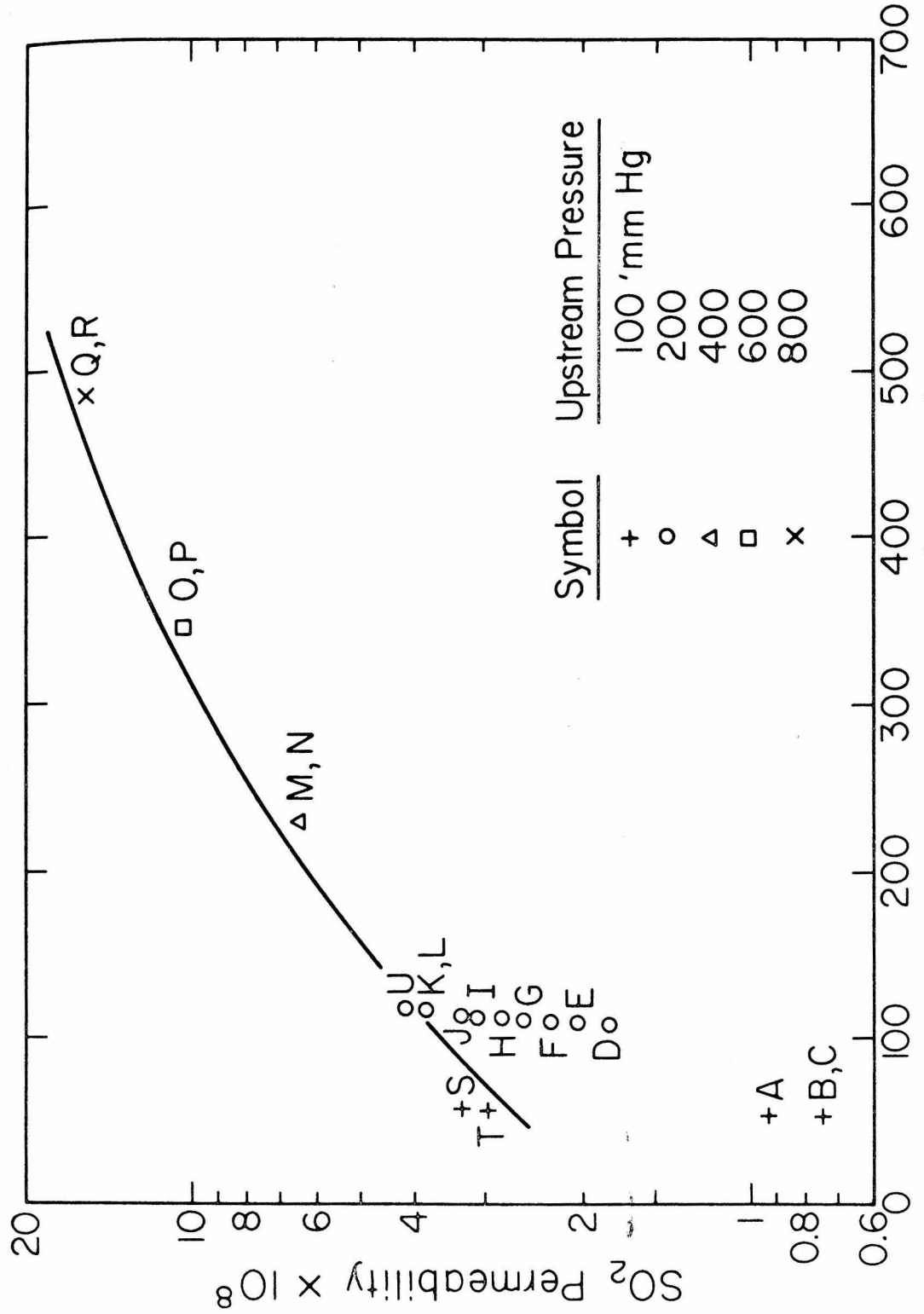
SO_2 Permeability x 10^8
Mean Pressure (mm Hg)
Symbol
Upstream Pressure
100 'mm Hg
200
400
600
800
+A
+B,C
+S
T+
U
K,L
J&I
H
G
F
E
D
M,N
O,P
Q,R

Figure 3.6

that the polymer chains were undergoing a slow change in orientation to accommodate more SO_2. At higher upstream pressures the rate of change was much faster so that no transient behavior was observed. After testing at 800 mm Hg upstream pressure,experiments were immediately rerun at 100 and 200 mm Hg, and higher values of the SO_2 permeability were obtained than previously. This confirms that the polymer structure changes according to the amount of SO_2 present.

Figure 3.6 shows that the highest results for the constant-ΔP experiments are close to the curve representing the variable-ΔP results. The points which fall far below the curve at 100 and 200 mm Hg upstream pressure illustrate the effect of conditioning the membrane. These data were taken after the membrane had spent three weeks in the permeation cell under vacuum. During this time volatile species were degassed and the polymer segments underwent changes in orientation which made the membrane less permeable. After the membrane was tested with SO_2 at the higher upstream pressures, the polymer structure returned to a more open configuration. These experiments show how sensitive the SO_2 permeability is to the previous exposure or conditioning of the membrane. The two methods of measurement yielded similar results when the polymer chains were in the same configuration.

Higher permeation rates can be achieved by operating a membrane at elevated pressure. Only CTA/PA-43 and CTA/PA-58 were adequate for testing at upstream pressures from 1 to 10 atm. The pressure

dependence of the N_2 permeability for these membranes is shown in Figure 3.7. For CTA/PA-43 the N_2 permeability increased linearly with pressure and returned to its initial value when the pressure was reduced. The performance of CTA/PA-58 was similar, except that the N_2 permeability did not return to its initial value at 1 atm after testing at 10 atm.

The pressure dependence of the N_2 permeability was unexpected because N_2 does not interact with the polymer. The pressure dependence may be caused by physical deformation of the membrane. A comparison of Figures 3.4 and 3.7 indicates that the SO_2 permeability has a much steeper pressure dependence than the N_2 permeability. This means that increasing the upstream pressure will favor SO_2 permeation over N_2 permeation and increase the selectivity for SO_2.

3.4.3 Results for Binary Mixtures

CTA/PA-43 and CTA/PA-58 were tested on the flow system with binary mixtures of SO_2 and N_2, and the results are given in Tables 3.3 and 3.4. The upstream and downstream pressures were 10 and 0.2 atm, respectively, and the temperature was 25-27 °C. All runs with the same number were performed on the same day. The flow rate refers to the gas mixture entering the upstream chamber of the permeation cell. SO_2 concentrations are given for the gas streams entering and leaving the upstream chamber and for the permeant stream. N_2 and SO_2 permeabilities were calculated from

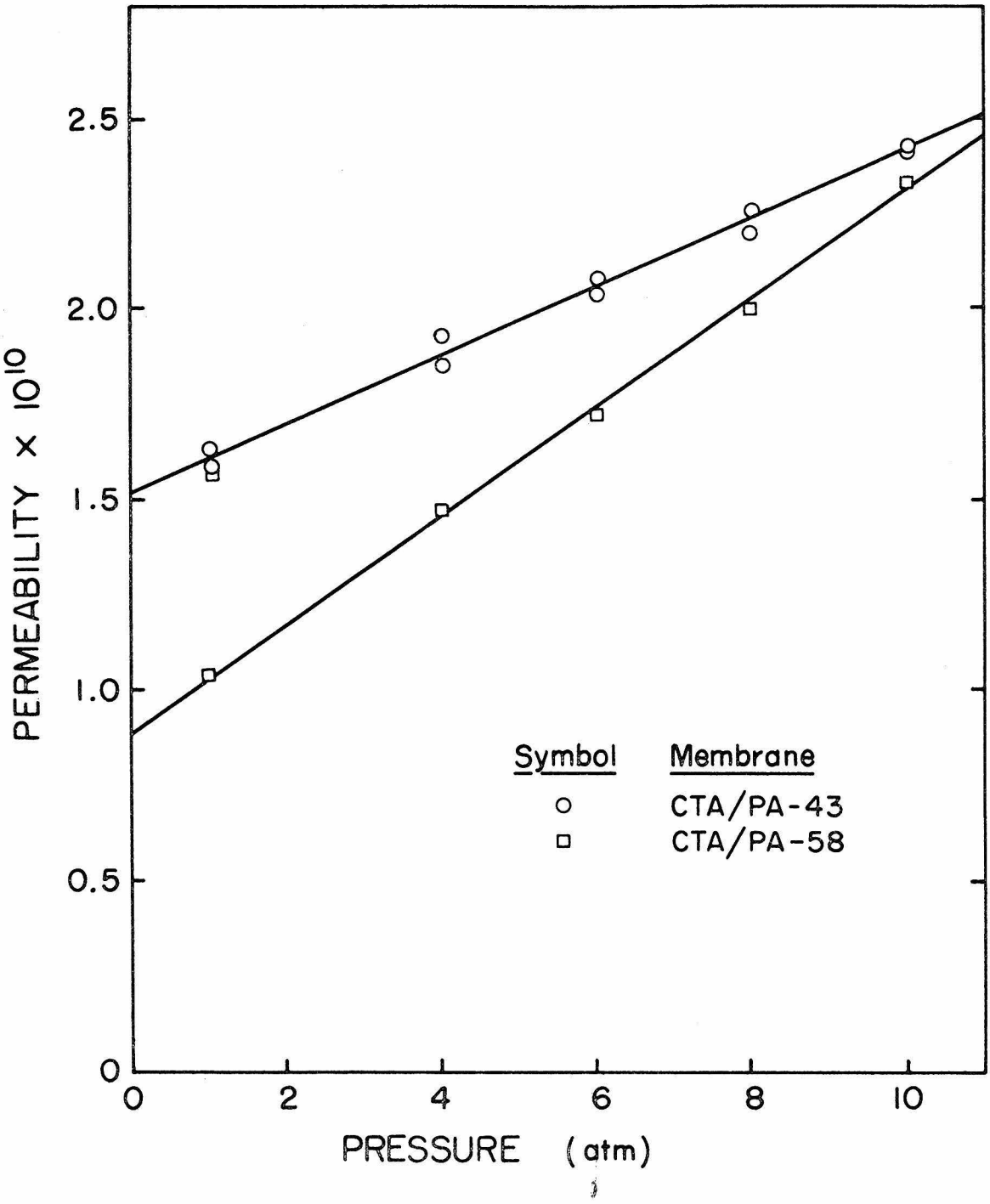

Figure 3.7 Pressure dependence of the N_2 permeability.

Table 3.3

Gas Separation Results for CTA/PA-43

Run	Flow Rate*	SO_2 Concentrations (%) Upstream Inlet	Upstream Outlet	Downstream	Permeation Rate**	$Q(N_2)^{\dagger}$	$Q(SO_2)^{\dagger}$	$\frac{Q(SO_2)}{Q(N_2)}$
4J	-	0	0	0	0.547	2.32	-	-
4K	2.0	2.02	1.86	35.2	1.09	3.05	136	44.6
4L	2.0	5.06	4.63	70.1	2.32	3.06	203	66.3
4M	1.0	9.94	7.71	87.9	4.31	2.36	261	111.
4N	2.0	9.94	8.55	91.0	5.15	2.12	288	136.
4O	4.0	9.94	9.05	92.3	6.11	2.16	326	151.
4P	-	100	100	100	12.78	-	596	-
5A	-	0	0	0	0.541	2.30	-	-
5B	4.0	0.110	0.108	1.95	0.606	2.53	71.1	28.1
5C	2.0	0.210	0.203	3.76	0.574	2.35	69.0	29.4
5D	2.0	0.523	0.500	9.50	0.608	2.34	76.4	32.6
5E	2.0	0.921	0.881	17.5	0.632	2.23	85.0	38.1
5F	-	0	0	0	0.531	2.26	-	-

* ℓ/min at 25°C, 1 atm

** $cm^3(STP)/(cm^2 \cdot min)$

† $\frac{cm^3(STP) \cdot cm}{cm^2 \cdot sec \cdot cm\ Hg} \times 10^{10}$

Table 3.4

Gas Separation Results for CTA/PA-58

Run	Flow Rate*	SO_2 Concentrations (%) Upstream Inlet	Upstream Outlet	Downstream	Permeation Rate**	$Q(N_2)$ †	$Q(SO_2)$ †	$\frac{Q(SO_2)}{Q(N_2)}$
N_2	-	0	0	0	0.295	3.21	-	-
1A	2.0	1.84	1.79	34.1	0.645	4.65	205	44
1B	2.0	4.70	4.19	65.9	1.17	4.45	279	63
1C	2.0	9.48	7.70	86.2	2.61	4.16	395	95
1D	-	0	0	0	0.311	3.38	-	-
4I	-	100	100	100	6.46	-	758	-
5G	-	0	0	0	0.218	2.36	-	-
5H	4.0	0.105	0.102	2.44	0.220	2.32	103	44.4
5I	2.0	0.204	0.194	4.45	0.226	2.34	97.0	41.5
5J	2.0	0.522	0.495	11.1	0.250	2.42	104	43.0
5K	2.0	0.921	0.872	21.3	0.284	2.44	138	56.6
5L	-	0	0	0	0.223	2.42	-	-

* ℓ/min at 25°C, 1 atm

** $cm^3(STP)/(cm^2 \cdot min)$

† $\frac{cm^3(STP) \cdot cm}{cm^2 \cdot sec \cdot cm\ Hg} \times 10^{10}$

the measured SO_2 concentrations and the permeation rate. The SO_2 concentration of the gas mixtures entering the permeation cell ranged from 0.1 to 10%. Pure N_2 at 10 atm and pure SO_2 at 1.1 atm were also tested for comparison with the results for the gas mixtures.

The results in the concentration columns indicate that the permeant stream is greatly enriched in SO_2. For example, CTA/PA-43 produced an enriched stream of 2% SO_2 from 0.1% SO_2 upstream, 35% from 2%, and over 90% from 10%. The performance of CTA/PA-58 was similar. The permeability results for N_2 and SO_2 suggest that there is some interaction between the two gases. The N_2 permeabilities of both membranes were enhanced when they were first tested with concentrated SO_2 mixtures and later returned to the values for pure N_2. The N_2 results for CTA/PA-58 are difficult to understand because the permeability of pure N_2 changed several times. The SO_2 permeability of the mixtures had the anticipated pressure dependence, though it was not as large as for pure SO_2 at the higher concentrations. This can be seen by comparing the SO_2 permeabilities for runs 40 and 4P in Table 3.3. The upstream partial pressures of SO_2 are nearly the same, but the permeability of pure SO_2 is almost twice as large as the permeability of SO_2 in the mixture.

To better understand how the SO_2 permeability was affected by the presence of N_2, experiments were run on CTA/PA-58 at different flow rates and upstream pressures while holding the SO_2 partial

pressure constant. The results are presented in Table 3.5. Increasing the flow rate increased the SO_2 permeability slightly, which means that there may have been some gas phase resistance or incomplete mixing in the upstream chamber. A much greater increase in the SO_2 permeability was achieved by reducing the partial pressure of N_2. This may be attributed to competition between the N_2 and SO_2 molecules for the absorption sites on the surface of the polymer. At lower N_2 partial pressures a larger fraction of the sites were occupied by SO_2 molecules and, consequently, the SO_2 permeability was closer to the value for pure SO_2. Another possible explanation is that at 10 atm upstream pressure the membrane was prevented from swelling as much as it did at lower pressures.

The above phenomena are illustrated in Figures 3.8 and 3.9 in which the permeability of pure SO_2 is compared with the permeability of SO_2 in the mixtures. The permeability of pure SO_2 was determined from constant-ΔP experiments on the manometric system, similar to those described previously for CTA/PA-59. The data were correlated with the three-parameter exponential model. The upstream and downstream partial pressure of SO_2 for each flow system run were then substituted into the model to obtain values for the SO_2 permeability, which are connected by the curves in Figures 3.8 and 3.9. Pure SO_2 at 1.1 atm was also tested on the flow system; the permeability data agreed well with those obtained on the manometric system. This means that the two systems were well calibrated.

Table 3.5

Effect of Upstream Pressure and Flow Rate on the SO_2 Permeability of CTA/PA-58

Run	Flow Rate*	Upstream Pressure	SO_2 Concentrations (%) Upstream Inlet	Upstream Outlet	Downstream	Permeation Rate**	$Q(N_2)^{\dagger}$	$Q(SO_2)^{\dagger}$	$\frac{Q(SO_2)}{Q(N_2)}$
4A	-	10	0	0	0	0.246	2.67	-	-
4B	1.0	10	9.94	7.26	86.1	2.06	3.30	333	101
4C	2.0	10	9.94	8.09	89.0	2.60	3.31	383	116
4D	4.0	10	9.94	8.90	91.0	3.05	3.21	413	129
4E	1.2	3	34.0	30.8	99^{+}	3.85	-	557	-
4F	0.8	2	54.9	48.8	99^{+}	4.05	-	547	-
4G	2.0	2	50.4	48.0	99^{+}	4.16	-	577	-
4H	2.0	3	32.3	30.2	99^{+}	3.90	-	581	-
4I	-	1.1	100	100	100	6.46	-	758	-

* ℓ/min at 25°C, 1 atm

** $cm^3(STP)/(cm^2 \cdot min)$

† $\frac{cm^3(STP) \cdot cm}{cm^2 \cdot sec \cdot cm\ Hg} \times 10^{10}$

Figure 3.8 Comparison of the permeability of pure SO_2 and the permeability of SO_2 with N_2 present for CTA/PA-43. The permeation data for pure SO_2 were obtained from constant-ΔP experiments on the manometric system and were correlated with the three-parameter exponential model (Eq. (2.24) with $Q_o = 4.71 \times 10^{-9}$, $\alpha = 9.50 \times 10^{-3}$, and $\beta = 1.59 \times 10^{-3}$). The curve connects the predicted values of the permeability of pure SO_2 for the upstream and downstream SO_2 partial pressures of N_2/SO_2 mixtures run on the flow system. The plotted points are data from Table 3.3 for the N_2/SO_2 mixtures and pure SO_2.

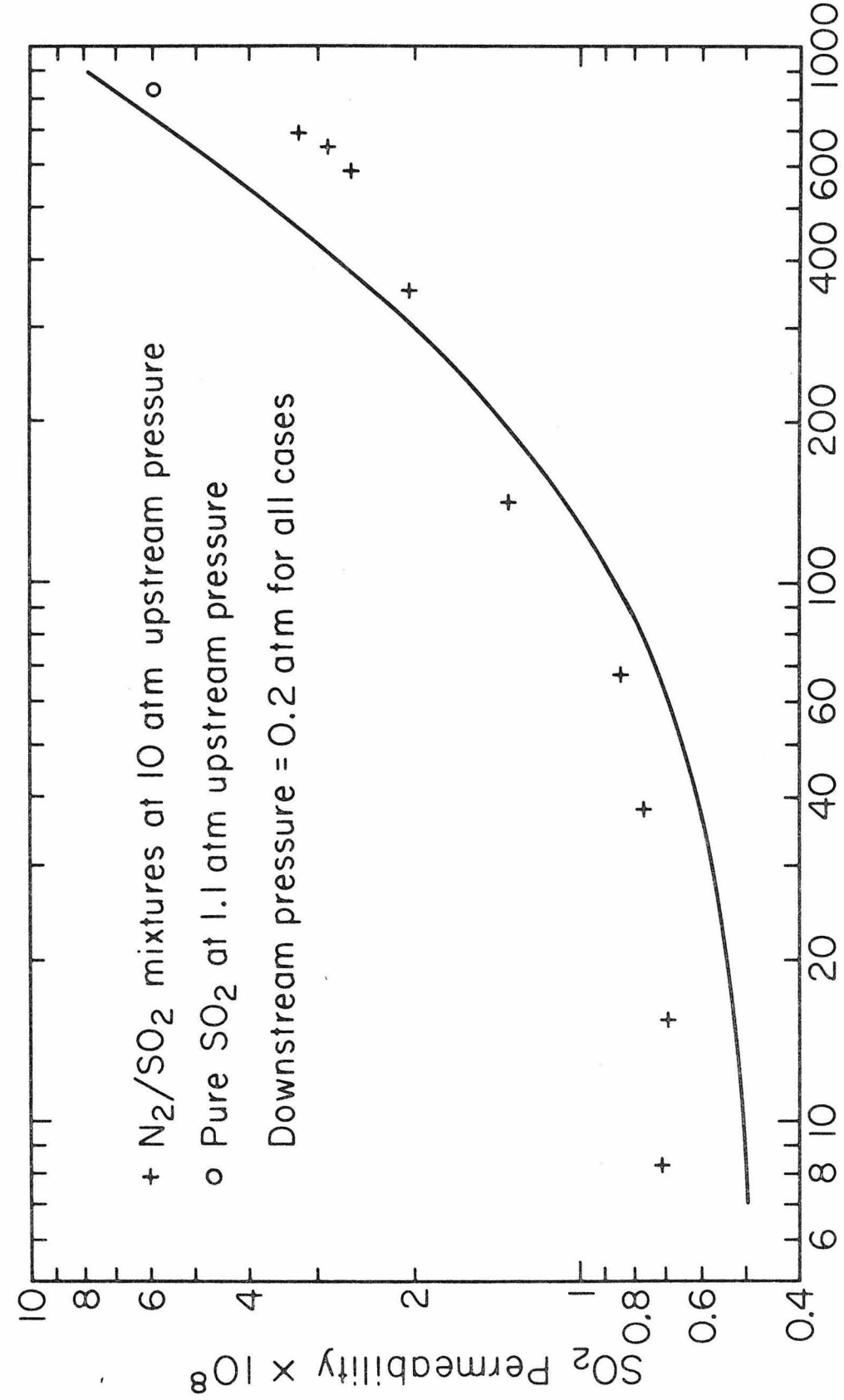
+ N_2/SO_2 mixtures at 10 atm upstream pressure
o Pure SO_2 at 1.1 atm upstream pressure
Downstream pressure = 0.2 atm for all cases
SO_2 Permeability x 10^8
Upstream Partial Pressure of SO_2 (mm Hg)
10
8
6
4
2
1
0.8
0.6
0.4
6
8
10
20
40
60
100
200
400
600
1000

Figure 3.8

Figure 3.9 Comparison of the permeability of pure SO_2 and the permeability of SO_2 with N_2 present for CTA/PA-58. The permeation data for pure SO_2 were obtained from constant-ΔP experiments on the manometric system and were correlated with the three-parameter exponential model (Eq. (2.24) with $Q_0 = 6.64 \times 10^{-9}$, $\alpha = 1.06 \times 10^{-2}$, and $\beta = 2.17 \times 10^{-3}$). The curve connects the predicted values of the permeability of pure SO_2 for the upstream and downstream SO_2 partial pressures of N_2/SO_2 mixtures run on the flow system. The plotted points are data from Tables 3.4 and 3.5 for the N_2/SO_2 mixtures and pure SO_2. The two clusters of points in the upper right corner of the figure show the effects of increasing the flow rate and reducing the upstream pressure.

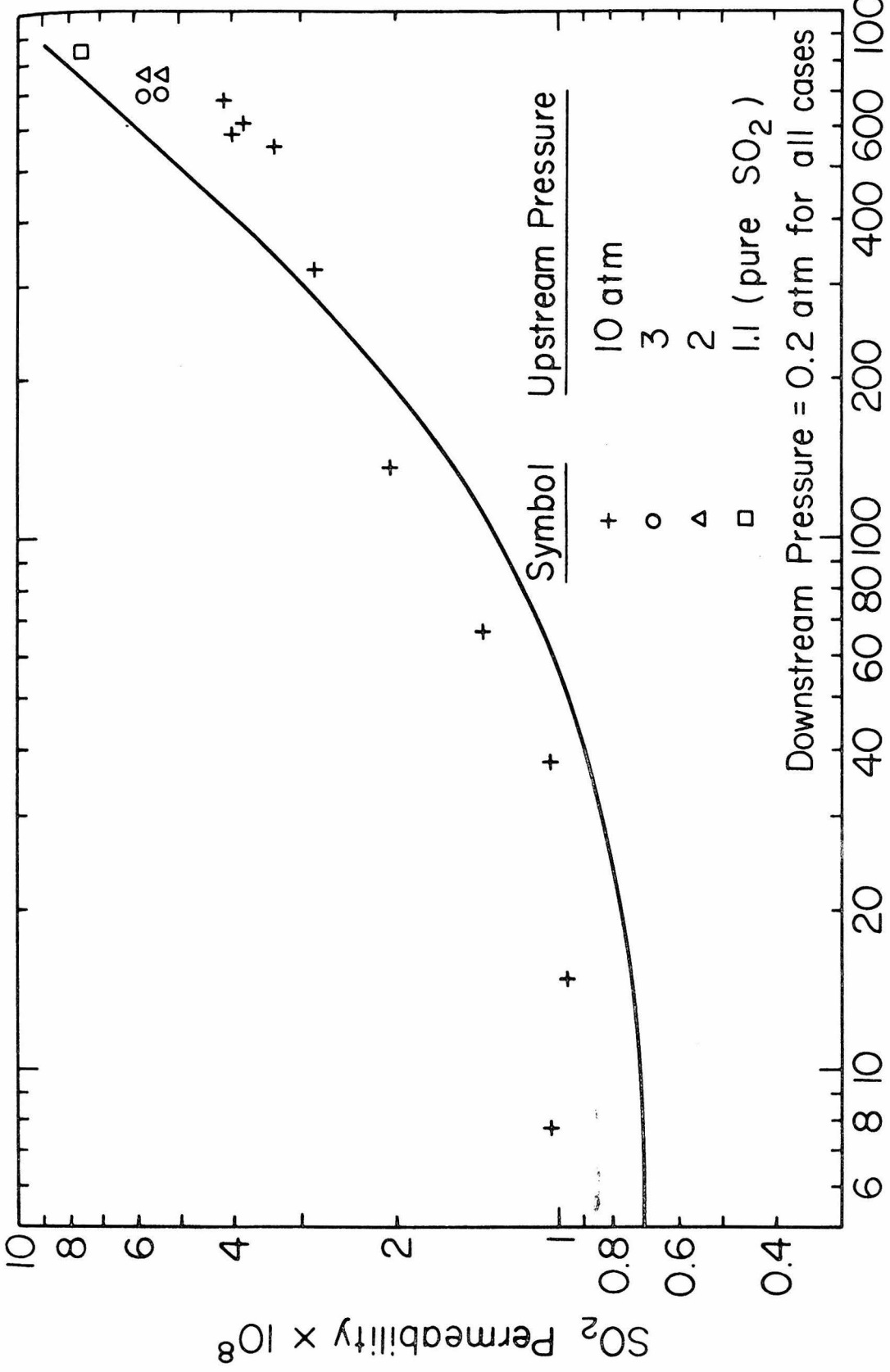
SO_2 Permeability x 10^8
10
8
6
4
2
1
0.8
0.6
0.4
6 8 10 20 40 60 80 100 200 400 600 1000
Upstream Partial Pressure of SO_2 (mm Hg)
Downstream Pressure = 0.2 atm for all cases
Symbol Upstream Pressure
+ 10 atm
o 3
Δ 2
□ 1.1 (pure SO_2)

Figure 3.9

At low SO_2 concentrations the results for the mixtures are higher than those for pure SO_2. The simultaneous permeation of N_2 may prevent the SO_2 molecules from becoming immobilized in clusters and thus enhance the SO_2 permeability. There is also greater uncertainty in the permeability of pure SO_2 at low pressures because of its dependence on the history of the membrane. Above 200 mm Hg upstream partial pressure the mixture data fall below the curve for pure SO_2. The logarithmic scale in these figures makes the effect look smaller than it actually is. At 600 mm Hg upstream partial pressure of SO_2, the SO_2 permeability of the mixture is only 60% of the value for pure SO_2. The effects of increasing the flow rate and reducing the upstream pressure are depicted by the two clusters of points in the upper right corner of Figure 3.9. Increasing the flow rate has almost negligible effect, but reducing the upstream pressure narrows the difference between the mixture data and the curve for pure SO_2. In conclusion, the SO_2 permeability of the mixtures can only be predicted qualitatively from the data for pure SO_2.

3.5 Discussion

3.5.1 Evaluation of Composite Membrane Performance

Ward and Neulander (1970) proposed five design goals for membranes for recovering SO_2 from combustion or smelter gases. These pertain to the SO_2 flux, selectivity, operating temperature, chemical stability, and life. The goal for the SO_2 flux was

4×10^{-3} cm^3 (STP)/(cm^2·sec·cm Hg). This was based on economic analysis which was not included in their report. Because of uncertainty in the SO_2 flux goal, it will only be used as a guideline in evaluating composite membrane performance. For the results in Table 3.2, the SO_2 fluxes in the limit of zero pressure ($Q_o(SO_2)/\ell$) fall below the goal by factors of 4-15. Higher SO_2 fluxes and selectivity can be achieved by operating the membranes at elevated pressures, which is why the flow system experiments were run at 10 atm upstream pressure.

The second goal was an SO_2/CO_2 permeability ratio of several hundred for applications involving combustion gases and at least 10 for smelter gas applications. The SO_2/CO_2 permeability ratios in the last column of Table 3.2 are less than 10, which means that these membranes would be limited to smelter gas and other applications involving high SO_2 concentrations. In practice, higher SO_2/CO_2 permeability ratios would be observed because of the pressure dependence of the SO_2 permeability.

The third goal was a minimum operating temperature of 100 °C. The polyacrylate elastomers have a service temperature range of -40-200 °C; however, their transport properties would change drastically at high temperatures. Typically, the permeability of the noncondensable species would increase much faster than that of the condensable species, resulting in a decline in selectivity. The chemical stability and life of the membranes have not been studied specifically; however, CTA/PA-43 and CTA/PA-58

performed well over a period of 10 months of intermittent testing at 1 and 10 atm pressure.

Ward and Neulander (1970) developed immobilized liquid membranes which were able to meet the SO_2 flux goal. However, the membranes were unable to withstand even 1 atm pressure difference across them. Operating a membrane at a pressure differential is essential for producing an enriched gas stream. The immobilized liquid membranes also had low SO_2/CO_2 permeability ratios.

Seibel and McCandless (1974) and Zavaleta and McCandless (1976) found that polyvinylidene fluoride membranes plasticized with sulfolane and sulfolene were effective in separating binary mixtures of N_2 and SO_2. The thickness of the membranes was about 2 mils, so gas fluxes were very low. No attempt was made to cast ultra-thin films to achieve higher fluxes. Gas permeabilities were determined with a permeation cell operated at atmospheric pressure downstream and elevated pressures upstream. Based on the results for pure gases, the SO_2/CO_2 permeability ratio was on the order of a hundred. This large ratio is misleading because of the relatively high pressure at which the SO_2 permeability was measured. At the low SO_2 partial pressures encountered in most applications, the SO_2 permeability would be much smaller because of its pressure dependence.

Direct comparison of the results of this study with those mentioned above is difficult because of differences in the experimental methods and the presentation of the results. Never-

theless, the overall performance of the CTA/PA composite membranes is qualitatively superior. None of the membranes meets all the design goals for large-scale industrial applications. Specific ways in which the performance of the composite membranes can be improved will be enumerated later.

3.5.2 Design of Membrane Gas Separators

A detailed discussion of the engineering aspects of the design of gas separators is beyond the scope of this study. To illustrate the applicability of this work, however, some design considerations will be presented here. References on this subject include Michaels and Bixler (1968), Stern and Walawender (1969), Ward and Neulander (1970), and McCandless (1972).

A good starting point in the design of gas separators is to look at how the downstream mole fraction, x_d, depends on the other parameters of the system. According to Equation (3.6), which was derived for a well-mixed permeation cell, x_d is a function of the upstream mole fraction, x_u, the pressure ratio, P_u/P_d, and the permeability ratio, $Q(SO_2)/Q(N_2)$. Equation (3.6) was solved for X_u = 0.001-0.2, P_u/P_d = 50, and $Q(SO_2)/Q(N_2)$ = 25-1000, and the results were plotted in Figure 3.10. The pressure ratio is the same as the one for most of the flow system experiments. x_d increases with x_u and $Q(SO_2)/Q(N_2)$ as expected; however, the rate of increase diminishes rapidly for large values of x_u. The dashed curve in Figure 3.10 connects the experimental results for

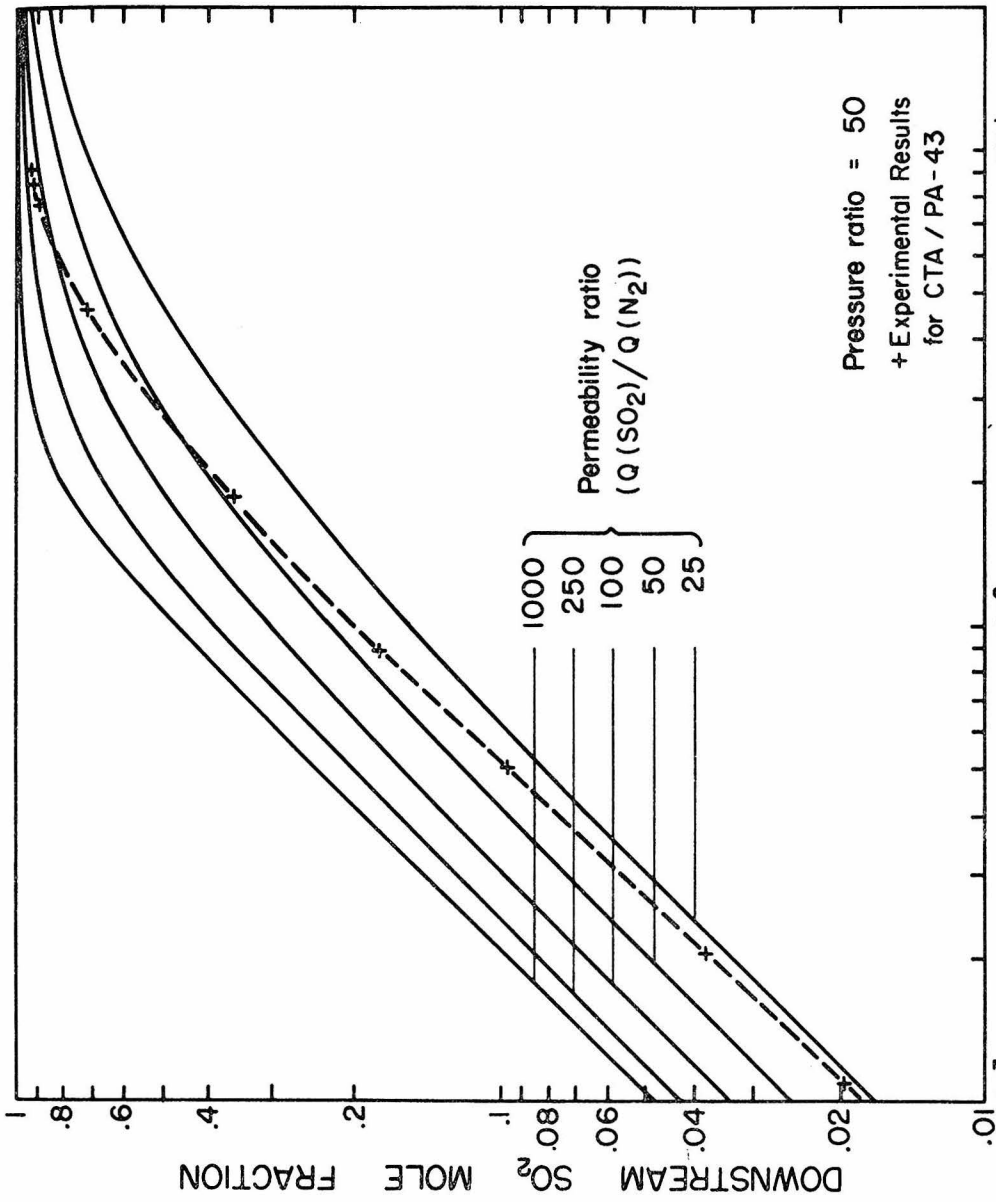

Figure 3.10 Dependence of the downstream SO_2 mole fraction on flow system parameters.

CTA/PA-43. It crosses over the other curves because of the pressure dependence of the permeability ratio.

To determine the effect of the pressure ratio, Equation (3.6) was resolved for P_u/P_d = 1000, and the results were plotted in Figure 3.11. Increasing the pressure ratio shifted all the curves upward. The effect was more pronounced for small x_u than large x_u. This means that the pressure ratio is equally as important as the membrane properties in determining the performance of a gas separator. Furthermore, the choice of the membrane and the pressure ratio depends on the application. For concentrated mixtures ($x_u > 0.1$) a membrane with low selectivity is adequate and the pressure ratio is not critical. For dilute mixtures both the selectivity and the pressure ratio must be large for optimum performance.

The two limiting flow configurations for gas separators are perfect mixing and no mixing (plug flow). Models for both cases have been described in the references cited at the beginning of this section. The most accurate models require numerical integration and are not as convenient for illustrative purposes. With additional assumptions or approximations, analytical expressions for the membrane area can be obtained. The membrane area required for a particular gas separator is an important quantity in determining the technical feasibility and capital cost of the membrane system.

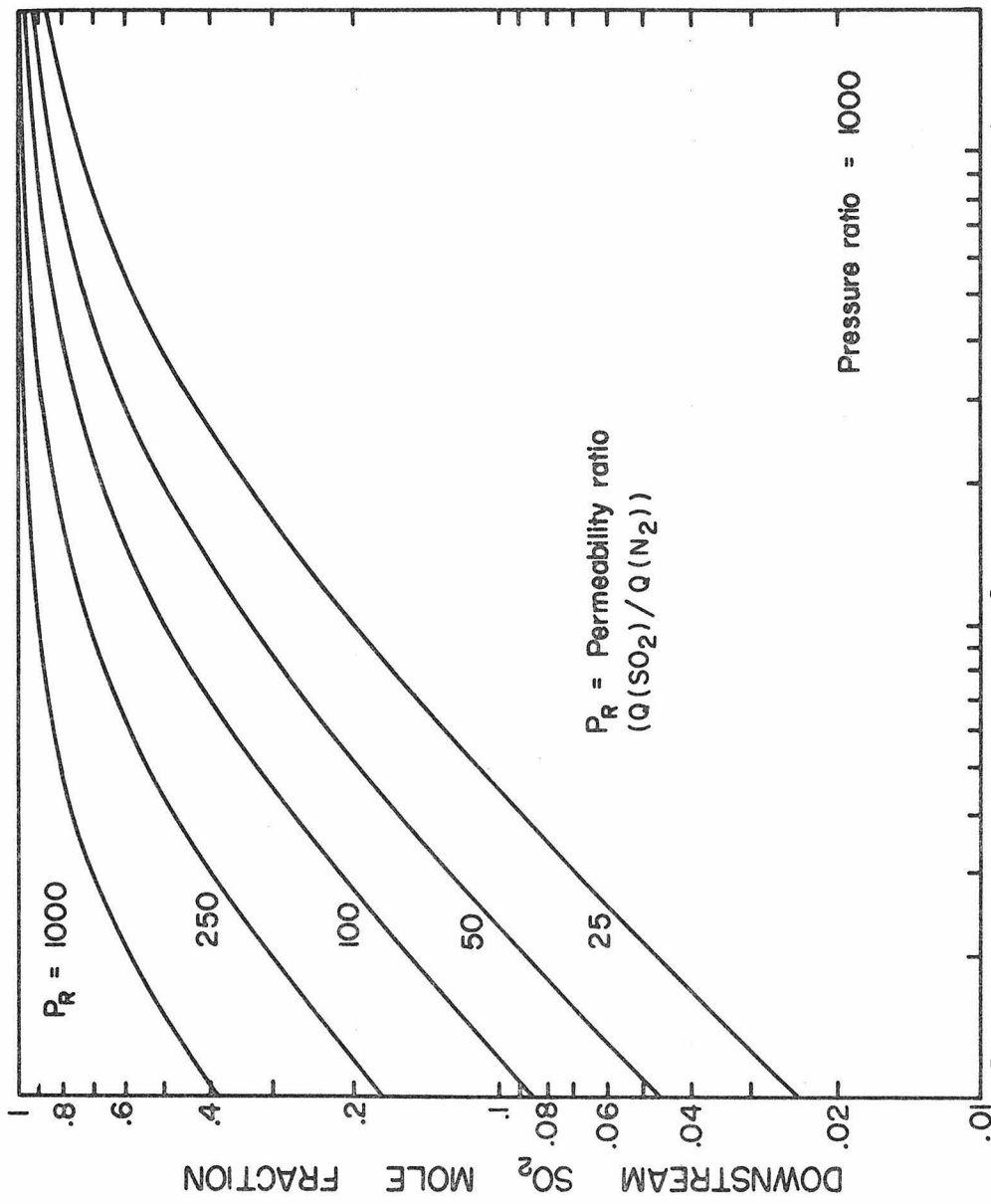

Figure 3.11 Dependence of the downstream SO_2 mole fraction on flow system parameters.

For the case of perfect mixing, the membrane area can be calculated exactly from the permeability results for the composite membranes. The nomenclature in Figure 3.1 and the results for CTA/PA-43 will be used in the following analysis. If $n_{u,in}$, $x_{u,in}$, $x_{u,out}$, P_d, and P_u are specified, then $n_{u,out}$, n_d, x_d, and A can be determined. $Q(SO_2)/Q(N_2)$ and x_d are found in Figure 3.10; $Q(SO_2)$ is given in Figure 3.8. From these quantities $Q(N_2)$ can be calculated. An expression for n_d is given in Equation (3.11), and A follows from Equation (3.10). A simple mass balance yields $n_{u,out}$.

The above procedure can be further simplified for low SO_2 concentrations, and a single analytical expression for A is obtained. Assuming that the upstream molar flow rate is constant,

$$n_{u,in} = n_{u,out} = n_u \tag{3.15}$$

From a mass balance on SO_2,

$$x_d n_d = n_u(x_{u,in} - x_{u,out}) \tag{3.16}$$

From Equations (3.5) and (3.10),

$$x_d n_d = \frac{AP_s}{RT_s} J(SO_2) \tag{3.17}$$

Equating (3.16) and (3.17) and solving for A yields

$$A = \frac{RT_s n_u (x_{u,in} - x_{u,out})}{P_s J(SO_2)} \tag{3.18}$$

Substituting for $J(SO_2)$ from (3.4) gives

$$A = \frac{RT_s n_u \ell (x_{u,in} - x_{u,out})}{P_s Q(SO_2)(x_{u,out} P_u - x_d P_d)} \tag{3.19}$$

If $x_d P_d$ is small compared to $x_{u,out} P_u$, then

$$A = \frac{RT_s n_u \ell}{P_s P_u Q(SO_2)} \left(\frac{x_{u,in}}{x_{u,out}} - 1 \right) \tag{3.20}$$

Equation (3.20) is the perfect-mixing result for low SO_2 upstream concentrations and negligible SO_2 back pressure.

To derive the membrane area for plug flow, suppose that permeation occurs in a long, narrow channel of length L and width W. An SO_2 mass balance over an incremental membrane area Wdz yields

$$n_u dx_u = \frac{-P_s J(SO_2) W dz}{RT_s} \tag{3.21}$$

Substituting for $J(SO_2)$ from (3.4) gives

$$n_u dx_u = \frac{-P_s Q(SO_2)(x_u P_u - x_d P_d) W dz}{RT_s \ell} \tag{3.22}$$

To find the total length or area, (3.22) must be rearranged and integrated:

$$\int_{x_{u,in}}^{x_{u,out}} \frac{-n_u dx_u}{(x_u P_u - x_d P_d)} = \int_0^L \frac{P_s Q(SO_2) W dz}{RT_s \ell} \tag{3.23}$$

For low SO_2 concentrations n_u and $Q(SO_2)$ are assumed to be constant; $x_d P_d$ must also be negligible or constant. Then, integration and rearrangement of (3.23) gives

$$A = WL = \frac{RT_s n_u \ell}{P_s P_u Q(SO_2)} \ln\left(\frac{x_{u,in} P_u - x_d P_d}{x_{u,out} P_u - x_d P_d}\right) \tag{3.24}$$

If $x_d P_d$ is small compared to $x_{u,out} P_u$,

$$A = \frac{RT_s n_u \ell}{P_s P_u Q(SO_2)} \ln\left(\frac{x_{u,in}}{x_{u,out}}\right) \tag{3.25}$$

Equation (3.25) is the plug flow result for low SO_2 upstream concentrations and negligible SO_2 back pressure.

The ratio of the areas for the limiting cases of perfect mixing and plug flow takes a simple form if the above models are used. Dividing Equation (3.20) by (3.25) yields

$$\frac{A_{\text{perfect mixing}}}{A_{\text{no mixing}}} = \left(\frac{x_{u,in}}{x_{u,out}} - 1 \right) / \ln \left(\frac{x_{u,in}}{x_{u,out}} \right) \qquad (3.26)$$

The two areas are the same in the limit of $x_{u,in}/x_{u,out} = 1$ and diverge for large values of $x_{u,in}/x_{u,out}$.

The above models may be used to estimate the membrane area for possible applications. For example, suppose that the composite membranes were being considered to control SO_2 emissions from a 500 MW power plant in which the flue gas rate is on the order of 10^6 CFM. The power plant burns high-sulfur coal, and the flue gas initially contains 1% SO_2. It is desired to remove 90% of the SO_2 with a membrane system. To simplify the calculations, suppose that the membranes have the same properties as CTA/PA-43 and are operated at the same temperature and upstream and downstream pressures as the flow system. Then, the following conditions apply:

$$n_{u,in} = 1.93 \times 10^4 \text{ mole/sec } (10^6 \text{ CFM at } 25\ ^\circ\text{C}, 1 \text{ atm})$$

$$\ell = 1.9 \times 10^{-5} \text{ cm}$$

$x_{u,in} = 0.01$

$x_{u,out} = 0.001$

$P_u = 760$ cm Hg (10 atm)

$P_d = 15.2$ cm Hg (0.2 atm)

The units in (3.20) and (3.25) are easily confused because of the cumbersome form of the permeability units. Correct results are obtained if cgs units are used throughout, including cm Hg for pressure.

The exact method for perfect mixing yields a membrane area of 24.7×10^6 ft^2. The approximate result from (3.20) is only 15.0×10^6 ft^2. The membrane area is underestimated by 40% when the SO_2 back pressure is neglected. A much lower downstream pressure is required to eliminate the effect of the SO_2 back pressure. From the plug flow model, Equation (3.25), the membrane area is only 3.8×10^6 ft^2. The no mixing flow configuration requires the smallest membrane area to perform this gas separation. The area for perfect mixing could be reduced by connecting several stages in series.

A membrane system having on the order of several million square feet of area is probably not practical to build and operate. Other studies have shown that packing densities of 100-500 ft^2/ft^3 are possible for small systems, but many engineering problems would be encountered in designing a large system. For example, it would be difficult to achieve a high packing density and at the same time

maintain a low pressure drop through the system. To meet the SO_2 flux design goal, the membranes were made very thin and were operated at high pressure. Both of these factors are likely to shorten membrane life, particularly when corrosive species and particulate matter are present in the gas. Running a membrane system at high pressure would also result in high operating costs.

3.5.3 Applications

Membrane performance was evaluated in terms of design goals for combustion and smelter gas cleaning. The composite membranes came close to meeting the SO_2 flux and selectivity goals when tested at 10 atm pressure. However, their physical durability may not be adequate for long periods of continuous operation with corrosive gases. Problems would be encountered in packaging the membranes and scaling up to industrial size.

Another area of application is in the measurement of ambient or source levels of SO_2. The composite membranes could be used to concentrate SO_2 in the atmosphere for more accurate measurement. For SO_2 sources the membranes would be effective in separating SO_2 from fine particles and other species which could damage or interfere with the detection equipment. Several recent publications have described analytical techniques utilizing membranes. Cheney et al. (1976) developed a method for detecting source levels of SO_2 using a piezo-electric detector and a dimethylsilicone membrane.

Treece et al. (1976) used polymeric interfaces for continuous SO_2 monitoring in process and power plant stacks. Jefferson and Khalafalla (1976) were able to measure SO_2 in the presence of SO_3 with a gas diffusion membrane electrode.

The composite membranes were intended for SO_2 applications but should not be limited to them. Further testing would probably reveal that they are selective to other gases and liquids. With recent advances in membrane technology, membranes are finding applications in new areas. In his review of the history of polymeric membranes, Michaels (1976) cited novel applications in the fields of biology and medicine. For example, membranes can control the release of drugs at specific sites in the body. Membranes have not yet realized their full potential.

3.5.4 Recommendations for Future Work

Several areas may be proposed for future work. More attention should be focused on optimizing membrane performance, which is determined by the properties of the microporous support and the layers of the composite film. The microporous media for supporting the thin films had several drawbacks and should be replaced with better materials. A substitute for cellulose triacetate is needed which has the same nonadhesive properties but higher permeability. The polyacrylate layer consisted of uncrosslinked polymer which had low physical strength and tended to flow under applied pressure. Improved physical properties could be achieved by curing the

polyacrylate layer before removing the composite film from the glass plate. If the composite films were stronger, they could be made even thinner to obtain higher transport rates.

Another area which needs further study is the characterization of the permeation of pure gases through the composite membranes. The SO_2 permeability exhibited a strong pressure dependence and other anomalous behavior which are not well understood. The three-parameter exponential model for correlating the SO_2 permeability results was shown to have the same mathematical form as the free volume theory. Other molecular theories should be investigated to see how well they can correlate the SO_2 permeation data. An explanation is needed for the unexpected pressure dependence of the N_2 permeability at elevated pressures.

A final area is the permeation of gas mixtures through the composite membranes. The results for binary mixtures of N_2 and SO_2 were not simply related to those for the pure gases. A molecular theory is needed in which interactions between the components of the mixture and the membrane are taken into account. Meanwhile, accurate predictions of membrane performance will depend on experimental results. The composite membranes should be tested with multicomponent mixtures before they are recommended for specific applications. Other gases such as O_2, CO_2, and H_2O will be present in many applications and may alter membrane performance and life.

3.6 Summary

Polyacrylate has properties which make it attractive for separating SO_2 from a mixture of gases. In Chapter 2 difficulties were encountered in preparing thin, durable membranes from this polymer. In this chapter a technique was described for casting 0.2-0.5 μm films of polyacrylate on glass plates on which a 0.002-0.005 μm layer of cellulose triacetate, a nonadhesive polymer, had been previously applied. The resulting two-layer films were easily removed from the glass and placed on microporous supports. This technique is applicable to any polymer which is completely soluble in a common organic or inorganic solvent.

Cellulose triacetate/polyacrylate composite membranes were made by the above procedure and initially tested with pure N_2, CO_2, and SO_2. The permeation of N_2 and CO_2 was nearly ideal. The N_2 permeability exhibited a slight pressure dependence when the upstream pressure was raised from 1 to 10 atm. The SO_2 permeability increased rapidly with increasing pressure and was well correlated with a three-parameter exponential model found empirically but having the same mathematical form as the free volume theory. This observation enables the determination of the free volume theory parameters from steady-state permeation experiments; the usual practice is to calculate them from unsteady absorption or desorption experiments. Constant- and variable-ΔP permeation experiments yielded similar results for the SO_2 permeability. At low SO_2 pressures the SO_2 permeability changed slowly with time and was

affected by conditioning of the membrane. There were indications that some SO_2 molecules became immobilized in clusters within the membrane.

The composite membranes were tested with binary mixtures of N_2 and SO_2 at 10 atm upstream pressure with a steady-state flow system. A typical membrane produced an enriched permeant stream of 2% SO_2 from 0.1% SO_2 upstream, 35% from 2%, and over 90% from 10%. The N_2 permeability was enhanced by the presence of SO_2, particularly at high SO_2 concentrations. At low SO_2 partial pressures the SO_2 permeability of the mixtures was higher than the permeability of pure SO_2 at the same pressure. The opposite was true at high SO_2 partial pressures where the presence of N_2 inhibited SO_2 permeation. The interactions between N_2 and SO_2 made it difficult to accurately predict the permeation rates of the mixtures from the data for the pure gases.

Membrane performance was evaluated in terms of design goals for combustion and smelter gas applications (Ward and Neulander, 1970). The composite membranes were able to meet the SO_2 flux goal when operated at 10 atm pressure. However, the selectivity and durability of the membranes were inadequate for large-scale industrial applications involving low SO_2 concentrations. The performance of the composite membranes was superior to that of membranes previously developed by others for SO_2 separations. The unique properties of the composite membranes make them attractive for instrumentation and other specialty applications.

Appendix A

IDENTIFICATION OF MATERIALS SELECTIVE TO SULFUR DIOXIDE

A comprehensive literature survey and testing of commercial samples was done to identify materials selective to sulfur dioxide. Only the most attractive materials were included in Table 1.3. The survey covered elastomers first and later was extended to other polymeric materials.

Samples of elastomers were obtained from DuPont and Rubbercraft. The materials from DuPont were coated on both sides of fabrics for added strength. The fabric materials included nylon, dacron, cotton, and fiber glass. The nominal thickness of the coated fabrics ranged from 6 to 32 mils. The elastomers from Rubbercraft were homogeneous sheets with no inner support. Table A.1 gives the supplier's code number and the nominal thickness for each elastomer.

Cellulosic polymers were also identified as potential candidates for SO_2 separations. Commercial samples of cellulosic polymers and other materials were obtained from Lustro Plastics Co., Thalco, Plastic Suppliers, Hercules Inc., and Nuclepore Corp. Table A.2 gives the supplier's code number and the nominal thickness for these materials.

Ethyl cellulose was received as a powder. Sample films were prepared by dissolving an appropriate amount of the polymer in a

Table A.1

List of Elastomers with Suppliers' Specifications

Elastomer	Supplier	Code Number	Thickness (in.)
Buna N on Nylon	Du Pont	BN-5027	0.006
Neoprene on Nylon	Du Pont	NN-5009	0.014
Polyacrylate on Dacron	Du Pont	AD-5776	0.010
Silicone on Glass	Du Pont	SG-5801	0.010
Hypalon on Cotton	Du Pont	HC-1477E	0.0075
Viton on Dacron	Du Pont	VD-0001	0.0085
Epichlorohydrin on Dacron	Du Pont	CD-0001	0.014
Ethylene/propylene on Dacron	Du Pont	DX-0001	0.032
Fluorosilicone on Dacron	Du Pont	FD-0005	0.017
Neoprene Sheet	Rubbercraft	R/C 19432	0.032
Buna N Sheet	Rubbercraft	R/C 5062	0.031
Natural Rubber Sheet	Rubbercraft	-	0.036

Table A.2

List of Polymeric Materials with Suppliers' Specifications

Material	Supplier	Code Number	Thickness (in.)
Cellophane (PT)	Lustro Plastics Co.	-	0.001
Poly(vinyl alcohol)	Thalco	-	0.003
Cellulose Diacetate	Plastic Suppliers	-	0.001
Cellulose Triacetate	Lustro Plastics Co.	Clear HP550	0.003
Cellulose Acetate-Butyrate	Lustro Plastics Co.	-	0.005
*Ethyl Cellulose	Hercules Inc.	N-Type	-
Polycarbonate	Nuclepore Corp.	N 000 CP6	0.00079

*Obtained in powder form

4:1 mixture of benzene and methanol and evaporating the resulting polymer solution to dryness in a petri dish. Film thickness ranged from 4 to 5 mils.

The permeability of the samples was determined according to the procedure described in Section 2.3.2. The apparatus underwent several modifications during the initial phase of this work and only the final design is given in Section 2.3.2. The first permeation cell was a Millipore Stainless 47 mm Pressure Holder (type XX40 047 00) which was difficult to seal gas tight. The accuracy of the permeability results was questionable because of leakage into the vacuum side of the cell and low permeation rates through the thick samples.

Table A.3 contains permeability data compiled from this study and the literature for selected elastomers. The data of this study were initially obtained by testing the elastomers with air and SO_2 using the Millipore filter holder. The air data were not included because of the leakage problem which affected the accuracy. Later, some elastomers were retested with N_2, CO_2, and SO_2 using the stainless steel cell described in Section 2.3.2. A range of values is given for the SO_2 permeability of some elastomers because of an observed pressure dependence.

Permeability data for other polymeric materials are given in Table A.4. Most of these were selected because of their large water permeabilities and were expected to have large SO_2 permeabilities, too. This was true for the cellulosic materials.

Permeability of Selected Elastomers

Elastomer	N_2	O_2	CO_2	SO_2	H_2O	Ref.
1a. Natural Rubber	8.4	23	131	-	300	6
1b. Natural Rubber Sheet	-	-	-	400-920	-	1
2. Polybutadiene	6.4	19	138	-	470	6
3. Poly(styrene-butadiene)	6.4	17	124	-	90-2000	6
4. Butyl Rubber	0.32	1.3	5.2	-	120	6
5a. Ethylene-Propylene	4.44	-	-	-	-	4
5b. Ethylene-Propylene on Dacron	-	-	-	120	-	1
6a. Poly(butadiene-acrylonitrile)	2.5	8.2	64	-	890	6
6b. Buna N on Nylon	1.8	-	39.7	800-1100	-	1
6c. Buna N Sheet	-	-	-	680	-	1
7. Epichlorohydrin on Dacron	-	-	-	710	-	1
8a. Neoprene	1.2	4.0	25	-	1300	6
8b. Neoprene Sheet	-	-	-	580	-	1
8c. Neoprene on Nylon	-	-	-	80	-	1
9a. Hypalon	1.16	2.8	20.8	-	-	2
9b. Hypalon on Cotton	-	-	-	380	-	1
10. Urethane	-	2.1	7.2	-	-	5
11. Polysulfide	-	0.29	3.2	-	4400	6
12a. Silicone	229	458	2470	11500	27500	3
12b. Silicone on Glass	-	-	-	10600	-	1
13a. Viton	-	2.2	5.1	-	-	5
13b. Viton on Dacron	-	-	-	17	-	1

Table A.3 (continued)

Elastomer	N_2	O_2	CO_2	SO_2	H_2O	Ref.
14. Polyacrylate on Dacron	2.04	-	46.7	1920-2370	-	1
15. Fluorosilicone on Dacron	-	-	-	2330	-	1

References: 1 - Present Study, 2 - Baer (1964), 3 - General Electric (1970), 4 - Hwang et al. (1974), 5 - Major and Kammermeyer (1962), 6 - Rogers et al. (1972)

Units of Permeability: $\frac{cm^3(STP)\cdot cm}{cm^2\cdot sec\cdot cm\ Hg} \times 10^{10}$

Table A.4

Permeability of Other Polymeric Materials

Polymer	N_2	O_2	CO_2	SO_2	H_2O	Ref.
1a. Cellophane	0.0005	0.002	0.006	-	12800	6
1b. Cellophane	-	-	-	< .02	-	1
2a. Poly(vinyl alcohol)	0.0008	0.003	0.01	-	13000	6
2b. Poly(vinyl alcohol)	-	-	-	undetectable	-	1
3. Cellulose Acetate	0.28	0.8	8.7	-	6800-15000	6
4. Cellulose Diacetate	-	-	-	110-200	-	1
5a. Cellulose Triacetate	0.17	1.0	5.7	-	-	4
5b. Cellulose Triacetate	0.20	-	5.6-7.0	270-470	-	1
6a. Cellulose Acetate-Butyrate	1.6	6.0	31.0	-	10000	6
6b. Cellulose Acetate-Butyrate	1.5	-	39.2	720-760	-	1
7a. Ethyl Cellulose	8.4	27.0	41.0	-	24000	6
7b. Type N-7	-	-	-	970-1080	-	1
7c. Type N-50	4.7	-	104	970-1080	-	1
7d. Type N-300	-	-	-	1040-1080	-	1
8a. Polycarbonate	0.3	1.5	8.5	-	1400	6
8b. Polycarbonate	-	-	-	10.7-11.2	-	1
9. Parylene N	0.046	0.24	1.3	11.3	-	7
10. Polyethylene Glycol	1.65	4.63	92.7	4100	-	8
11. Polyvinylidene Fluoride (w/18 wt % sulfolene)	0.093	-	2.0	430	-	9

References: 1 - Present Study, 4 - Hwang et al. (1974), 6 - Rogers et al. (1972), 7 - Union Carbide (1974), 8 - Ward (1972), 9 - Zavaleta and McCandless (1976)

Units of Permeability: Same as Table A.3.

Ethyl cellulose films prepared in this study were of the N-type, having 47.5-49.0% ethoxyl content. The number following the type in Table A.4 refers to the viscosity (cp) of a 4:1 toluene:ethanol solution containing 5 weight percent ethyl cellulose at 25 °C (Hercules, 1970). The SO_2 permeability of ethyl cellulose was unaffected by the molecular weight, as indicated by the data for different viscosities.

The last three materials in Table A.4 were included for their special properties. Parylene N films can be made as thin as 250 Å by a special vapor deposition process developed by Union Carbide (1974). Polyethylene glycol was prepared as an immobilized liquid membrane which utilized the mechanism of facilitated transport to enhance the selectivity for SO_2 (Ward, 1972). The polyvinylidene fluoride film was plasticized with sulfolene, a good SO_2 solvent, to improve its properties for SO_2 separations (Zavaleta and McCandless, 1976).

Appendix B

DETAILS OF MEMBRANE PREPARATION

The general procedures for making the polyacrylate, cellulose triacetate, and composite membranes were summarized in Sections 2.2.2 and 3.2. Additional information about the materials and methods are given in the following sections.

B.1 Polyacrylate Membranes

Polyacrylate films were prepared by dissolving Hycar 4041CG (B. F. Goodrich Chemical Company) in reagent grade toluene and casting the solution on mercury in a $3\frac{1}{2}$-in. diameter petri dish. After the toluene evaporated, a $2\frac{1}{4}$-in. diameter disk of Celgard 2500, a porous polypropylene film manufactured by Celanese, was laid on top of the thin polymer film followed by a piece of paper of slightly larger diameter. The thin film adhered to the Celgard and the paper and was easily removed from the mercury with a pair of tweezers. The stepwise procedure is given below:

(1) Select a desired thin film thickness.

(2) Calculate the amount of polymer required per 5 ml of solution.

(3) Weigh out enough polymer for 50 ml of solution.

(4) Cut the polymer into small pieces and place them in a 100-ml beaker.

(5) Add enough toluene to make 50 ml of solution. Cover the beaker with aluminum foil and wait 12 hr for dissolution.

(6) Stir the solution briefly to achieve a uniform distribution of polymer. Allow the solution to set several hours undisturbed so that particles and residue in the polymer can settle to the bottom.

(7) Prepare the mercury by washing it twice with toluene to remove the residue from previous membranes. Remove the toluene from the mercury with a pipet. Allow the remaining toluene to evaporate.

(8) Remove all the remaining residue and oxide from the mercury by dabbing the surface with old membranes, which have an adhesive surface.

(9) With a clean pipet, withdraw 5 ml of polymer solution from the 100-ml beaker without disturbing the residue at the bottom. Empty the pipet into the petri dish containing the mercury.

(10) Check for particles on the surface of the mercury. If there are any large ones, try to direct them to the edge of the petri dish with a stainless steel spatula.

(11) Cover the petri dish with a bell jar, allowing just a small space at the bottom for solvent vapors to escape. This slows down evaporation and prevents large particles from settling on the solution.

(12) Wait at least 5 hr for the toluene to evaporate. For films less than about 1.5 μm thick, interference patterns may be seen on the surface.

(13) Weigh a Celgard disk.

(14) Lay the Celgard disk gently on the surface of the polymer film.

(15) Lay a paper disk of slightly larger diameter over the Celgard disk. Press firmly against the polymer film to achieve good contact.

(16) Cut the polymer film away from the edge of the petri dish with a razor blade.

(17) Remove the paper and the membrane from the mercury with a pair of forceps.

(18) Cut the paper to the size of the Celgard disk and remove it.

(19) Weigh the Celgard disk with its attached polymer film and measure the diameter.

(20) Calculate the thickness of the polymer film.

This method works well for film thicknesses from 1 to 25 μm.

Another standard procedure was devised for sealing the membranes in the permeation cell. This was necessary to prevent damage to the fragile membranes. The procedure is given below:

(1) Place a $2\frac{1}{4}$-in. diameter piece of smooth, thin filter material over the porous stainless steel disk in the

permeation cell. Mitex teflon filters (Millipore Corporation) and Whatman 41 ashless paper filters were satisfactory for this purpose.

(2) Place the membrane on the filter.

(3) Place a stainless steel gasket (1.750 I.D. x 2.234 O.D. x .004 in.) on the membrane.

(4) Place a rubber gasket over the stainless steel gasket.

(5) Slowly apply a vacuum to the downstream side of the cell.

(6) Close the cell and tighten the bolts uniformly.

(7) Observe the pressure rise on the downstream side with air on the upstream side.

(8) If the pressure rise is much faster than expected, remove the membrane from the cell and seal the inner edge of the stainless steel gasket with nail polish.

(9) Determine the reduced membrane area for permeation.

(10) Reassemble the permeation cell as stated above.

(11) If the air permeation rate is the correct magnitude, evacuate the system and check for leaks.

(12) Test the membrane with N_2, CO_2, and SO_2.

B.2 Cellulose Triacetate Membranes

Cellulose triacetate (CTA) films were made by lowering a clean glass plate into a dilute solution of CTA in chloroform and withdrawing the plate at constant velocity. The films were removed from the plate by floating them onto a water surface. All the apparatus was

enclosed in a glove box, except for a variable-speed motor which was mounted on top to raise and lower the glass plate.

Solutions of 0.25 and 0.5 weight percent CTA were prepared by dissolving 4.5 and 9 gm, respectively, of CTA (type 436-80S, Eastman Chemical Products) in 1200 ml of reagent grade chloroform in 1500-ml beakers. To hasten the dissolution process, the solutions were agitated with a teflon-coated magnetic stirrer. The solutions were then filtered with a 150-ml Buchner funnel having a fritted glass disk of M pore size (Corning Glass Works). The 1500-ml beakers were covered with Saran wrap and aluminum foil to retard solvent evaporation.

Glass plates ($3\frac{1}{2} \times 3\frac{1}{2} \times \frac{1}{8}$ in.) which were made by the tin-float process were obtained from Pacific Universal Products. This type of glass is relatively free of surface imperfections and is smooth enough so that films as thin as 0.05 μm will not stick to the surface. The plates were washed with a nonabrasive liquid soap, rinsed with distilled water, blown dry with a stream of compressed N_2, and placed in the glove box where they were inspected for defects and dust particles. The plates were held in a spring-loaded Y-shaped holder which was connected to the variable-speed motor by a fine wire.

The CTA films were supported on 9.0-cm diameter MF-Millipore filters of 0.05 μm pore size and Celgard 3501 (Celanese), a porous hydrophilic polypropylene film. The support media were rinsed with distilled water and taped to a plexiglass block ($4 \times 4 \times \frac{7}{16}$

in.) which was lowered into a water bath ($7\frac{1}{4}$ in. in diameter x $3\frac{3}{4}$ in. deep) via two fine wires attached to the four corners of the block. The water bath rested on an aluminum tray so that it could be filled to overflowing with distilled water.

The mean thickness of the films was determined by weighing a known area. Prior to making the thin films, aluminum foil strips ($\frac{3}{8}$ x 1 in.) were weighed on a microbalance of six-decimal-place accuracy. Films that were not used for membranes were removed from the water bath with a pair of forceps, placed on these strips, and dried in an oven. After at least 12 hr had elapsed, the strips were weighed again. A mean thickness was calculated from the mass and dimensions of the thin film and the bulk density of CTA.

After the above preliminary steps were completed, CTA membranes were made by the procedure given below:

(1) Select a desired thin film thickness.

(2) From Equation (2.3) determine the solution concentration and withdrawal rate to make this thickness.

(3) Place a clean glass plate in the Y-shaped holder and suspend it over the appropriate CTA solution.

(4) Lower the glass plate into the solution until it is submerged up to, but not including, the holder. Allow a few minutes for the solution to become quiescent.

(5) Raise the plate at constant velocity. It dries almost instantaneously.

(6) Score the edges of the plate with a sharp razor blade.

(7) Measure the length and width of the film.

(8) Dip the plate in the water bath at a slight angle from the horizontal. The film will slowly detach from the plate and float on the surface of the water.

(9) Withdraw the plate from the water bath.

(10) Slowly raise the porous support from the bottom of the water bath until the thin film rests on it.

(11) Remove the plexiglass block completely from the water bath and allow the attached membrane to dry.

(12) Clean a stainless steel gasket (1.750 I.D. x 2.234 O.D. x .004 in.) and apply vacuum grease to one side.

(13) Lay the gasket on the membrane and press down firmly.

(14) Cut away excess membrane around the gasket with a razor blade.

(15) Follow the procedure given in the previous section for sealing the membrane in the permeation cell.

B.3 Composite Membranes

The procedure for making the composite membranes is nearly the same as that described in the previous section. Modifications to this procedure have been explained in Section 3.2.

Appendix C

CALIBRATION OF FLOW SYSTEM INSTRUMENTS

C.1 Pressure Gauges

The upstream pressure was measured with an Ashcroft test gauge (No. 1377-SS-XTISA) with a range of 0-200 psig. It was factory calibrated to an accuracy of 0.25% of full scale. The downstream pressure was measured with a Matheson vacuum test gauge (No. 63-5601) with a range of 760-0 mm Hg. Its accuracy was specified as 0.25% of full scale and was checked with an absolute manometer. The reading on the vacuum gauge was a differential pressure. To obtain the absolute pressure, the differential pressure had to be corrected for the prevailing atmospheric pressure.

C.2 Rotameters

The rotameters were calibrated with a wet test meter or a bubble flow meter, depending on the flow rate. The three rotameters on the upstream side of the permeation cell (Figure 3.3) had No. 603 tubes (Matheson Gas Products) and the one on the downstream side a No. 601 tube. Calibration curves were needed for pure N_2 and SO_2 and mixtures of the two gases at several pressures. The wet test meter could not be used if SO_2 was present because of the high solubility of SO_2 in water.

A method for doing all the calibration with pure N_2 was devised by applying the dimensional analysis of McCabe and Smith (1956). Their dimensional analysis of rotameters yields the following functional relationship:

$$\frac{\dot{m}}{D_f[m_f g \rho(1-\rho/\rho_f)]^{1/2}} = f\left(\frac{[m_f g \rho(1-\rho/\rho_f)]^{1/2}}{\mu}, \frac{D_t}{D_f}\right) \qquad (C.1)$$

where $\dot{m}$ is the mass flow rate, ρ and μ are the density and viscosity, respectively, of the fluid, and D_f, m_f, and ρ_f are the diameter, mass, and density, respectively, of the float. D_t is the diameter of the tube, which increases from the bottom to the top, and g is the gravitational constant. For low density gases ρ/ρ_f is small compared to 1 and may be neglected in Equation (C.1). D_t/D_f is related to the scale reading on the tube. For a single float (C.1) can then be simplified to give

$$\frac{\dot{m}}{\sqrt{\rho}} = f\left(\frac{\sqrt{\rho}}{\mu}, \text{scale reading}\right) \qquad (C.2)$$

Equation (C.2) implies that calibration curves of the form $\dot{m}/\sqrt{\rho}$ versus scale reading will be identical for gases which have the same value of $\sqrt{\rho}/\mu$.

The above result was verified by obtaining calibration data for N_2 and Ar at the same value of $\sqrt{\rho}/\mu$. Figure C.1 shows that the

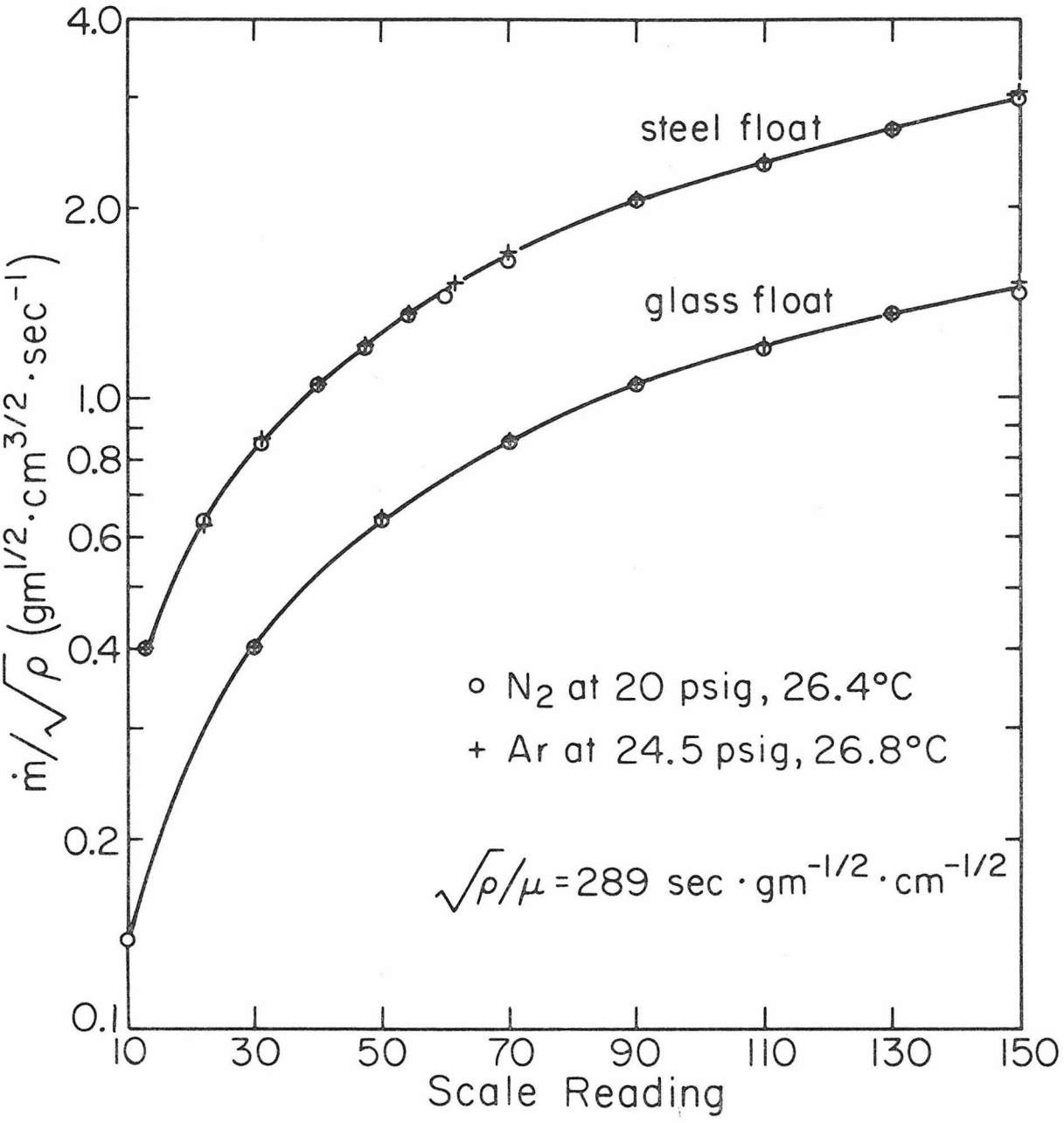

Figure C.1 Comparison of rotameter calibration curves for N_2 and Ar with $\sqrt{\rho}/\mu$ constant.

calibration curves are identical. Because the densities of N_2 and Ar are nearly the same, it may be argued that these results are not conclusive evidence that this approach will work for all gases. A second verification was done with N_2 and He in which the densities are quite different. Figure C.2 shows that there is only a slight discrepancy in the calibration curves. The He curve is lower than the N_2 curve because the He flow rate through the wet test meter exceeded its normal operating range.

To use this approach, density and viscosity data are needed for the pure gases and the mixtures. The density, ρ, is obtained from the gas law:

$$\rho = \frac{PM}{ZRT} \tag{C.3}$$

where Z is the compressibility factor. Z may be estimated from a universal correlation (Smith and Van Ness, 1959). Compressibility factor data for SO_2 were published by Kang et al. (1961). The density of the mixtures is given by

$$\rho_m = \frac{PM_m}{Z_m RT} \tag{C.4}$$

M_m and Z_m are obtained from a mole fraction weighting of the values for the pure gases.

Viscosity data for pure gases at 1 atm are available in the "Handbook of Chemistry and Physics" (Chemical Rubber Co., Cleveland,

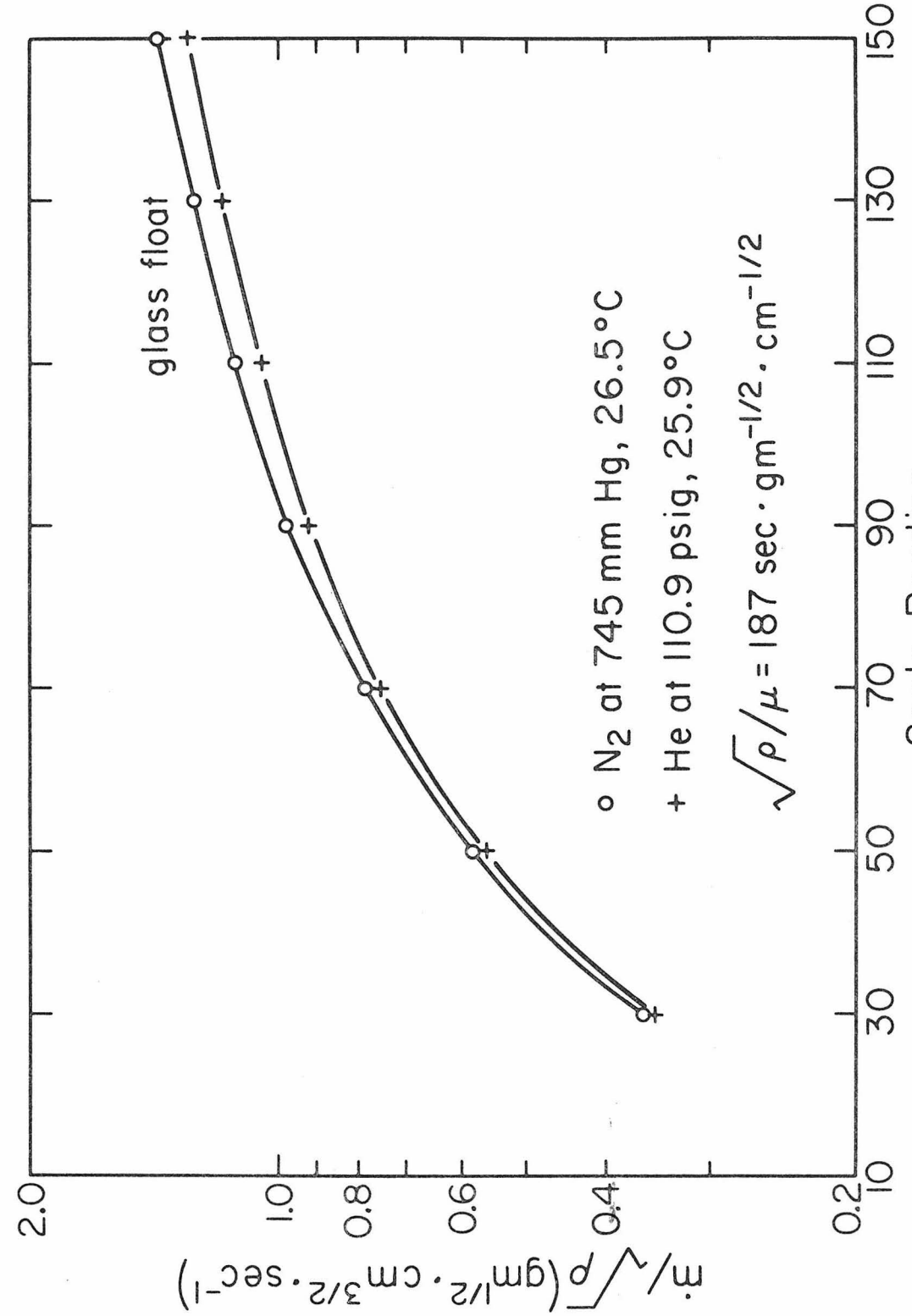

Figure C.2 Comparison of rotameter calibration curves for N_2 and He with $\sqrt{\rho}/\mu$ constant.

Ohio). The pressure dependence of the viscosity of noncondensable gases such as N_2, Ar, and He is negligible (Kestin and Wang, 1958). The viscosity of pure gases can also be calculated by using the theory of Hirschfelder et al. (1954). A method for calculating the viscosity of polar gas mixtures was given by Mason and Monchick (1962).

The viscosities of pure N_2 and SO_2 are 178.2 and 127.8 μp, respectively, at 26 °C and 1 atm. The method of Mason and Monchick combined with the formulas and tables of Hirschfelder et al. was used to calculate the viscosity of mixtures of N_2 and SO_2. The results of these rigorous calculations were less than 1% different from the values obtained with just a mole fraction weighting of the viscosities of the pure gases.

Mass flow rates were determined by substituting wet test meter data into the following equation:

$$\dot{m} = \frac{CMV(P-p_w)}{760RTt} \quad \text{(gm/sec)} \qquad \text{(C.5)}$$

where C = wet test meter calibration factor

M = molecular weight of gas

P = ambient pressure (mm Hg)

p_w = vapor pressure of water (mm Hg)at temperature T

R = gas constant = 0.08206 (l·atm)/(gm mole· °K)

T = temperature of wet test meter (°K)

t = time (sec) for volume V to flow through meter

V = volume of gas (l)

Numerous rotameter calibrations were done with N_2 at different pressures to cover all operating conditions of interest. For a single float the shape of the curves was the same, and curves for different pressures could be superimposed by shifting them vertically. This observation could greatly reduce the amount of data required for accurate rotameter calibration. For example, the data in Figures C.1 and C.2 would be well-correlated by a three-parameter exponential function of the form given in Equation (2.19). Only the pre-exponential parameter would change for different pressures. It could be determined from 2 or 3 experimental points, much fewer than the number required for an entire calibration curve.

C.3 Gas Chromatograph

The analysis of N_2/SO_2 mixtures was done with a Beckman GC-2A thermal conductivity gas chromatograph. The column (6 ft x $\frac{1}{8}$ in. O.D. teflon) was packed with Chromosil 310 (Supelco, Inc.) and operated at a helium flow rate of 50 ml/min. Moisture affected the performance of the column and, therefore, was excluded from gases to be analyzed. The current and temperature were set at 200 ma and 400 °C. A minimum of 12 hr were allowed for the instrument to stabilize.

The gas chromatograph was calibrated over the range of 0.05-100% SO_2 by diluting pure SO_2 and known SO_2 mixtures with pure N_2. Mixtures containing approximately 1 and 10% SO_2 were obtained

from Matheson Gas Products. Dilution was done with the previously calibrated rotameters. Gas samples were taken with a 1.0-ml gas-tight syringe (Hamilton) and injected into the gas chromatograph. Output from the gas chromatograph was displayed on a strip chart recorder. Calibration curves were plotted as SO_2 peak height versus SO_2 concentration. The calibration of the gas chromatograph varied slightly from one day to another. This required the use of a correction factor with the original calibration curves.

Appendix D

DATA ANALYSIS

D.1 Methods for Evaluating Permeability

Gas permeability may be evaluated by integral or differential methods. The integral approach was used in the derivation of Equations (2.8) and (2.10). The permeability is easy to calculate from these equations because $P(\ell)$ versus t data may be substituted directly into them.

The differential approach requires the determination of $dP(\ell)/dt$ by graphical or numerical methods. Van Amerongen (1946) computed the permeability with the following equation:

$$Q = \frac{dP(\ell)}{dt} \times \frac{V}{P(0)} \times \frac{\ell}{A} \times \frac{273}{T} \qquad (D.1)$$

where the variables are the same as those defined in Section 2.4.1. For Q to have the conventional cgs units, (D.1) must be divided by 76. Equation (D.1) applies for constant upstream pressure, P(0), constant downstream volume, V, and downstream pressures which are negligible compared to P(0).

An equation with more general applicability will be derived below. The gas flux through a membrane of area A is given by

$$J = \frac{1}{A}\frac{dn}{dt}\left(\frac{\text{moles}}{\text{cm}^2\cdot\text{sec}}\right) \qquad (D.2)$$

where dn/dt is the rate of change of the number of moles of gas in the downstream chamber. If n obeys the ideal gas law and $V = a + bP(\ell)$, then

$$\frac{dn}{dt} = \frac{[a+2bP(\ell)]}{RT} \frac{dP(\ell)}{dt} \tag{D.3}$$

In the units of $cm^3(STP)/(cm^2.sec)$, (D.2) becomes

$$J = \frac{273[a+2bP(\ell)]}{76AT} \frac{dP(\ell)}{dt} \tag{D.4}$$

An expression for Q is obtained by multiplying J by the membrane thickness and dividing by the pressure difference across the membrane:

$$Q = \frac{3.592\ell}{AT} \frac{[a+2bP(\ell)]}{[P(0)-P(\ell)]} \frac{dP(\ell)}{dt} \tag{D.5}$$

Equation (D.5) is analogous to Equation (2.10).

D.2 Description of Computer Programs

Data analysis was performed with computer programs written in the BASIC language. The programs were run on a PDP-10 time-sharing system which enabled the programmer to follow the execution. Data were entered through INPUT statements at appropriate points in the programs. Numerical integration was done with a library program based on Simpson's Rule.

Most of the programs employed either a quadratic or a Newton-Raphson convergence routine for finding the optimum values of certain parameters. The quadratic routine was suitable for two-parameter searches, only. It was based on the fact that a parabola can be drawn through any three points in a plane. The x-coordinate was an estimated value for one of the parameters. The y-coordinate was the relative error in a set of values for the other parameter which was calculated from the experimental data. The relative error was determined by finding the root-mean-square error and dividing it by the average of the calculated values. For three initial values of the first parameter, three values of the relative error for the second parameter were computed and a parabola was fit to the three points. The x-coordinate at which the first derivative was zero was selected as one of the new values for the first parameter. The other new values were chosen above and below this value by an amount based on the relative error. This routine converged if the initial values were near the minimum in the relative error. A provision was made for entering new values if the routine did not converge after five iterations.

To fit a curve to three or more parameters, a more sophisticated technique was needed. Stagner (1970) suggested a generalized Newton-Raphson method which takes a set of experimental data (x_1,y_1), $(x_2,y_2),\cdots,(x_m,y_m)$ and fits it to a curve $y = f(x)$ with parameters $p_1, p_2,\cdots, p_n$. A variance function, V, is defined which is a measure of the mean square error of the curve fit:

$$V = \sum_{i=1}^{m} \left[y_i - f(p_1, p_2, \cdots, p_n, x_i) \right]^2 \tag{D.6}$$

V is to be minimized subject to the following constraints:

(1) $p_j \geq 0$, $j = 1,2,\cdots,n$

(2) $m > n$.

If V is differentiable and the parameters initially have the approximate values $\xi_1, \xi_2, \cdots, \xi_n$, the minimum will be at $\xi_1+\delta_1$, $\xi_2+\delta_2, \cdots, \xi_n+\delta_n$ and is given by

$$\left[\frac{\partial V(\hat{p})}{\partial p_j} \right]_{\hat{p}=\hat{\xi}+\hat{\delta}} = 0, \quad j=1,2,\cdots,n \tag{D.7}$$

Expanding (D.7) in a Taylor series yields

$$\frac{\partial V(\hat{\xi})}{\partial p_j} + \sum_{k=1}^{n} \left[\frac{\partial^2 V(\hat{\xi})}{\partial p_j \partial p_k} \right] \delta_k + \frac{\partial \phi(\hat{\xi}^2)}{\partial p_j} = 0, \quad j=1,2,\cdots,n \tag{D.8}$$

With the following notation,

$$g_j = \frac{\partial V(\hat{\xi})}{\partial p_j} \tag{D.9}$$

$$G_{jk} = \frac{\partial^2 V(\hat{\xi})}{\partial p_j \partial p_k} \tag{D.10}$$

$$\Phi_j = \frac{\partial \phi(\hat{\xi}^2)}{\partial p_j} \tag{D.11}$$

(D.8) becomes

$$\hat{g} + G\hat{\delta} + \hat{\Phi} = 0 \tag{D.12}$$

Sovling for $\hat{\delta}$ yields

$$\hat{\delta} = -G^{-1}(\hat{g}+\hat{\Phi}) \tag{D.13}$$

Using ℓ as the iteration number, the iteration procedure for $\hat{\xi}$ is

$$\hat{\xi}_{\ell+1} = \hat{\xi}_{\ell}+\hat{\delta} = \hat{\xi}_{\ell}-G^{-1}\hat{g} \tag{D.14}$$

where the contribution of $\hat{\Phi}$ has been assumed negligible.

Several difficulties may be encountered with the Newton-Raphson method. The initial estimate of $\hat{\xi}$ must be close to the actual solution because there is no devise to force convergence from a poor approximation. The procedure breaks down if G is singular. Convergence may be slow if the data extend over several orders of magnitude. This last problem can be alleviated by dividing each term of Equation (D.6) by y_i.

The computer programs are described briefly below. Complete listings of the programs are included in the next section.

(1) QCALC - computes permeability from experimental data using Equation (2.10).

(2) DFIT2 - finds the optimum values of D_0 and γS in Equation (2.27) using the quadratic convergence routine.

(3) QFIT2 - finds the optimum values of Q_0 and γS in Equations (2.15) and (2.16) using the quadratic convergence routine on data for a single permeation run.

(4) QFIT3 - finds the optimum values of Q_0 and γS in Equations (2.15) and (2.16) using the quadratic convergence routine on data for several permeation runs at different upstream pressures.

(5) QFIT7 - finds the optimum values of Q_0, α, and β in Equation (2.24) using the Newton-Raphson convergence routine.

D.3 Computer Program Listings

QCALC

Data Input:

B2 = 2b (cu cm/mm Hg), constant in Equation (2.9)
D = membrane thickness (cm)
A = membrane area (sq cm)
TO = absolute temperature (°K)
VO = a (cu cm), constant in Equation (2.9)
PO = ambient pressure (mm Hg)
P = downstream pressure vector (mm Hg)
G = gauge pressure vector (mm Hg), upstream pressure minus ambient pressure
T = time vector (min or hr)

QCALC (cont.)

Data Output:
P = same as above
G = same as above
AVE P = average of upstream and downstream pressures
T = same as above
Q1 = permeability in cgs units

Listing:

```
2 DIM P(20), G(20), T(20), Q1(20), P2(20)
5 PRINT "WHAT IS B2 (CU CM/MM HG)";
10 INPUT B2
15 PRINT "DO YOU WISH TO CONTINUE";
20 INPUT A$
25 IF A$="NO" GO TO 999
30 PRINT "WHAT ARE D, A, TO, VO, AND PO";
35 INPUT D, A, TO, VO, PO
40 PRINT "WHAT IS P (MM HG)";
45 MAT INPUT P
50 PRINT "WHAT IS G (MM HG)";
55 MAT INPUT G
60 PRINT "WHAT IS T (MIN OR HR)";
65 MAT INPUT T
70 N=NUM
75 PRINT "T IN MIN OR HR";
80 INPUT C$
85 IF C$="MIN" THEN 95
90 C1=3600
92 GO TO 100
95 C1=60
100 C2=(273*D)/(C1*A*TO)
102 PRINT
104 PRINT
106 PRINT
108 PRINT
110 PRINT " P", " G", " AVE P", " T", "   Q1"
112 PRINT
114 PRINT P(1), G(1),, T(1)
116 FOR K=2 TO N
120 P1=PO+(G(K)+G(K-1))/2
122 P2(K)=P1/2+(P(K)+P(K-1))/4
125 C3=(B2*(P(K-1)-P(K))+(VO+B2*P1)*LOG((P1-P(K-1))/(P1-P(K))))
130 Q1(K)=C2*C3/76/(T(K)-T(K-1))
140 PRINT P(K), G(K), P2(K), T(K), Q1(K)
145 NEXT K
150 PRINT
152 PRINT
154 PRINT
156 PRINT
160 GO TO 15
999 END
```

DFIT2

Data Input: L = membrane thickness (cm)
P = upstream pressure vector (mm Hg)
T = time lag vector (sec)
S = vector of initial values of γS $(mm\ Hg)^{-1}$

Data Output: S = γS $(mm\ Hg)^{-1}$
DO = mean value of D_o (sq cm/sec)
RMS ERROR = root-mean-square error in D_o
REL ERROR = relative error in D_o

Listing:

```
5 DIM P(10), T(10), DO(10)
8 PRINT "WHAT IS L";
9 INPUT L
10 PRINT "WHAT IS P";
15 MAT INPUT P
20 PRINT "WHAT IS T";
25 MAT INPUT T
30 N=NUM
35 PRINT "ENTER THREE INITIAL VALUES FOR S";
40 MAT INPUT S
45 PRINT
47 PRINT
50 PRINT "ITERATION", "S", "DO", "RMS ERROR", "REL ERROR"
55 FOR I=1 TO 5
60 PRINT
65 FOR J=1 TO 3
70 DO(N+1)=0
75 FOR K=1 TO N
80 Y=EXP(S(J)*P(K))
81 Z=EXP(2*S(J)*P(K))
82 DO(K)=L*L*(4*Y-1+Z*(2*S(J)*P(K)-3))/(4*T(K)*(Y-1)**3)
85 DO(N+1)=DO(N+1)+DO(K)
90 NEXT K
95 DO(N+1)=DO(N+1)/N
100 F1=0
105 FOR L1=1 TO N
110 F1=F1+(DO(N+1)-DO(L1))**2
115 NEXT L1
120 DO(N+2)=SQR(F1/N)
125 E(J)=DO(N+2)/DO(N+1)
130 PRINT I, S(J), DO(N+1), DO(N+2), E(J)
```

DFIT2 (cont.)

```
135 NEXT J
140 XO=(S(1)**2-S(2)**2)*(S(1)-S(3))-(S(1)**2-S(3)**2)*(S(1)-S(2))
145 X3=((E(1)-E(2))*(S(1)-S(3))-(E(1)-E(3))*(S(1)-S(2)))/XO
150 X2=(E(1)-E(2)-X3*(S(1)**2-S(2)**2))/(S(1)-S(2))
155 S(2)=-X2/(2*X3)
160 S(1)=S(2)*(1-E(2))
165 S(3)=S(2)*(1+E(2))
170 NEXT I
172 PRINT
173 PRINT
175 PRINT "DO YOU WISH TO CHANGE THE VALUES OF S";
180 INPUT B$
185 IF B$="YES" GO TO 35
999 END
```

QFIT2

Data Input:
- TO = absolute temperature (°K)
- BO = b (cu cm/mm Hg), constant in Equation (2.9)
- D = membrane thickness (cm)
- AO = membrane area (sq cm)
- VO = a (cu cm), constant in Equation (2.9)
- PO = ambient pressure (mm Hg)
- P = downstream pressure vector (mm Hg)
- G = gauge pressure vector (mm Hg), upstream pressure minus ambient pressure
- T = time vector (min or hr)
- S = vector of initial values of γS $(\text{mm Hg})^{-1}$

Data Output:
- S = γS $(\text{mm Hg})^{-1}$
- Q = mean value of Q_o in cgs units
- RMS ERROR = root-mean-square error in Q_o
- REL ERROR = relative error in Q_o
- P = same as above
- G = same as above
- T = same as above
- Q2 = vector of calculated values of Q_o

QFIT2 (cont.)

Listing:

```
2 DIM P(20), G(20), T(20), Q(3,20), S(3), E(3)
5 PRINT "WHAT ARE TO (K) AND BO (CU CM/MM HG)";
10 INPUT TO, BO
15 PRINT "DO YOU WISH TO CONTINUE";
20 INPUT A$
25 IF A$="NO" GO TO 99999
30 PRINT "WHAT ARE D (CM), AO (SQ CM), VO (CU CM), AND PO (MM HG)";
35 INPUT D, AO, VO, PO
40 PRINT "WHAT IS P (MM HG)";
45 MAT INPUT P
50 PRINT "WHAT IS G (MM HG)";
55 MAT INPUT G
60 PRINT "WHAT IS T (MIN OR HR)";
65 MAT INPUT T
70 N=NUM
75 PRINT "T IN MIN OR HR";
80 INPUT C$
85 IF C$="MIN" THEN 95
90 C1=3600
92 GO TO 96
95 C1=60
96 C2=(273*D)/(76*C1*AO*TO)
100 PRINT "ENTER THREE INITIAL VALUES FOR S";
101 MAT INPUT S
102 PRINT
103 PRINT
104 PRINT "ITERATION", "S", "Q", "RMS ERROR", "REL ERROR"
105 FOR I=1 TO 5
106 PRINT
110 FOR J=1 TO 3
117 Q(J,N+1)=0
120 FOR K=2 TO N
125 P1=PO+(G(K)+G(K-1))/2
132 C3=EXP(S(J)*P1)
135 DEF FNY(X)=(VO+2*BO*X)/(C3-EXP(S(J)*X))
137 A=P(K-1)
139 B=P(K)
140 GOSUB 70700
145 Q(J,K)=(C2*S(J)*Z)/(T(K)-T(K-1))
148 Q(J,N+1)=Q(J,N=1)+Q(J,K)
150 NEXT K
155 Q(J,N+1)=Q(J,N+1)/(N-1)
157 F1=0
160 FOR L=2 TO N
165 F1=F1+(Q(J,N+1)-Q(J,L))**2
175 NEXT L
```

QFIT2 (cont.)

```
180 Q(J,N+2)=SQR(F1/(N-1))
181 E(J)=Q(J,N+2)/Q(J,N+1)
182 PRINT I, S(J), Q(J,N+1), Q(J,N+2), E(J)
185 NEXT J
188 X0=(S(1)**2-S(2)**2)*(S(1)-S(3))-(S(1)**2-S(3)**2)*(S(1)-S(2))
190 X3=((E(1)-E(2))*(S(1)-S(3))-(E(1)-E(3))*(S(1)-S(2)))/X0
195 X2=(E(1)-E(2)-X3*(S(1)**2-S(2)**2))/(S(1)-S(2))
205 S(2)=-X2/(2*X3)
210 S(1)=S(2)*(1-E(2))
215 S(3)=S(2)*(1+E(2))
220 NEXT I
225 PRINT
226 PRINT
227 PRINT "P", "G", "T", "Q2"
228 PRINT
230 PRINT P(1), G(1), T(1)
235 FOR Y=2 TO N
240 PRINT P(Y), G(Y), T(Y), Q(2,Y)
245 NEXT Y
246 PRINT
247 PRINT
248 PRINT
250 PRINT "DO YOU WISH TO CHANGE THE VALUES OF S";
255 INPUT B$
260 IF B$="YES" GO TO 100
280 GO TO 15
49999 STOP
70700 LET U(8)=0.0
70701 LET U(6)=0.0
70702 LET U(1)=B-A
70704 LET U(2)=1
70706 LET U(3)=FNY(A)+FNY(B)
70708 LET U(4)=U(1)/U(2)
70710 LET U(5)=U(4)/2
70712 LET U(7)=0.0
70714 FOR W=1 TO U(2)
70716 LET X=A+(W-1)*U(4)
70718 LET U(7)=U(7)+FNY(X+U(5))
70719 NEXT W
70720 LET Z+(U(3)+2*U(6)+4*U(7))*U(5)/3
70722 IF ABS(Z)<1.E-5 THEN 70744
70724 IF ABS((Z-U(8))/Z)<=1E-5 THEN 70736
70726 IF U(2)>1000 THEN 70736
70728 LET U(8)=Z
70730 LET U(6)=U(6)+U(7)
70732 LET U(2)=2*U(2)
70734 GO TO 70708
70736 IF Z=0 THEN 70744
```

QFIT2 (cont.)

```
70738 IF ABS((Z-U(8))/Z)<=1E-5 THEN 70744
70740 PRINT "SIMSON"  Z DID NOT CONVERGE TO RELATIVE ERROR OF 1E-5"
70742 PRINT "IN 10 ITERATIONS"
70744 RETURN
99999 END
```

QFIT3

Data Input:
- BO = b (cu cm/mm Hg), constant in Equation (2.9)
- D = membrane thickness (cm)
- AO = membrane area (sq cm)
- DO = number of data sets
- TO = absolute temperature (°K)
- VO = a (cu cm), constant in Equation (2.9)
- PO = ambient pressure (mm Hg)
- P = downstream pressure vector (mm Hg)
- G = gauge pressure vector (mm Hg), upstream pressure minus ambient pressure
- T = time vector (min)
- S = vector of initial values of γS $(\text{mm Hg})^{-1}$

Data Output:
- S = γS $(\text{mm Hg})^{-1}$
- Q = mean value of Q_o in cgs units
- RMS ERROR = root-mean-square error in Q_o
- REL ERROR = relative error in Q_o

Listing:

```
2 DIM H(20), C(20), R(20)
5 PRINT "WHAT IS BO (CU CM/MM HG)";
10 INPUT BO
15 PRINT "DO YOU WISH TO CONTINUE";
20 INPUT A$
25 IF A$="NO" GO TO 99999
26 PRINT "WHAT ARE D (CM) AND AO (SQ CM)";
27 INPUT D, AO
28 PRINT "HOW MANY SETS OF DATA";
29 INPUT DO
30 DIM P(10,20), G(10,20), T(10,20), Q(3,100)
31 NO=0
32 FOR M=1 TO DO
33 PRINT "WHAT ARE TO (K), VO (CU CM), PO (MM HG)";
34 INPUT F(M), V(M), O(M)
35 PRINT "WHAT IS P (MM HG)";
```

QFIT3 (cont.)

```
40 MAT INPUT H
42 PRINT "WHAT IS G (MM HG)";
44 MAT INPUT C
46 PRINT "WHAT IS T (MIN)";
48 MAT INPUT R
50 N(M)=NUM
52 FOR M1=1 TO N(M)
54 P(M,M1)=H(M1)
56 G(M,M1)=C(M1)
58 T(M,M1)=R(M1)
60 NEXT M1
62 NO=NO+N(M)-1
63 NEXT M
64 C2=(273*D)/(76*60*AO)
65 PRINT "ENTER THREE INITIAL VALUES FOR S";
70 MAT INPUT S
75 PRINT
77 PRINT
80 PRINT "ITERATION", "S", "Q", "RMS ERROR", "REL ERROR"
85 FOR I=1 TO 5
90 PRINT
95 FOR J=1 TO 3
100 Q(J,NO+1)=0
102 M3=1
105 FOR M2=1 TO DO
110 FOR K=2 TO N(M2)
115 P1=O(M2)+(G(M2,K)+G(M2,K-1))/2
120 C3=EXP(S(J)*P1)
125 DEF FNY(X)=(V(M2)+2*BO*X)/(C3-EXP(S(J)*X))
130 A=P(M2,K-1)
135 B=P(M2,K)
140 GOSUB 70700
145 Q(J,M3)=(C2*S(J)*Z)/(F(M2)*(T(M2,K)-T(M2,K-1)))
146 Q(J,NO+1)=Q(J,NO+1)+Q(J,M3)
147 M3=M3+1
150 NEXT K
152 NEXT M2
155 Q(J,NO+1)=Q(J,NO+1)/NO
157 F1=0
160 FOR L=1 TO NO
165 F1=F1+(Q(J,NO+1)-Q(J,L))**2
175 NEXT L
180 Q(J,NO+2)=SQR(F1/NO)
181 E(J)=Q(J,NO+2)/Q(J,NO+1)
182 PRINT I, S(J), Q(J,NO+1), Q(J,NO+2), E(J)
185 NEXT J
188 XO=(S(1)**2-S(2)**2)*(S(1)-S(3))-(S(1)**2-S(3)**2)*(S(1)-S(2))
190 X3=((E(1)-E(2))*(S(1)-S(3))-(E(1)-E(3))*(S(1)-S(2)))/XO
195 X2=(E(1)-E(2)-X3*(S(1)**2-S(2)**2))/(S(1)-S(2))
205 S(2)=-X2/(2*X3)
210 S(1)=S(2)*(1-E(2))
```

QFIT3 (cont.)

```
215 S(3)=S(2)*(1+E(2))
220 NEXT I
246 PRINT
247 PRINT
248 PRINT
250 PRINT "DO YOU WISH TO CHANGE THE VALUES OF S";
255 INPUT B$
260 IF B$="YES" GO TO 65
280 GO TO 15
49999 STOP
70700 LET U(8)=0.0
70701 LET U(6)=0.0
70702 LET U(1)=B-A
70704 LET U(2)=1
70706 LET U(3)=FNY(A)+FNY(B)
70708 LET U(4)=U(1)/U(2)
70710 LET U(5)=U(4)/2
70712 LET U(7)=0.0
70714 FOR W=1 TO U(2)
70716 LET X=A+(W-1)*U(4)
70718 LET U(7)=U(7)+FNY(X+U(5))
70719 NEXT W
70720 LET Z=(U(3)+2*U(6)+4*U(7))*U(5)/3
70722 IF ABS(Z)<1.E-5 THEN 70744
70724 IF ABS((Z-U(8))/Z)<=1E-5 THEN 70736
70726 IF U(2)>1000 THEN 70736
70728 LET U(8)=Z
70730 LET U(6)=U(6)+U(7)
70732 LET U(2)=2*U(2)
70734 GO TO 70708
70736 IF Z=0 THEN 70744
70738 IF ABS((Z-U(8))/Z)<=1E-5 THEN 70744
70740 PRINT "SIMSON:  Z DID NOT CONVERGE TO RELATIVE ERROR OF 1E-5"
70742 PRINT "IN 10 ITERATIONS"
70744 RETURN
99999 END
```

QFIT7

Data Input:
- P(L) = downstream pressure vector (mm Hg)
- P(0) = upstream pressure vector (mm Hg)
- Q = permeability vector (arbitrary units)
- A = initial value for Q_o (same units as Q)
- B = initial value for α $(mm\ Hg)^{-1}$, constant in Equation (2.24)
- C = initial value for β $(mm\ Hg)^{-1}$, constant in Equation (2.24)

QFIT7 (cont.)

Data Output:
- A = value of Q_o (same units as Q)
- B = value of α $(mm\ Hg)^{-1}$
- C = value of β $(mm\ Hg)^{-1}$
- REL ERROR = mean relative error in permeabilities calculated from model
- P(L) = same as above
- P(O) = same as above
- QX = same as Q above
- QC = vector of calculated values of permeability (same units as Q)
- REL ERROR = vector of relative error in QC

Listing:

```
4 DIM Y(3), F(3), V(3,3), S(3,3)
5 DIM L(100), H(100), D(100), Q(100), E(100)
10 PRINT "DO YOU WISH TO CONTINUE";
15 INPUT A$
20 IF A$="NO" GO TO 99999
25 PRINT "WHAT IS P(L) (MM HG)";
30 MAT INPUT L
35 PRINT "WHAT IS P(O) (MM HG)";
40 MAT INPUT H
45 PRINT "WHAT IS Q (E10)";
50 MAT INPUT D
55 N=NUM
60 PRINT "ENTER INITIAL VALES FOR A, B, C";
65 INPUT AO, BO, CO
70 PRINT
75 PRINT
80 PRINT "ITERATION", "A", "B", "C", "REL ERROR"
85 PRINT
90 FOR J=1 TO 1
95 MAT Y=ZER
100 MAT V=ZER
105 EO=0
110 FOR I=1 TO N
115 Z1=AO/(H(I)-L(I))
120 A=L(I)
125 B=H(I)
130 DEF FNA(X)=EXP(BO*X/(1+CO*X))
135 GOSUB 71450
140 Q(I)=Z1*Z
145 Z2=D(I)-Q(I)
150 E(I)=ABS(Z2)/D(I)
152 EO=EO+E(I)
155 Y(1)=Y(1)+2*Z2*Q(I)/AO/D(I)
```

QFIT7 (cont.)

```
160 DEF FNB(X)=(X/(1+CO*X))*EXP(BO*X/(1+CO*X))
165 GOSUB 71400
170 Y2=Z1*Z
175 Y(2)=Y(2)+2*Z2*Y2/D(I)
180 DEF FNC(X)=(-BO*X*X/(1+CO*X)**2)*EXP(BO*X/(1+CO*X))
185 GOSUB 71350
190 Y3=Z1*Z
195 Y(3)=Y(3)+2*Z2*Y3/D(I)
200 V(1,1)=V(1,1)+2*Q(I)*(2*Q(I)-D(I))/AO**2/D(I)
205 V(1,2)=V(1,2)+2*Y2*(2*Q(I)-D(I))/AO/D(I)
210 V(1,3)=V(1,3)+2*Y3*(2*Q(I)-D(I))/AO/D(I)
215 V(2,1)=V(1,2)
220 DEF FND(X)=EXP(BO*X/(1+CO*X))*(X/(1+CO*X))**2
225 GOSUB 71300
230 V4=Z1*Z
235 V(2,2)+V(2,2)+(-2*V4*Z2+2*Y2*Y2)/D(I)
240 DEF FNE(X)=-EXP(BO*X/(1+CO*X))*(X/(1+CO*X))**2
245 GOSUB 71250
250 V5=Z
255 DEF FNF(X)=-BO*EXP(BO*X/(1+CO*X))*(X/(1+CO*X))**3
260 GOSUB 71200
265 V5=(V5+Z)*Z1
270 V(2,3)=V(2,3)+(-2*V5*Z2+2*Y2*Y3)/D(I)
275 V(3,1)=V(1,3)
280 V(3,2)=V(2,3)
285 DEF FNG(X)=BO*BO*EXP(BO*X/(1+CO*X))*(X/(1+CO*X))**4
290 GOSUM 71150
295 V6=Z
300 DEF FNH(X)=2*BO*EXP(BO*X/(1+CO*X))*(X/(1+CO*X))**3
305 GOSUB 71100
310 V6=(V6+Z)*Z1
315 V(3,3)=V(3,3)+(-2*V6*Z2+2*Y3*Y3)/D(I)
320 NEXT I
325 EO=EO/N
330 PRINT J, AO, BO, CO, EO
335 MAT S=INV(V)
340 MAT F=S*Y
345 AO=AO+F(1)
350 BO=BO+F(2)
355 CO=CO+F(3)
356 PRINT J+1, AO, BO, CO
360 NEXT J
365 PRINT "DO YOU WISH TO CHANGE THE INITIAL VALUES";
370 INPUT B$
375 IF B$="YES" GO TO 60
380 PRINT
385 PRINT
390 PRINT "P(L)", "P(O)", "QX", "QC", "REL ERROR"
```

QFIT7 (cont.)

```
395 PRINT
400 FOR K=1 TO N
405 PRINT L(K), H(K), D(K), Q(K), E(K)
410 NEXT K
415 PRINT
420 PRINT
425 GO TO 10
49999 STOP
71100 LET U(8)=0.0
71102 LET U(6)=0.0
71104 LET U(1)=B-A
71106 LET U(2)=1
71108 LET U(3)=FNH(A)+FNH(B)
71110 LET U(4)=U(1)/U(2)
71112 LET U(5)=U(4)/2
71114 LET U(7)=0.0
71116 FOR W=1 TO U(2)
71118 LET X=A+(W-1)*U(4)
71120 LET U(7)=U(7)+FNH(X+U(5))
71122 NEXT W
71124 LET Z=(U(3)+2*U(6)+4*U(7))*U(5)/3
71126 IF ABS(Z)<1.E-5 THEN 71148
71128 IF ABS((Z-U(8))/Z)<1E-5 THEN 71140
71130 IF U(2)>1000 THEN 71140
71132 LET U(8)=Z
71134 LET U(6)=U(6)+U(7)
71136 LET U(2)=2*U(2)
71138 GO TO 71110
71140 IF Z=0 THEN 71148
71142 IF ABS((Z-U(8))/Z)<=1E-5 THEN 71148
71144 PRINT "SIMSON:  Z DID NOT CONVERGE TO RELATIVE ERROR OF 1E-5"
71146 PRINT "IN 10 ITERATIONS"
71148 RETURN
71150 LET U(8)=0.0
71152 LET U(6)=0.0
71154 LET U(1)=B-A
71156 LET U(2)=1
71158 LET U(3)=FNG(A)+FNG(B)
71160 LET U(4)=U(1)/U(2)
71162 LET U(5)=U(4)/2
71164 LET U(7)=0.0
71166 FOR W=1 TO U(2)
71168 LET X=A+(W-1)*U(4)
71170 LET U(7)=U(7)+FNG(X+U(5))
71172 NEXT W
71174 LET Z=(U(3)+2*U(6)+4*U(7))*U(5)/3
71176 IF ABS(Z)<1.E-5 THEN 71198
71178 IF ABS((Z-U(8))/Z)<=1E-5 THEN 71190
71180 IF U(2)>1000 THEN 71190
71182 LET U(8)=Z
```

QFIT7 (cont.)

```
71184 LET U(6)=U(6)+U(7)
71186 LET U(2)=2*U(2)
71188 GO TO 71160
71190 IF Z=0 THEN 71198
71192 IF ABS((Z-U(8))/Z)<=1E-5 THEN 71198
71194 PRINT "SIMSON:  Z DID NOT CONVERGE TO RELATIVE ERROR OF 1E-5"
71196 PRINT "IN 10 ITERATIONS"
71198 RETURN
71200 LET U(8)=0.0
711202 LET U(6)=0.0
71204 LET U(1)=B-A
71206 LET U(2)=1
71208 LET U(3)=FNF(A)+FNF(B)
71210 LET U(4)=U(1)/U(2)
71212 LET U(5)=U(4)/2
71214 LET U(7)=0.0
71216 FOR W=1 TO U(2)
71218 LET X=A+(W-1)*U(4)
71220 LET U(7)=U(7)+FNF(X+U(5))
71222 NEXT W
71224 LET Z=(U(3)+2*U(6)+4*U(7))*U(5)/3
71226 IF ABS(Z)< 1.E-5 THEN 71248
71228 IF ABS((Z-U(8))/Z)<=1E-5 THEN 71240
71230 IF U(2)>1000 THEN 71240
71232 LET U(8)=Z
71234 LET U(6)=U(6)+U(7)
71236 LET U(2)=2*U(2)
71238 GO TO 71210
71240 IF Z=0 THEN 71248
71242 IF ABS((Z-U(8))/Z)<1E-5 THEN 71248
71244 PRINT "SIMSON:  Z DID NOT CONVERGE TO RELATIVE ERROR OF 1E-5"
71246 PRINT "IN 10 ITERATIONS"
71248 RETURN
71250 LET U(8)=0.0
71252 LET U(6)=0.0
71254 LET U(1)=B-A
71256 LET U(2)=1
71258 LET U(3)=FNE(A)+FNE(B)
71260 LET U(4)=U(1)/U(2)
71262 LET U(5)=U(4)/2
71264 LET U(7)=0.0
71266 FOR W=1 TO U(2)
71268 LET X=A+(W-1)*U(4)
71270 LET U(7)=U(7)+FNE(X+U(5))
71272 NEXT W
71274 LET Z=(U(3)+2*U(6)+4*U(7))*U(5)/3
71276 IF ABS(Z)<1.E-5 THEN 71298
71278 IF ABS((Z-U(8))/Z)<=1E-5 THEN 71290
71280 IF U(2)>1000 THEN 71290
```

QFIT7 (cont.)

```
71282 LET U(8)=Z
71284 LET U(6)=U(6)+U(7)
71286 LET U(2)=2*U(2)
71288 GO TO 71260
71290 IF Z=0 THEN 71298
71292 IF ABS((Z=U(8))/Z)<=1E-5 THEN 71298
71294 PRINT "SIMSON:  Z DID NOT CONVERGE TO RELATIVE ERROR OF 1E-5"
71296 PRINT "IN 10 ITERATIONS"
71298 RETURN
71300 LET U(8)=0.0
71302 LET U(6)=0.0
71304 LET U(1)=B-A
71306 LET U(2)=1
71308 LET U(3)=FND(A)+FND(B)
71310 LET U(4)=U(1)/U(2)
71312 LET U(5)=U(4)/2
71314 LET U(7)=0.0
71316 FOR W=1 TO U(2)
71318 LET X=A+(W-1)*U(4)
71320 LET U(7)=U(7)+FND(X+U(5))
71322 NEXT W
71324 LET Z=(U(3)+2*U(6)+4*U(7))*U(5)/3
71326 IF ABS(Z)<1.E-5 THEN 71348
71328 IF ABS((Z-U(8))/Z)<=1E-5 THEN 71340
71330 IF U(2)>1000 THEN 71340
71332 LET U(8)=Z
71334 LET U(6)=U(6)+U(7)
71336 LET U(2)=2*U(2)
71338 GO TO 71310
71340 IF Z=0 THEN 71348
71342 IF ABS((Z-U(8))/Z)<=1E-5 THEN 71348
71344 PRINT "SIMSON:  Z DID NOT CONVERGE TO RELATIVE ERROR OF 1E-5"
71346 PRINT "IN 10 ITERATIONS"
71348 RETURN
71350 LET U(8)=0.0
71352 LET U(6)=0.0
71354 LET U(1)=B-A
71356 LET U(2)=1
71358 LET U(3)=FNC(A)+FNC(B)
71360 LET U(4)=U(1)/U(2)
71362 LET U(5)=U(4)/2
71364 LET U(7)=0.0
71366 FOR W=1 TO U(2)
71368 LET X=A+(W-1)*U(4)
71370 LET U(7)=U(7)+FNC(X+U(5))
71372 NEXT W
71374 LET Z=(U(3)+2*U(6)+4*U(7))*U(5)/3
71376 IF ABS(Z)<1.E-5 THEN 71398
71378 IF ABS((Z-U(8))/Z)<=1E-5 THEN 71390
71380 IF U(2)>1000 THEN 71390
71382 LET U(8)=Z
```

QFIT7 (cont.)

```
71384 LET U(6)=U(6)+U(7)
71386 LET U(2)=2*U(2)
71388 GO TO 71360
71390 IF Z=0 THEN 71398
71392 IF ABS((Z-U(8))/Z)<=1E-5 THEN 71398
71394 PRINT  "SIMSON:  Z DID NOT CONVERGE TO RELATIVE ERROR OF 1E-5"
71396 PRINT "IN 10 ITERATIONS"
71398 RETURN
71400 LET U(8)=0.0
71402 LET U(6)=0.0
71404 LET U(1)=B-A
71406 LET U(2)=1
71408 LET U(3)=FNB(A)+FNB(B)
71410 LET U(4)=U(1)/U(2)
71412 LET U(5)=U(4)/2
71414 LET U(7)=0.0
71416 FOR W=1 TO U(2)
71418 LET X=A+(W-1)*U(4)
71420 LET U(7)=U(7)+FNB(X+U(5))
71422 NEXT W
71424 LET Z=(U(3)+2*U(6)+4*U(7))*U(5)/3
71426 IF ABS(Z)<1.E-5 THEN 71448
71428 IF ABS((Z-U(8))/Z)<=1E-5 THEN 71440
71430 IF U(2)>1000 THEN 71440
71432 LET U(8)=Z
71434 LET U(6)=U(6)+U(7)
71436 LET U(2)=2*U(2)
71438 GO TO 71410
71440 IF Z=0 THEN 71448
71442 IF ABS((Z-U(8))/Z)<=1E-5 THEN 71448
71444 PRINT "SIMSON:  Z DID NOT CONVERGE TO RELATIVE ERROR OF 1E-5"
71446 PRINT "IN 10 ITERATIONS"
71448 RETURN
71450 LET U(8)=0.0
71452 LET U(6)=0.0
71454 LET U(1)=B-A
71456 LET U(2)=1
71458 LET U(3)=FNA(A)+FNA(B)
71460 LET U(4)=U(1)/U(2)
71462 LET U(5)=U(4)/2
71464 LET U(7)=0.0
71466 FOR W=1 TO U(2)
71468 LET X=A+(W-1)*U(4)
71470 LET U(7)=U(7)+FNA(X+U(5))
71472 NEXT W
71474 LET Z=(U(3)+2*U(6)+4*U(7))*U(5)/3
71476 IF ABS(Z)<1.E-5 THEN 71498
71478 IF ABS((Z-U(8))/Z)<=1E-5 THEN 71490
71480 IF U(2)>1000 THEN 71490
71482 LET U(8)=Z
```

QFIT7 (cont.)

```
71484 LET U(6)=U(6)+U(7)
71486 LET U(2)=2*U(2)
71488 GO TO 71460
71490 IF Z=0 THEN 71498
71492 IF ABS((Z-U(8))/Z)<=1E-5 THEN 71498
71494 PRINT "SIMSON:  Z DID NOT CONVERGE TO RELATIVE ERROR OF 1E-5"
71496 PRINT "IN 10 ITERATIONS"
71498 RETURN
99999 END
```

REFERENCES

Agrawal, J. P., and Sourirajan, S. (1970). High flux freeze-dried cellulose acetate reverse osmosis membranes as microporous barriers in gas permeation and separation. J. Appl. Polymer Sci., 11, 1303.

Baer, E., Ed. (1964). "Engineering Design for Plastics," pp. 682-86. Reinhold, New York.

Barrer, R. M., and Fergusson, R. R. (1958). Diffusion of benzene in rubber and polythene. Trans. Faraday Soc., 54, 989.

Cadotte, J. E., and Rozelle, L. T. (1972). In situ-formed condensation polymers for reverse osmosis membranes. U.S. Department of the Interior, Office of Saline Water Research and Development Report, Contract 14-30-2883, North Star Research and Development Institute.

Carnell, P. H. (1965). Preparation of thin polymer films. J. Appl. Polymer Sci., 9, 1863.

Carnell, P. H. and Cassidy, H. G. (1961). The preparation of membranes. J. Polymer Sci., 55, 233.

Cheney, J., Norwood, T., and Homolya, J. (1976). The detection of source levels of sulfur dioxide using a piezo-electric detector and permeation membrane. Anal. Lett., 9, 557.

Crank, J. (1953). A theoretical investigation of the influence of molecular relaxation and internal stress on diffusion in polymers. J. Polymer Sci., 11, 151.

Crank, J., and Park, G. S., Eds. (1968a). "Diffusion in Polymers." Academic Press, New York.

Crank, J., and Park, G. S. (1968b). Methods of measurement. Chap. 1 in "Diffusion in Polymers," ed. by J. Crank and G. S. Park. Academic Press, New York.

Daynes, H. A. (1920). Diffusion through a rubber membrane. Proc. Roy. Soc., A97, 286.

Felder, R. M., Spence, R. D., and Ferrell, J. K. (1975). Permeation of sulfur dioxide through polymers. J. Chem. Eng. Data, 20, 235.

Fels, M., and Li, N. N. (1974). Separation of hydrocarbons by selective permeation through polymeric membranes. In "Permeability of Plastic Films and Coatings to Gases, Vapors, and Liquids," pp. 357-73. Ed. by H. B. Hopfenberg. Plenum Publishing Corp., New York.

Frisch, H. L. (1957). The time lag in diffusion. J. Phys. Chem., Wash. 61, 93.

Fujita, H. (1968). Organic vapors above the glass transition temperature. Chap. 3 in "Diffusion in Polymers," ed. by J. Crank and G. S. Park. Academic Press, New York.

Fujita, H., Kishimoto, A., and Matsumoto, K. (1960). Concentration and temperature dependence of diffusion coefficients for systems polymethyl acrylate and N-alkyl acetates. Trans. Faraday Soc., 56, 424.

General Electric (1970). "General Electric Permselective Membranes." Medical Development Operation, Chemical and Medical Division, Schenectady, N.Y.

Hercules (1970). "Ethyl Cellulose - Properties and Uses." Polymers Department, Hercules Inc., Wilmington, Del.

Hirschfelder, J. O., Curtiss, C. F., and Bird, R. B. (1954). "Molecular Theory of Gases and Liquids." Wiley, New York.

Hwang, S.-T., and Kammermeyer, K. (1974). Effect of thickness on permeability. In "Permeability of Plastic Films and Coatings to Gases, Vapors, and Liquids." pp. 197-205. Ed. by H. B. Hopfenberg. Plenum Publishing Corp., New York.

Hwang, S.-T., and Kammermeyer, K. (1975). "Membranes in Separations, Techniques of Chemistry Vol.VII," ed. by A. Weissberger. Wiley, New York.

Hwang, S.-T, Choi, C. K., and Kammermeyer, K. (1974). Gaseous transfer coefficients in membranes. Separ. Sci., 9, 461.

Industrial Environmental Research Laboratory - RTP (1977). "Annual Report." Office of Research and Development, U.S. Environmental Protection Agency, Research Triangle Park, N.C.

Jefferson, R. H., and Khalafalla, S. E. (1976). Gas diffusion membrane electrode to determine sulfur dioxide in presence of sulfur trioxide. U.S. Bur. Mines, Rep. Invest. (RI 8200).

Juliano, P. C., and Ward, W. J., III (1972). Block copolymer membrane for separating polar contaminants from gaseous mixtures. U.S. Patent 3,653,180.

Kang, T. L., Hirth, L. J., Kobe, K. A., and McKetta, J. J. (1961). Pressure-volume-temperature properties of sulfur dioxide. J. Chem. Eng. Data, 6, 220.

Kestin, J., and Wang, H. E. (1958). Viscosity of five gases: Re-evaluation. Trans. Am. Soc. Mech. Engrs., 80, 11.

Lange, S. A., and Evdokimova, Zh. A. (1970). Solubility of sulfur dioxide in sulfolane and in sulfolene solutions in sulfolane. Neftepererab. Neftekhim. (Moscow), 3, 27.

Lesky, J. S., and Fuest, R. W. (1972). Process for removal of acidic materials from fluids. U.S. Patent 3,646,594.

Levich, V. G. (1962). "Physiochemical Hydrodynamics." Prentice-Hall, Englewood Cliffs, N.J.

Li, N. N., and Long, R. B. (1970). Plasticizing effect of permeates on membrane permeation and separation. In "Progress in Separation and Purification," Vol. 3, pp. 153-89. Ed. by E. S. Perry and C. J. Van Oss. Wiley, New York.

Loeb, S., and Sourirajan, S. (1964). The preparation of high-flow semi-permeable membranes for separation of water from saline solutions. U. S. Patent 3,133,132.

Long, F. A., and Richman, D. (1960). Concentration gradients for diffusion of vapors in glassy polymers and their relation to time dependent diffusion phenomena. J. Am. Chem. Soc., 82, 513.

Lonsdale, H. K., Riley, R. L., Lyons, C. R., and Carosella, D. P., Jr. (1971). Transport in composite reverse osmosis membranes. In "Membrane Processes in Industry and Biomedicine," pp. 101-22. Ed. by M. Bier, Plenum Press, New York.

McCabe, W. L., and Smith, J. C. (1956). "Unit Operations of Chemical Engineering," pp. 235-38. McGraw-Hill, New York.

McCandless, F. P. (1972). Separation of binary mixtures of CO and H_2 by permeation through polymeric films. Ind. Eng. Chem., Process Des. Dev., 11, 470.

Machin, D., and Rogers, C. E. (1972). Free volume theories for penetrant diffusion in polymers. Makromol. Chem., 155, 269.

Major, C. J., and Kammermeyer, K. (1962). Gas permeability of plastics. Modern Plastics, Vol. 39, No. 11, 135.

Mason, E. A., and Monchick, L. (1962). Transport properties of polar-gas mixtures. J. Chem. Phys., 36, 2746.

Matson, S. L., Herrick, C. S., and Ward, W. J., III (1977). Progress on the selective removal of hydrogen sulfide from gasified coal using an immobilized liquid membrane. Ind. Eng. Chem., Process Des. Dev., 16, 370.

Meares, P. (1958). Diffusion of allyl chloride in polyvinyl acetate. Part II. The transient state of permeation. J. Polymer Sci., 27, 405.

Meares, P. (1965). Transient permeation of organic vapors. J. Appl. Polymer Sci., 9, 917.

Michaels, A. S. (1976). Synthetic polymeric membranes: Practical applications - past, present and future. Pure Appl. Chem., 46, 193.

Michaels, A. S., and Bixler, H. J. (1968). Membrane permeation: Theory and practice. In "Progress in Separation and Purification," pp. 143-86. Ed. by E. S. Perry. Interscience, New York.

Pasternak, R. A., Schimscheimer, J. F., and Heller, J. (1970). A dynamic approach to diffusion and permeation measurements. J. Polymer Sci.: Part A-2, 8, 467.

Perkins, H. C. (1974). "Air Pollution," pp. 46-48. McGraw-Hill, New York.

Petropoulos, J. H., and Roussis, P. P. (1974). A discussion of theoretical models of anomalous diffusion of vapors in polymers. In "Permeability of Plastic Films and Coatings to Gases, Vapors, and Liquids." pp. 219-32. Ed. by H. B. Hopfenberg. Plenum Publishing Corp., New York.

Ponder, W. H., Stern, R. D., and McGlamery, G. G. (1976). SO_2 control technologies - commercial availabilities and economics. Presented at the Third Annual International Conference on Coal Gasification and Liquefaction: What Needs to be Done Now? Pittsburgh, Pa., Aug. 3-5.

Riley, R. L., Lonsdale, H. K., Lyons, C. R., and Merten, U. (1967). Preparation of ultrathin reverse osmosis membranes and the attainment of theoretical salt rejection. J. Appl. Polymer Sci., 11, 2143.

Riley, R. L., Hightower, G. R., and Lyons, C. R. (1973). Thin-film composite membrane for single-stage seawater desalination by reverse osmosis. Appl. Polymer Symp. No. 22, 255.

Riley, R. L., Hightower, G. R., Lyons, C. R., and Tagami, M. (1974). Thin-film composite membrane performance in a spiral wound single-stage reverse osmosis seawater pilot plant. In "Permeability of Plastic Films and Coatings to Gases, Vapors, and Liquids," pp. 375-88. Ed. by H. B. Hopfenberg. Plenum Publishing Corp., New York.

Riley, R. L., Fox, R. L., Lyons, C. R., Milstead, C. E., Seroy, M. W., and Tagami, M. (1976). Spiral-wound poly(ether/amide) thin-film composite membrane systems. Desalination, 19, 113.

Rogers, C. E. (1965). Transport through polymers with a gradient of inhomogeneity. J. Polymer Sci., C10, 93.

Rogers, C. E., Stannett, V., and Szwarc, M. (1957). Permeability valves - permeability of gases and vapors through composite membranes. Ind. Eng. Chem., 49, 1933.

Rogers, C. E., Fels, M., and Li, N. N. (1972). Separation by permeation through polymeric membranes. In "Recent Developments in Separation Science," Vol. 2, pp. 107-55. Ed. by N. N. Li. Chemical Rubber Co., Cleveland, Oh.

Schell, W. J. (1975). Separation of coal hydrogasification gases by permselective membranes. Am. Chem. Soc., Div. Fuel Chem., Prepr., 20, 253.

Seibel, D. R., and McCandless, F. P. (1974). Separation of sulfur dioxide and nitrogen by permeation through a sulfolane plasticized vinylidene fluoride film. Ind. Eng. Chem., Process Des. Dev., 13, 76.

Smith, J. M., and Van Ness, H. C. (1959). "Introduction to Chemical Engineering Thermodynamics," p. 95. McGraw-Hill, New York.

Stagner, J. R. (1970). ALSEP SWS curve-fit theory. Jet Propulsion Laboratory, Pasadena, Ca.

Stern, S. A., and Walawender, W. P. (1969). Analysis of membrane separation parameters. Separ. Sci., 4, 129.

Stern, S. A., Fang, S.-M., and Jobbins, R. M. (1971). Permeation of gases at high pressures. J. Macromol. Sci. Phys., B5, 41.

Treece, L. C., Felder, R. M., and Ferrell, J. K. (1976). Polymeric interfaces for continuous SO_2 monitoring in process and power plant stacks. Env. Sci. Tech., 10, 457.

Union Carbide (1974). "Parylene Conformal Coatings." Commercial Development Department, Union Carbide Corp., New York.

Van Amerongen, G. J. (1946). The permeability of different rubbers to gases and its relation to diffusivity and solubility. J. Appl. Phys., 17, 972.

Ward, W. J., III (1971). Ultra-thin liquid membrane construction. U.S. Patent 3,625,734.

Ward, W. J., III (1972). Immobilized liquid membranes. In "Recent Developments in Separation Science," Vol. 1, pp. 153-61. Ed. by N. N. Li. Chemical Rubber Co., Cleveland, Oh.

Ward, W. J., III, and Neulander, C. K. (1970). Immobilized liquid membranes for sulfur dioxide separation. PB-191-769, U.S. Dept. of Commerce.

Ward, W. J., III, Browall, W. R., and Salemme, R. M. (1976). Ultrathin silicone/polycarbonate membranes for gas separation processes. J. Membr. Sci., 1, 99.

Wellons, J. D., and Stannett, V. (1966). Permeation, sorption, and diffusion of water in ethyl cellulose. J. Polymer Sci.: Part A-1, 4, 593.

Williams, M. L., Landel, R. F., and Ferry, J. D. (1955). The temperature dependence of relaxation mechanisms in amorphous polymers and other glass-forming liquids. J. Am. Chem. Soc., 77, 3701.

Zavaleta, R., and McCandless, F. P. (1976). Selective permeation through modified polyvinylidene fluoride membranes. J. Membr. Sci., 1, 333.